Population Coding and Reconstruction of Complex Stimuli in the Locust Olfactory System

Thesis by

Bede Michael Broome

In Partial Fulfillment of the Requirements

For the Degree of

Doctor of Philosophy

California Institute of Technology

Pasadena, California

2006

(Defended January 6, 2006)

To my family and my love.

Without you, this would never have been possible.

Acknowledgements

Although the act of receiving a PhD is a singular achievement, the process of performing graduate research is a highly collaborative one. I would like to thank my advisor, Gilles Laurent, for his analytical and critical assessment of the material covered in this dissertation. His constant skepticism and methodical approach to understanding problems, without losing sight of the big picture, has affected me deeply. Also, I would like to thank my committee members: Michael Dickinson, Mark Konishi, Thanos Siapas, and Erin Schuman. Their suggestions and encouragement have guided me through the sometimes difficult process of finding a good research project and sticking to it.

I would also like to thank the members of the Laurent Lab for endless hours of encouragement and assistance with everything from minute experimental details to my overall understanding of neuroscience. In particular, I would like to thank Vivek Jaramayan, who collaborated with me extensively on the work in chapter 2 and under whose guidance I have become far more knowledgeable about the principles of neural coding, Matlab programming, and data analysis. Also, I owe great thanks to a visiting member of our lab, Markus Meister. Markus' sabbatical turned into a very productive collaboration and the contents of chapter 3. It was very interesting to learn about science from a different viewpoint, and his technical expertise was essential for developing the electronic nose and the stimulus protocols used with it.

I would like to recognize the individuals whose early encouragement led me to pursue a career in science: Fernando Nottebohm, Edward Ziff, James Schwartz, Ashok Hegde, and Edward Vates. I owe particular thanks to Ed for getting me interested in research at an early age and for providing such a good career model.

I am extremely appreciative of the help I have received from my friends and family, and I am eternally indebted to my parents for their love and encouragement throughout medical and graduate school.

Finally, I would like to thank my best friend Oceana Blueskyes, my partner in life, for her unwavering support throughout my PhD years. Her love and companionship have provided me with the stability both in body and mind that were necessary for completing this degree.

Abstract

Odors evoke complex sequences of activity in antennal lobe projection neurons (PNs), the insect analogs of mitral/tufted cells. These PN activity patterns evolve over hundreds of milliseconds, are consistent across trials, and contain information about odor identity and concentration. However, in natural settings animals must often identify odor blends or multiple odorants that occur in short temporal succession. We explored the effects of such stimulus history on single cell PN activity, PN ensemble responses, and downstream Kenyon cell (KC) responses by performing two experiments with novel stimulus paradigms. In the first experiment two different odors with variable intervening delays were presented while recording from PN and KC ensembles in the locust. We found that PN ensemble representations rapidly tracked odor stimulus changes and, in conditions of temporary odor overlap, often corresponded to the representation of neither odor alone nor their binary mixture. KC responses tracked the specificity of the instantaneous state of the PN representation: for example, for stimulus conditions that lead to unique and unpredictable PN population activity, we could find KCs with correspondingly unique spiking. These results support the hypotheses that PN population dynamics are history dependent and that PN output is read broadly in space (over the PN population) and piecewise in time by its target population.

In the second experiment two different odors were presented either as single pulses or complex M-sequence odor stimuli while we recorded PN activity and the time-varying stimulus using a specially adapted electronic sensor. Our results describe the numerous similarities between the processing of stimuli with diverse frequencies and highlight several important differences. We found that PN response types are varied, low dimensional, and that individual PNs do not fall into stable functional classes. Also, PN ensembles occupy different regions of high dimensional coding space and follow trajectories that depend on stimulus history. Finally, an observer's ability to reconstruct either the concentration or identity of an odor improves with PN number. These results add support to a growing body of evidence that Kenyon cells, the targets of PNs in the mushroom bodies, carry out a pattern classification on PN activity vectors sampled over large sets of PNs.

Table of Contents

Chapter 1

Introduction

"Last of all he will be able to see the sun, and not mere reflections of him in the water, but he will see him in his own proper place, and not in another; and he will contemplate him as he is."

-Plato, The Republic, The Allegory of the Cave

The process by which sensory events transform into subjective experiences is a matter of great mystery and inquiry. First, the brain receives information through specially tuned receptors, each with their own properties and sensitivities. Then, the output of these sensors is conveyed to other brain regions, transformed, and processed so that representations (platonic shadows) of the outside world are formed within our minds. Thus, the richness that we see, hear, feel, taste, and smell in the outside world is in fact both a filtered and a rebuilt version of reality. We will never escape our cave, the internally reconstructed version of the world around us. The representations that we form are fundamentally based upon and constrained by the complex rules that govern our cellular biology, our systems level interactions, and the world around us.

Understanding how the brain forms these representations is critical for appreciating the human experience. In this thesis I will address several issues related to the formation of odor representations in the insect olfactory system. By elaborating on the mechanisms behind the neural coding processes that drive these constructs, I hope to bring new understanding to the principles that underlie our perceptions of the world around us.

1.1 Neural Coding

To understand how the brain forms representations of sensory events, we must first decipher the language that the brain uses to encode information. At a basic level, all neural systems employ similar biochemical/electrical mechanisms to generate and propagate information. Electro-chemical gradients across neuronal membranes give rise to action potentials ("spikes") when input to gating mechanisms within the membrane exceed threshold voltages as a result of external stimuli (Bernstein, 1902; Hodgkin and Huxley, 1952). These spikes travel the length of the neuron and stimulate the release of pooled neurotransmitters at the synapse (Eccles, 1976; Loewi and Navratil, 1926). This, in turn, activates downstream neurons. Variations in either the anatomical organization of the cells or the mechanisms related to spike generation/propagation act as mechanisms to store information and adapt to the outside environment (Kandel et al., 2000).

At the periphery, single neurons in a sensory system detect some form of energy (e.g., a photon, or kinetic energy) or chemicals (in the case of taste and olfaction) and transform those into electrical signals. Those signals are transmitted to and received by other neurons, and thus, they become the carriers of information about the physical world. For example, each photoreceptor captures photons of specific spectral quality and intensity in some volume of space. Collectively, photoreceptors provide signals from which a visual field can be constructed, even though each neuron "encodes" only a very small portion of that space. However, as those signals proceed from the periphery, they are combined in complex ways, and functionally relevant features are extracted. The mammalian visual system provides a clear example of this progression (Gilbert, 1994; Lagnado and Baylor, 1992; Reid and Alonso, 1996). As signals from photoreceptors proceed to further layers of the retina and ultimately to ganglion cells, information about constructed features —edges, concentric light/dark regions, wavelength—can be found in the activity of single neurons. Such information is often said to be explicit. The same information

is of course present, implicitly, in the collective activity of arrays of upstream neurons. Of particular interest is the recent realization that such features match the statistical structure of our physical world (Yang and Purves, 2003). From the retina, signals are conveyed to the lateral geniculate nucleus in the thalamus and then on to the visual cortex, where we find, for example, neurons sensitive to orientation, motion, and color (Livingstone and Hubel, 1988; Sincich and Horton, 2005). As individual neuronal responses become more specific or selective, it is obvious that a reconstruction of the world that matches our perception must require the pooling of activity from many neurons. Therefore, information is said to be distributed (Callaway, 2004; Martin, 2002).

How do brain networks process and use distributed signals? Different types of "coding" strategies can be found in neural systems; at one extreme are what are often called spatial representations (Rieke et al., 1997). Those can in turn be split into identity codes and truly spatial codes—i.e., ones in which neuronal position is intrinsically relevant for the encoding or decoding mechanisms. The encoding of spatial position by the retinal array of photoreceptors, or the encoding of spatial position by delay lines in the owl's nucleus laminaris (Konishi, 2003; Meister, 1996), for example, are true spatial codes. At the other extreme are "temporal codes" (Laurent, 1999). These can also be split according to whether the codes are representations of time or temporal encoding of features that do not, in and of themselves, vary in time. The latter are considered true temporal encoding schemes. These schemes are not necessarily exclusive of one another; they can often be superimposed depending on a system's specific requirements (Ahissar and Arieli, 2001). They are also to a significant extent dependent on the metrics used to characterize neuronal activity. For example, a temporal code is nearly always also an identity code simply because the identities of the neurons whose firing carries information are themselves informative. In addition, the information present in the timing of a population's spikes disappears as one uses longer and longer time windows to quantify it: essentially, a potentially temporal representation becomes a spatial one as one measures rates over long time periods. This reveals

that the nature of a code depends on the prior knowledge of the mechanisms by which this information is normally decoded.

Time codes do not depend on a cell's location but rather its activity. Within time coding a distinction is often made between rate codes and temporal codes. Again these two descriptions are not exclusive, but rather two ends of a spectrum (Shadlen and Newsome, 1994). A pure rate code conveys information using only the mean firing rate of its spikes (Parker and Newsome, 1998; Sanger, 2003). Early pioneers in neural coding discovered the first example of such a system while recording from mechano-sensitive stretch receptors, finding that stretch was directly proportional to the mean spike rate (Adrian, 1942). In contrast, a pure temporal code does not depend on the intensity of a particular spike burst but on the precise timing of spikes relative to one another (Shadlen and Newsome, 1994; Theunissen and Miller, 1995).

While theories about neuronal coding date back to the experiments of Lord Adrian in the 1930's, our understanding of temporal coding has, until recently, been quite spare. Perhaps the main reason for the relative dominance of rate coding in our models of the brain (in all but a few specialized cases) has been our inability to record from large sets of neurons (Nicolelis et al., 2003; Nicolelis and Ribeiro, 2002; Wilson and McNaughton, 1993; Wilson and McNaughton, 1994). While rate codes can be understood by monitoring the activity of a single cell, temporal codes often require the ability to monitor the responses of many cells simultaneously (Buzsaki, 2004; Deadwyler and Hampson, 1997). Thus, temporal coding has been studied relatively less than rate coding, but it is no less significant.

In fact, temporal coding is a particularly attractive way for information-rich signals to be processed. It could, for example, enable neurons to bind together their activity, working in parallel to represent information (Engel et al., 2001; Engel and Singer, 2001). Individual processing capabilities may be combined when groups of neurons project onto the same downstream target that acts as a coincidence detector. Each of the input neurons acts to bring the downstream neuron closer to threshold, summating their input (Dayan and Abbott, 2001; König

et al., 1996). For larger groups temporal coding can be used to organize activity through synchronous oscillations. In this situation neurons fire in time with an internally or externally (with respect to a specific brain region) generated synchronizing mechanism, and all of the information from one cycle is linked together by nature of its timing (Singer, 1999; Singer, 1995). Synchronized oscillations of this type have been observed across many different phyla. These include: primates - gamma oscillations (30-90Hz) have been linked to such diverse processes as attention (Fell et al., 2003; Tiesinga et al., 2004) and memory (Lee et al., 2005; Mehta, 2005); rodents - theta oscillations have been linked to hippocampal activity (Siapas et al., 2005; Siapas and Wilson, 1998); amphibians – oscillations are used to increase information transmission in the retina (Schnitzer and Meister, 2003); crustaceans – oscillations have been found to regulate activity in the stomatogastric ganglion (Bartos et al., 1999; Marder, 2002); and arthropods – oscillations are necessary for fine olfactory discrimination (Stopfer et al., 1997).

However, coincidence detection and oscillatory activity are not the only ways in which temporal coding can be used in the brain. Rank order coding is a strategy where the timing of a cell's first spike carries significance. This method has been demonstrated to be an efficient means for representing information both experimentally and theoretically in the visual system (Delorme and Thorpe, 2001; Thorpe et al., 2001; Van Rullen et al., 1998). In this model downstream neurons are very sensitive to the activation order of inputs by a feed-forward shunting mechanism that progressively reduces the sensitivity of the downstream neuron to its inputs. Investigations into this method of coding are ongoing. Finally, neurons can organize themselves into so-called synfire chains - systems capable of generating repeating patterns in response to a stimulus trigger (Ables, 1991; Aviel, 2003). To achieve this state, neurons are connected so that once activated groups of synchronously firing neurons will activate one another in a self-perpetuating manner. These many observations of complex structure in neuronal activity suggest a diversity of potential coding mechanisms in the brain. The hard part is to establish their functional relevance.

1.2 Insect Olfactory Anatomy

Animals are constantly bombarded with an enormous number of odors. The powerful ability of the olfactory system to detect and discriminate between these odorants allows animals to perform some of the most essential tasks for their survival: find food, find mates, and avoid predators. Olfaction is the oldest, most conserved sense, and many of its mechanisms are identical across phyla. For example, convergent anatomy, recurrent interactions, serial processing, and oscillatory activity have all been observed in both insects and mammals (Firestein, 2001; Hughes and Mazurowski, 1962; Laurent and Naraghi, 1994; Mombaerts, 1996; Nicoll, 1971b.). The insect system's similarity to the mammalian system, both structurally and functionally, enables one to probe the complexities of neural coding and use invasive techniques that would be difficult in larger organisms. Due to its smaller physical size, the insect is a far more tractable system. While in mammals the olfactory bulb contains four types of neurons and greater than one million cells, the insect antennal lobe contains only ~1000 neurons and two classes of cells (Firestein, 2001; Leitch and Laurent, 1996). This reduced complexity allows one to better understand the specific interactions that govern olfactory processing before testing these conclusions in mammals.

Insects in general and the locust (*Schistocerca americana)* in particular have advantages for the study of olfaction. Insects are highly olfactory animals and can find both food sources and potential mates (despite poor visual acuity) over large habitats using olfactory cues. Accordingly, a relatively large portion of their brain is dedicated to olfaction, making these areas experimentally accessible. Also, insects are not simple creatures and have been shown to exhibit complex behaviors previously ascribed only to larger animals. These include: associative learning (Bitterman, 1983), complex decision-making (Giurfa, 2003; Giurfa et al., 2001), and navigation through landscapes (Srinivasan, 2003). Most recently, social learning, the transference of

knowledge between individuals without outside instruction, has been demonstrated in crickets (Coolen et al., 2005). The fact that insects can accomplish such complex tasks allows us to investigate not only low level sensory systems but also higher level structures where information integration occurs and decisions are made. Finally, there are several unique advantages associated with locusts. They are large, easy to manipulate, capable of withstanding intrusive physiological recordings, and the subject of considerable prior physiological work (Burrows, 1996; Laurent, 1997). Also, locusts have certain populations of neurons whose anatomy and firing characteristics enable one to record the activity of specific large groups of neurons unambiguously (Perez-Orive et al., 2002).

The overall organization of both the mammalian and insect olfactory systems is shallow; at each one of few relays, transformations occur and representations change. Olfactory stimuli are initially transduced by olfactory receptor neurons (ORNs). In locusts these are exclusively found on the antenna; however, in other insects they also appear on the maxillary palps or elsewhere (Chapman, 1998). In mammals these receptors are located in the olfactory epithelium within the nasal cavity. While mammalian ORNs have no structure enclosing them, insect ORNs, are located within small, porous protrusions of the cuticle called sensilla (Chapman, 1998; Keil, 1989; Steinbrecht, 1980). Each sensillum typically possesses two or more ORNs with some locust sensilla containing up to 50 ORNs (Keil, 1989; Ochieng et al., 1998). Sensilla come in four different types, of which three are known to contain ORNs. Each different type of sensilla (basiconic, trichoid, coeloconic, chaetic) occurs with a different frequency and in different regions of the antenna (Lee and Strausfeld, 1990). Among those sensilla that are known to contain ORNs, basiconic and coeloconic sensilla are most densely clustered at the proximal and middle regions of the antenna, while trichoid sensilla are located more distally. Little is known about the arrangement of individual receptors, in contrast with the extensive knowledge about the mammalian olfactory epithelium (Buck, 1991; Mombaerts, 1999; Scott and Brierley, 1999; Scott et al., 1997).

Within the sensilla a wide variety of olfactory receptors (OR) bind with varying affinities to the large number of odorants encountered in nature (Hallem et al., 2004; Wilson et al., 2004). Work in round worms, insects (*Drosophila* and mosquitoes*),* and mammals (mice, dogs and humans) has uncovered several families of G-protein coupled receptor (GPCR) genes expressed in olfactory neurons. They form the largest gene super-family in the genome (Buck, 1991; Vosshall et al., 1999). In rats, an extreme case, ORs make up 6% of the genome, although many of these genes are non-functional pseudogenes. In *Drosophila,* 55 functional olfactory receptors have been identified, and in mammals approximately 1000 (~400 in humans, ~1400 in rats) are present (Couto et al., 2005; Hallem et al., 2004; Mombaerts, 1999; Vosshall et al., 2000). To date, there is no similar count of the unique ORNs types in locusts; however, we do know that there are 50,000-90,000 ORNs on each locust antenna (Burrows, 1996; Leitch and Laurent, 1996). ORNs arborize in glomeruli, roughly spherical regions of neuropil in the antennal lobe (AL), the insect equivalent of the mammalian olfactory bulb. Surprisingly, each *Drosophila* and mammalian ORN (this finding has yet to be replicated in other species) expresses only a single type of OR gene (2 in *Drosophila*, with one conferring binding specificity) from this large repertoire, and each ORN that shares the same OR projects to a single glomerulus (Mombaerts et al., 1996; Vosshall et al., 2000). This occurs regardless of the physical location of the ORN on the olfactory epithelium/antenna.

Odorant molecules bind to ORs associated with one of the two pathways for odor transduction: cAMP and IP_3. Odorant molecules that stimulate GPCRs cause them to activate GTP effectors that facilitate the production of cAMP. The rise in this intracellular second messenger causes a membrane bound cyclic-nucleotide gated Ca^{2+} channel to open, depolarizing the cell and giving rise to an action potential that carries the ORN's information downstream (Ache and Young, 2005; Zufall and Leinders-Zufall, 1998). The other intracellular messaging pathway, the IP_3 dependent pathway, has been molecularly identified primarily in crustaceans, but it is thought to exist in a diverse range of animals across phyla. In a similar fashion to the cAMP

pathway, odor reception triggers IP_3 production that then opens IP_3 gated Ca^{2+} channels, depolarizing the cell and eliciting a spike (Ache and Young, 2005; Boekhoff et al., 1990). It is currently unknown whether individual ORNs use both pathways simultaneously or what the functional effect of a redundant system might be (Ache and Young, 2005; Takeuchi et al., 2003).

In the locust, projections from ORNs travel ipsilaterally - in flies and mammals the projections are bilateral - to antennal lobe glomeruli (Hansson and Anton, 2000). There they synapse directly onto two different cell types: excitatory projection neurons (PNs) and inhibitory local neurons (LNs) (Fig. 1.1) (Ernst et al., 1977). Anatomical studies have demonstrated that in the locust there are 830 PNs and approximately 300 LNs (Leitch and Laurent, 1996). Cholinergic PNs extend dendrites to 10-14 coplanar glomeruli, equidistant from the center of the AL (R Jortner, SS Farivar, & G Laurent, in prep; Wehr and Laurent, 1999). The multiglomerular nature of locust PNs is relatively unique, having only been noted in locusts and wasps amongst the many species studied. *Drosophila* possess uniglomerular PNs, and honeybees have both uni- and multiglomerular PNs (Fonta et al., 1993; Homberg et al., 1988; Stocker et al., 1990). However, it is not known whether the multiglomerular PNs in locusts or bees all receive projections from the same OR, effectively making them uniglomerular systems. Projection neurons are the sole output neurons of the locust AL and project ipsilaterally to the calyx of the mushroom body and the lateral protocerebrum (Hansson and Anton, 2000). As with the PN inputs, the output pattern varies across different insect species. *Drosophila* and bee PNs do not all project to both destinations, and in contrast to the locust some PNs project only to the lateral protocerebrum (Jefferis et al., 2001; Wong et al., 2002).

Locust LNs project broadly across the AL and form dendrodendritic, GABAergic synapses with a large number of the PNs (Fig. 1.1)(R Jortner, SS Farivar, & G Laurent, in prep; Hansson and Anton, 2000). While different classes of LNs have been observed, each defined by its projection pattern, all are densely arborizing cells whose neurites are completely limited to the AL. In addition, LNs are axonless and in the locust do not produce action potentials, enabling us

to record from large groups of cells and unambiguously attribute the activity to PNs (Perez-Orive et al., 2002). LNs respond to odor stimuli with graded sub-threshold activity and calcium spikes (Laurent and Davidowitz, 1994; Leitch and Laurent, 1996). Just as with PNs, LNs are not identical in all insect species. In some insects systems (such as bees and cockroaches) LNs project only to limited portions of the AL, and in others they spike. However, they are consistently both inhibitory and GABAergic (Hansson and Anton, 2000; Homberg et al., 1989).

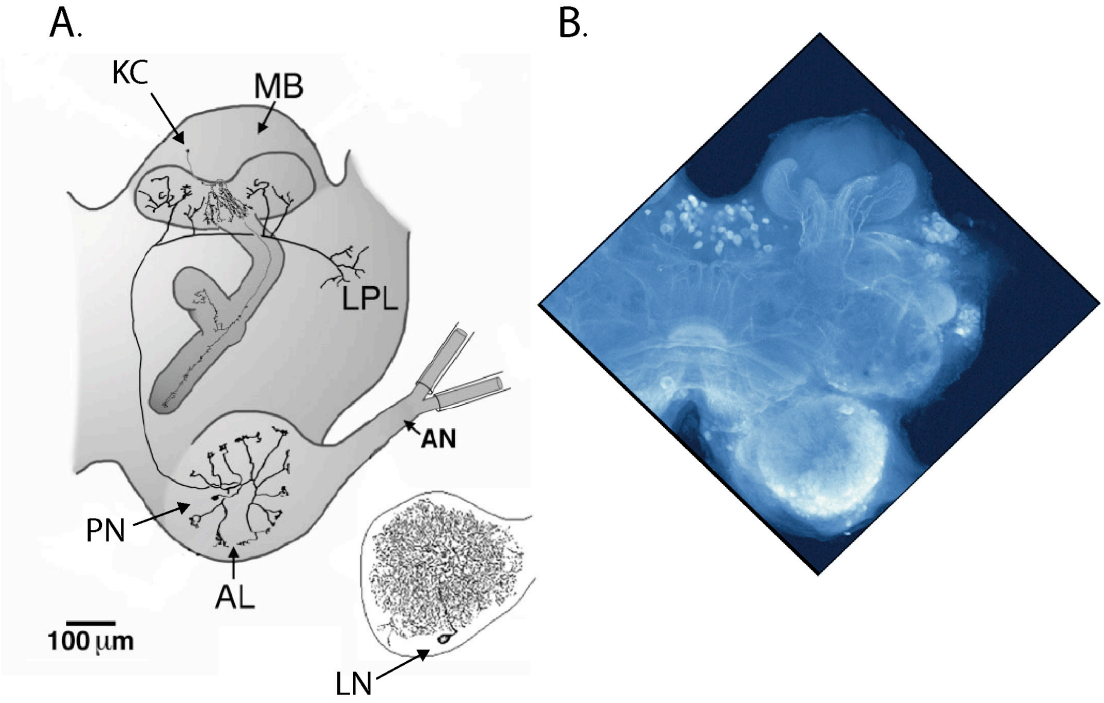

Figure 1.1 Anatomy of the locust olfactory system. **A**. Structures: AL - antennal lobe; AN - antennal nerve; KC - Kenyon cell; LN - local neuron; LPL - Lateral protocerebral lobe (lateral horn); MB - mushroom body; PN - projection neuron. LN is shown as a cut out to demonstrate its broad branching throughout the AL. **B**. Actual anatomy of locust brain shown using an anti-GABA stain. Figures adapted from Wehr & Laurent 1996 and Perez-Orive et al. 2002.

The mushroom body (MB) is a primary recipient of AL projections and is one of the integrative nexuses in the insect brain, receiving input from the visual, olfactory, and tactile sensory systems (Burrows, 1996; Gronenberg, 2001; Strausfeld et al., 1998). Projections from the AL follow the antennal tract to the calyx of the MB where they branch broadly throughout the MB calyx (Fig. 1.1). There are approximately 50,000 intrinsic neurons, termed Kenyon cells

(KCs), in the locust MB (Laurent and Naraghi, 1994). These small cells (3-8μm) have cell bodies located above the calyx and send their primary neurites down into the calyx where their neurites divide and fan out, projecting over a small region (Laurent and Naraghi, 1994; R Jortner, SS Farivar, & G Laurent, in prep). A single PN makes contact with approximately 1/2 of all KCs and covers approximately 10% of the MB calyx (R Jortner, SS Farivar, & G Laurent, in prep). As with the other cell types in the olfactory system, there are inter-species differences with respect to KC organization. For example, bees, cockroaches, and wasps have two calyces per MB, while locusts and *Drosophila* possess only one (Strausfeld et al., 1998; Strausfeld et al., 2003).

Kenyon cell axons all leave the MB via the pedunculus, a structure located at the base of the MB. These densely packed axons carry KC information to several different lobes. Locust KCs project to two lobes (the α- and β-lobes), while additional structures are present in other insects (α'-, β'-, and γ-lobes are present in *Drosophila*) (Strausfeld et al., 1998). In the lobes, KCs synapse onto MB extrinsic neurons that then project widely throughout the brain. While little is known about the anatomy or function of projections that follow after the MB, oscillations have been detected in their activity. Desynchronizing upstream PNs has been shown to decrease the specificity of their response, a result that has also been demonstrated in KCs (MacLeod et al., 1998). Further investigation into these downstream areas is ongoing.

In comparison to the MB, relatively little is known about the structure and function of the lateral horn, the second output region of the AL (Hansson and Anton, 2000). In locusts, lateral horn interneurons (LHIs) are GABAergic cells that project directly to the MB. There, the profuse axon branches overlap with KC dendrites. Experiments have shown that LHIs respond to most odors, suggesting a role for them in the modulation of MB activity (Perez-Orive et al., 2002).

1.3 Olfactory Coding in the Locust

While there is still much to discover about olfaction, a picture of how odors are represented at different points in the locust olfactory system has begun to emerge. Odors initially activate multiple odor receptors with varying affinities (Hallem et al., 2004; Wilson et al., 2004). This promiscuous activation, using sets of ORNs to represent an odor, allows locusts to perceive a virtually limitless number of odors. The alternative, where each odor activates only one specific receptor, would limit their perception to the number of different receptors on the antenna, ~1000.

As the signal progresses to the AL there is a dramatic reduction in the number of cells that represent the odor information. The highly convergent nature of this connection (100,000 ORNs → 800 PNs) is thought to reduce the significance of noise fluctuations on the odor signal in the AL (Laurent, 2002). Nonetheless, a very large fraction of PNs are activated by the ORNs. 90% of all PNs (in the locust) respond to the presence of an odor with either excitation (~50%) or inhibition (~40%) of their activity relative to their basal firing rate (Perez-Orive et al., 2002). This widespread activity appears to arise not only from the primary activation of the PNs by ORNs, but also by recurrent interactions within the AL (Leitch and Laurent, 1996; MacLeod and Laurent, 1996). It is notable that this activity does not occur only in specific regions, and odotopic mapping is not the primary means for representing information in the OB or AL (Laurent, 1999).

Recordings of local field potentials (LFP) in the mushroom body calyx indicate that PN activity occurs in 20-30Hz oscillatory cycles when odors are present and that the power of these oscillations drops significantly when odors are removed (Laurent and Davidowitz, 1994; Laurent and Naraghi, 1994). It is believed that PNs use this synchronous firing to bind together the activity of numerous PNs and form a representation of each unique odor. Thus, it appears that odors are not represented by the momentary activity of a single PN or even a single PN pattern, but by 830 dimensional PN ensembles occurring at the rate of 20-30Hz (Mazor and Laurent, 2005). It has also been shown that these 830-D representations are not static repeating patterns,

but patterns that evolve over time. Not all PNs fire in each oscillatory cycle; instead, PNs transiently synchronize their activity in ensembles that change over time and in an odor-specific manner (Laurent and Davidowitz, 1994; Laurent and Naraghi, 1994). A given PN that is highly synchronized with another PN for one cycle may be unsynchronized or silent in the next one. These evolving ensembles take advantage of the fact that odors are usually present for a prolonged period. As odor presentations continue, the ensembles that are activated become more and more dissimilar from one another. In zebrafish this decorrelation process was shown to reach its maximum in 200-300ms (Friedrich and Laurent, 2004), a time period that is consistent with rodent experiments as the point when discrimination between odors can be expected (Uchida and Mainen, 2003).

This oscillatory synchronization is mediated by the recurrent activity between PNs and LNs in the AL. While LNs do not spike in locusts, their contribution to synchrony has nonetheless been demonstrated in two ways. First, LNs sub-threshold activity has been directly monitored using intracellular recordings, showing strict locking to LFP phases observed downstream (R Jortner, SS Farivar, & G Laurent, in prep). Second, selective blocking of GABA (primarily associated with LNs) in the AL has been shown to stop oscillations of the downstream LFP (which reflects the activity of the AL PNs) (MacLeod et al., 1998; MacLeod and Laurent, 1996; Stopfer et al., 1997). Others have suggested that lateral inhibition (in the strict visual system sense, where feedback from neighboring cells acts to sharpen the tuning curve of a particular cell in respect to a certain odor) is present in the AL and modulates PN activity (Mori et al., 1999). However, this hypothesis is unlikely given the widespread PN activity that is detected across both the OB and the AL in response to odors and the lack of traditional tuning curves in the AL.

Behavioral evidence suggests that oscillatory synchronization of PNs is essential to an animal's ability to perform fine discriminations between odors. Using honeybees, it was demonstrated that abolishing oscillations using the GABA blocker picrotoxin inhibited the ability

of the animal to discriminate between similar single chain alcohols (1-hexanol and 1-octanol) (Stopfer et al., 1997). However, their ability to discriminate between dissimilar odorants (geraniol and 1-hexanol) was not disturbed. Similar oscillations have been found in all model organisms with the exception of *Drosophila*. However, the significance of oscillations in other systems has not been thoroughly examined.

It is important to note that this distributed method of representing odors may not be used in all circumstances. One prominent exception may be the case of pheromones. Pheromones are compounds that are used for communication between individuals of a particular species for a wide variety of purposes including: mating, alarm transmission, territorial marking, and group aggregation. Animals are highly tuned to these compounds and may use special receptors or processing areas to ensure that these signals are correctly interpreted (Amrein, 2004; Brennan and Keverne, 2004; Hassanali et al., 2005). In moths specific glomeruli have been identified that mediate pheromone activation, and it appears that all the activity necessary to represent sex pheromones at the AL level is confined to within two specific glomeruli (Christensen and Hildebrand, 2002). This may represent an instance of labeled lines, single pathways used for information transmission, in the AL. While some have suggested that a system of labeled lines is used for all odor representations, there is significant evidence to dispute this hypothesis. First, odors cause widespread activation in the AL, something that would not be expected with labeled lines. Second, the diversity of odorants that an animal can recognize suggests that it is not limited by the relatively small number of pathways present in a labeled line model. Thus, while there may be some specialized odors for which labeled lines are useful, most odors are probably represented in the AL by distributed coding strategies.

Until recently, the size and recording difficulty associated with the MB hampered our ability to investigate its function. The existing evidence for its function came mainly from genetic and developmental studies that demonstrated the MB's involvement in learning and memory for both olfactory and visual information (Dubnau et al., 2001; McGuire et al., 2001; Strausfeld et al.,

1998). More recent studies have begun to shine light on how the MB integrates olfactory information from incoming PN ensembles. Each KC responds to approximately 10% of the odors presented to it and does so with a few very tightly times spikes (Perez-Orive et al., 2002). This stands in stark contrast to the promiscuous and prolonged firing of PNs. KCs owe their specificity to their high firing thresholds, the highly divergent nature of the PN→MB connection (830→50,000), and the synchronous firing of PNs. Each PN projects to approximately 1/2 of all KCs, yet KCs only respond when they receive input from ~100PNs in a single oscillation cycle (Perez-Orive et al., 2002 ; R Jortner, SS Farivar, & G Laurent, in prep). The large number of ways in which PNs can be coincidently active on a single KC gives the system the ability to (at least theoretically) distinguish between a virtually limitless number of odors. Many PNs are necessary to activate a single KC because of the high activation thresholds that KCs possess. KCs will fire only when coincident activity exceeds this threshold and occurs before the feed-forward inhibition of LHIs at the end of each PN activation cycle resets them (Perez-Orive et al., 2002). Thus, the distributed odor representation found at the ORNs and PNs level is finally transformed into a sparse code at the level of the KCs. From this point on, the nature of olfactory coding is relatively unknown and the topic of much research.

1.4 Decoding Neuronal Activity

Our ability to reconstruct ("decode") stimuli from the neuronal responses that they elicit is a critical test of the coding principles that we attribute to specific sensory systems. Decoding is an objective way to evaluate how well one understands the coding mechanisms that are ascribed to given brain regions and can highlight limitations in one's methods. Furthermore, it provides a way of quantifying how much information is present in the activity of a given neuronal population and insight into how that information may be used at later stages in the brain (Dayan

and Abbott, 2001; Rieke et al., 1997). This remains true regardless of whether stimulus reconstruction is actually performed by the animal in the same manner as it is evaluated experimentally. Several different classes of reconstruction methods have been developed, including population vector coding, Bayesian inference, and spike train decoding. Each technique has advantages in certain situations and challenges with respect to its implementation in a real neural system.

1.4.1 Population Vector Coding

Tuning curves are a way of describing the preferential activity that certain cells exhibit for a specific range of a continuous parameter. These curves are specific to each cell and are measured empirically by presenting a wide range of stimuli while monitoring the responses. Cells that demonstrate tuning curves have been identified in many sensory and motor systems, and typically groups of cells cover an entire stimulus range with their preferred response ranges (Fig. 1.2A) (Pouget et al., 2000; Rieke et al., 1997).

Population vector coding uses tuning curves as the basis for calculating the "direction" of a stimulus or output (Dayan and Abbott, 2001; Foldiak, 2002; Oram et al., 1998). The preferential response of a given cell (its tuning curve) is mathematically represented as a direction vector with a magnitude equal to the difference between the given cell's activity (over a specific time period) and the mean activity of that neuron in all conditions (Fig. 1.2B). By sampling from a large group of cells and summating the resulting vectors, a population vector can be created which represents the collective direction of the population's activity (Fig. 1.3). Extensions of this method include multi-dimensional scaling of the individual cell vectors (Oram et al., 1998), which allows other applications that are not purely directional (e.g., face cells (Young and Yamane, 1992)), and methods for optimizing the coefficients used to estimate the vector direction (Dayan and Abbott, 2001). This method has been used with great success for predicting arm movements in monkeys

(Schwartz and Moran, 2000), deciphering place cell function in the hippocampus (Zhang et al., 1998), and other similar applications.

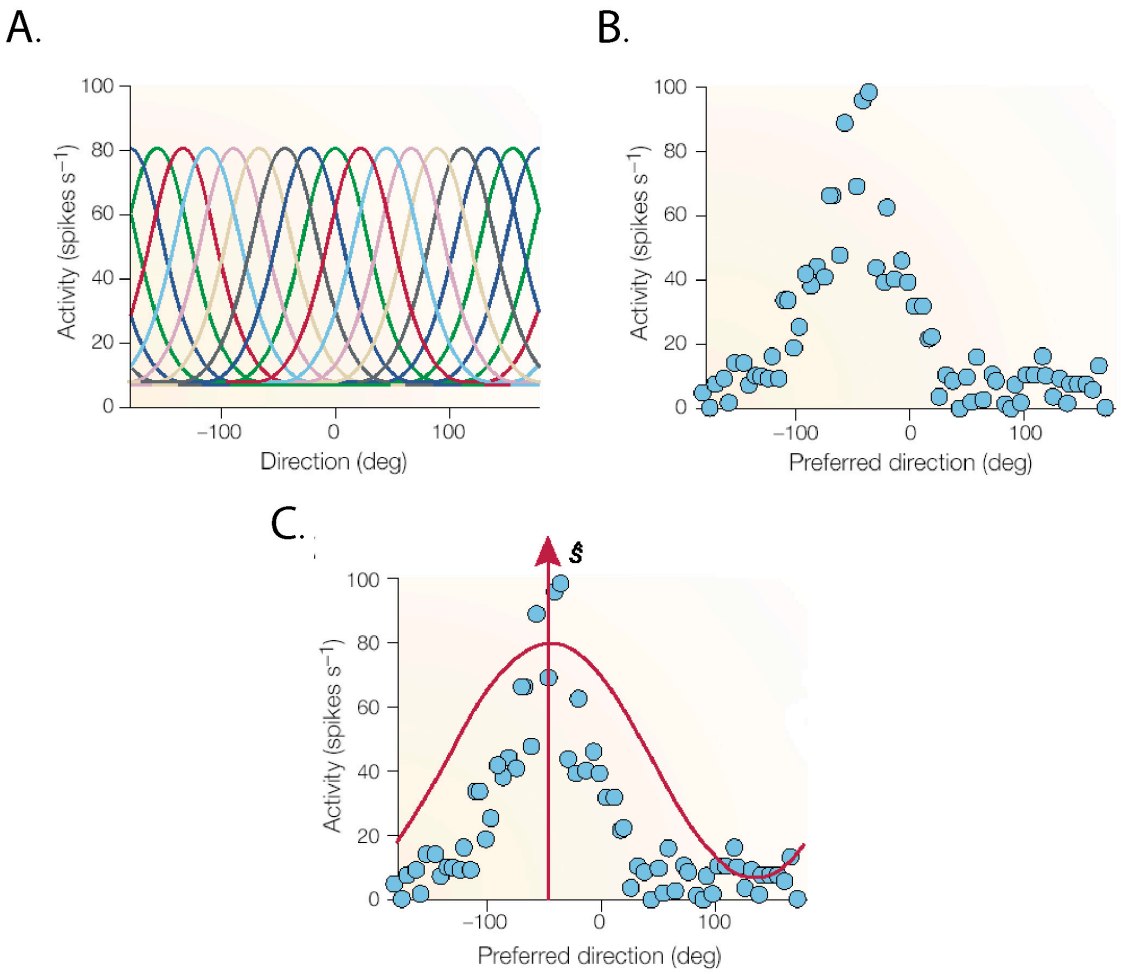

Figure 1.2 Tuning Curves. **A**. Several different tuning curves each with a preferred response direction that collectively cover a range of values. **B**. An example of the data that is used to calculate a given cell's tuning curve. **C**. Preferential direction and cosine waveform superimposed upon example data. Figure adapted from Pouget et al., 2000.

However, there are problems with this method (Foldiak, 2002). First, tuning curves may not have the properties necessary for accurate decoding. Neurons in real systems do not always have tuning curves that are evenly distributed across the entire range of values, which can lead to bias in the resulting population vector. Also, tuning curves may not have a cosine function shape, which would also bias the vector. Second, variability in the responses of individual neurons are

completely ignored. While it is assumed that the neurons will retain the shape of their tuning curve under all conditions, this may not be the case. Third, the method does not provide a mechanism to assess statistical confidence. Finally, the method is not easy to implement in neural systems. While this is not a requirement for decoding techniques, it does not argue in favor of this technique over others that have greater biological relevance.

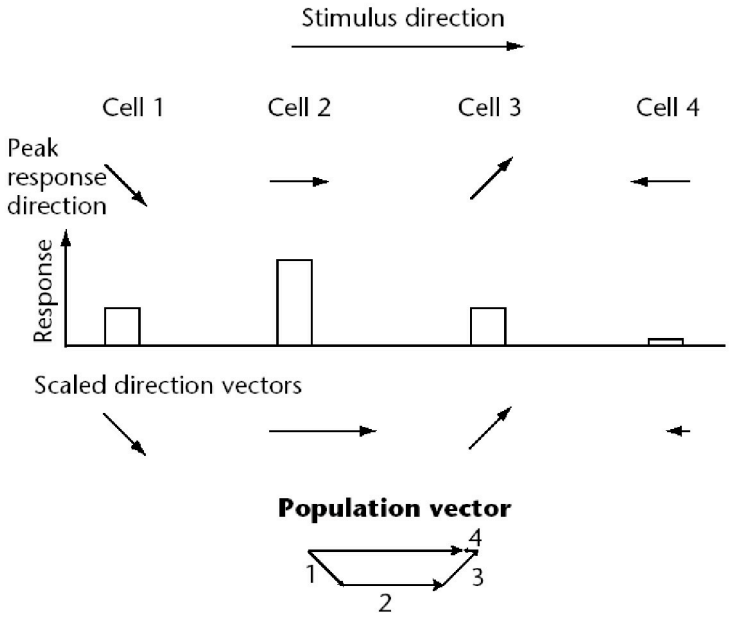

Figure 1.3 Example calculation of a population vector for a horizontal stimulus from the responses of four neurons. Figure adapted from Foldiak, 2002.

1.4.2 Bayesian Inference

As the limitations discussed above indicate, population vector methods are neither a universal nor optimal way to decode stimuli. To overcome some of the problems associated with this technique, methods have been developed to eliminate tuning curves and instead evaluate probability distributions that associate stimuli with neuronal responses. These Bayesian methods are generally more applicable to different sensory/motor applications and allow one to quantify the quality of the reconstruction (Foldiak, 2002; Rieke et al., 1997). In addition, Bayesian

methods are easier to implement in realistic neural systems using feed-forward networks (Dayan and Abbott, 2001; Funahashi, 1998).

At the core, Bayesian estimates involve determining the conditional probability that a response (r) will occur if a stimulus (s) is presented, P(r|s) (Fig1.4). The conditional probability of these two events occurring is related to the joint probabilities of each event occurring separately via Bayes' rule:

$$P(r|s) = P(r,s)/P(s). \qquad \text{EQ\#1}$$

However, in Bayesian decoding (working backwards from response to stimulus) one is interested in determining the reverse equation, termed the posterior distribution:

$$P(s|r) = P(r|s)P(s)/P(r) \qquad \text{EQ\#2}$$

or

$$P(s|r) = P(r,s)/P(r). \qquad \text{EQ\#3.}$$

To implement Bayesian decoding it is necessary to empirically determine the probability distributions for both the stimuli and responses. This can prove difficult because a large amount of data across a wide range of values is required. However, if the data is available, the values in the posterior distribution (EQ#2) are determined as follows: the histogram of responses across a range of stimuli provides P(r|s), P(s) is based on the characteristics of the known stimulus, and P(r) is determined with the relationship:

$$P(r) = \Sigma(P(r|s)P(s)). \qquad \text{EQ\#4}$$

Once the posterior distribution, P(s|r), has been determined, additional manipulations must be performed to extract single values from this function. Essentially, extracting single values involves identifying the single value at the peak of the probability distribution; i.e., maximizing the function to find the direction of the highest probability density. However, the exact shape of a probability distribution is not known, and given any additional data it may change. In a sense this process underlies all Bayesian techniques: a prior distribution of data is

refined as more data is presented, resulting in a distribution that more closely approximates the actual. One method, termed maximum a posteriori (MAP) estimation, accomplishes this task by minimizing a loss function that relates all possible peak values of the distribution to each hypothesized peak value and calculates a penalty. Minimizing this loss function is therefore equivalent to identifying the direction of highest probability density. A mathematical extension of this method is termed the maximum likelihood (ML) technique. ML arises logically from MAP in situations where a very large amount of data is present. In effect, these data allow one to base the entire estimate on observed data without any hypothesized prior distributions. It can be proven that in situations where the data set is sufficiently large, the ML method is optimal. Assessed theoretically, the ML method will approach an information-theory limit called the Cramer-Rao boundary, the theoretical limit for the accuracy of an unbiased estimator (Dayan and Abbott, 2001; Rieke et al., 1997).

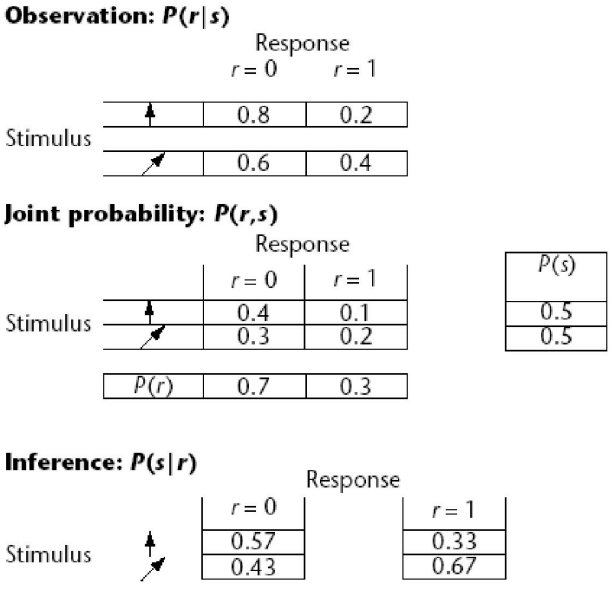

Figure 1.4 An example of Bayesian decoding using two stimuli and two responses (0 or 1) from a single neuron. The probabilities of each stimulus, vertical or diagonal, occurring is 0.5. The conditional probability P(rls) is measured separately for the two stimuli. Bayes' theorem gives the decoding for the two possible responses. Figure adapted from Foldiak, 2002.

1.4.3 Spike-Train Decoding

While vector and Bayesian methods are effective at decoding reasonably static stimuli, decoding stimuli that vary rapidly with time requires a different approach. Spike-train decoding is based on directly transforming spike trains from single cells or groups of cells into the stimuli that produced them. In conditions where a spike train closely and densely follows the evolution of a stimulus, a method using a linear combination of fixed kernels can be used; relating the occurrence of a spike to the preceding period of stimulus that generated it with time varying coefficients that are determined by the activity of individual cells (Bialek et al., 1991; Warland et al., 1997).

Bialek and colleagues implemented this technique to decode the visual information present in the activity of the fly H1 neuron by using the following protocol (Bialek et al., 1991). A fly was presented with a grating pattern whose motion velocity varied randomly across its visual field. Simultaneously, the activity of the H1 neuron, which encodes the velocity and direction of a stimulus, was recorded extracellularly. After the experiment was complete, spike-triggered stimulus averages (STSAs) were created for each H1 cell (2, one in each eye, were recorded). These STSAs were calculated by averaging a fixed period (100ms) of the known stimulus that preceded each spike occurrence for each cell (Fig. 1.5A). Roughly, this process yields a kernel that relates a spike to the input stimulus that elicits it. By linearly summating the STSAs that correspond to each cell after convolving them with the recording of spike occurrences over the duration of the recording, they were able to reconstruct the major features of the original grating stimulus (Fig. 1.5B).

One difficulty associated with this method is correctly determining the kernels. Bialek and colleagues addressed this issue by optimizing the STSAs in a recurrent process designed to minimize the reconstruction error over several iterations. At each step the quality of the reconstruction was tested with data that were not used in the original kernel construction. Overall, this method produced reconstructions that were very similar to the original time varying stimulus.

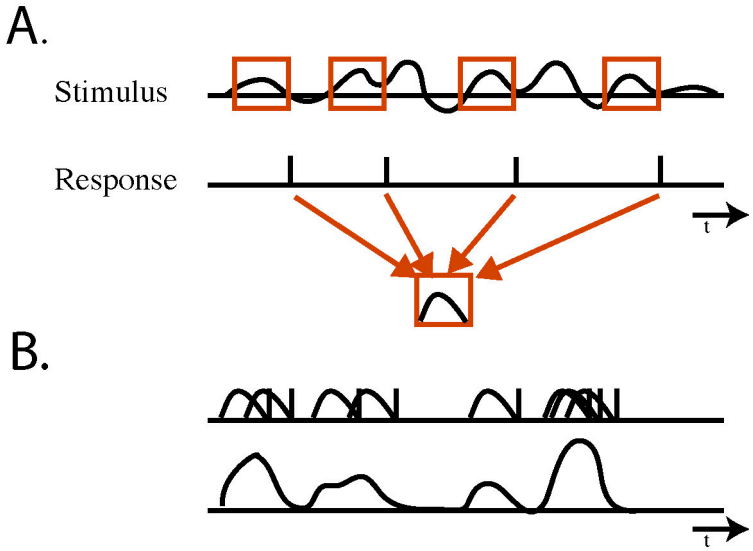

Figure 1.5 A. An example of the reverse correlation technique for extracting spike triggered stimulus averages (STSAs). A fixed period of time prior to each recorded spike is extracted from the stimulus recording and is averaged. **B**. Stimuli are reconstructed by combining the STSAs of each cell in accordance with the test spike pattern.

The work described in this dissertation will investigate applications of the spike-decoding method in the insect olfactory system. In that context this method will be used to provide the first high resolution reconstruction of an olfactory stimulus based solely on the activity of downstream neurons.

1.5 Outline

In this thesis I will investigate how information is encoded and decoded at various stages of the insect olfactory system. In particular, I will explore how this system responds to stimuli that are more naturalistic than those that have been used in previous work. I will test the applicability of our current theories in this different setting, determine if there are any conditions

in which our current understanding does not hold, and remark upon behavioral experiments that could be implemented to determine the perceptual relevancy of this work.

In the chapter 2 I will examine how the insect olfactory system responds to overlapping stimuli. Specifically, I will address certain paradoxes raised by our current model that inadequately explain situations where two odors are presented in a temporally overlapping fashion without being fully mixed. Several models, including dynamic resetting, have been proposed as solutions to this problem. The experiments that I will describe will sort through these competing theories and propose a new model for the processing of overlapping odors. In doing so I will investigate the role that prior conditions have on the ensemble processing of odors. Little is currently understood about how activated PN ensembles react when presented with a new odor. Applying analysis techniques partially developed in our laboratory, I will examine how PN ensemble representations adjust when odors are rapidly exchanged and investigate the downstream activity of the KCs to see if the activity predicted by the analysis is actually observed in the locust. Finally, this work will make predictions about unique overlapping odor conditions and the possibility that these states may lead to intermediate representations as a consequence of the coding principles used in the system - possibly causing the animal to experience perceptions that are unique from the individual components or their simple mixture. The work presented in this section has been submitted for publication as BM Broome, V Jayaraman, & G Laurent (2005).

In chapter 3 I will investigate how the insect olfactory system reacts to rapidly varying odors, a situation that animals might encounter in nature. I will explore how PNs respond both individually and as groups, applying many of the same experimental techniques described above. I will explain new technologies developed to meet the specific needs of this project. Specifically, I will describe an electronic nose sensor that was adapted for use with electrophysiology to obtain high resolution records of odor stimuli. This sensor was essential for making new insights into the existence of unique classes of PNs and for decoding the odor stimulus from the resulting spike

trains. I will describe the limited effects of history on PN activity in rapidly varying odor conditions and the unique odor specific responses that each cell can produce. Most significantly, I will propose that PN ensemble coding of odors fundamentally changes when odors are presented rapidly. Changes were observed in both the regions of odor space traversed and in the temporal response properties of the ensembles. Finally, detailed explanations will be given of the techniques that I used to reconstruct rapidly varying stimuli when single odors, overlapping odors, or complete mixtures of odors were present. Using these techniques I will explore how the quality of these reconstructions is dependent upon the number of cells used to create them. The work in this section is in preparation for publication as BM Broome, M Meister, & G Laurent (2005).

Chapter 2

Encoding and Decoding of Overlapping Odor Sequences

2.1 Introduction

In nature, animals rarely encounter stimuli in isolation and must often extract meaningful information from complex streams of overlapping signals. With odors this undertaking is further complicated by the inherently chaotic and often unpredictable nature of these signals' delivery (Koehl et al., 2001). Understanding how the brain treats such complex stimuli is further complicated by the observation that olfaction is a synthetic sense (Laing and Francis, 1989). That is, with the exception of specialized signals such as pheromones, allomones, or kairomones (Mustaparta, 1996; Suh et al., 2004; Vickers et al., 1998), odor segmentation appears to be limited in animals; similarly, humans can identify individual components in a mixture, but only if less than 3-4 odors are mixed together (Laing and Francis, 1989). How then, does the brain deal with multiple concurrent stimuli that are not correlated in time? Does it keep track of each one independently? Does it create a representation of the mixture when there is temporal overlap? Or does it behave yet differently?

While the answers to these questions ultimately contain perceptual and behavioral components, we can begin to address them relatively easily using neurophysiological methods. In our case, the interest in such stimuli and their neural representations resides in the fact that they

impose difficult constraints on the system; these constraints should in turn help us better understand the neural codes for odors. Our recent work on insects and fish olfactory systems shows that odors give rise to very different response profiles in two structures, separated by only one synapse (Friedrich and Laurent, 2001; Mazor and Laurent, 2005; Perez-Orive et al., 2002). In the antennal lobe odors are represented by distributed assemblies of promiscuous principal neurons, whose individual activities evolve deterministically over time in a PN- and odor-specific manner (Laurent and Naraghi, 1994; Laurent et al., 1996; Mazor and Laurent, 2005; Wehr and Laurent, 1996). In the mushroom body, the direct target of the antennal lobe, odors are represented by very small assemblies of highly specialized neurons called Kenyon cells, or KCs, that are silent at rest (Laurent and Naraghi, 1994; Perez-Orive et al., 2002). The mechanisms underlying this dramatic transformation of representations is beginning to be understood (Laurent, 1999; Perez-Orive et al., 2004; Perez-Orive et al., 2002): Kenyon cells accomplish a pattern matching between an activity (input) vector—a function of the state of the PN population at a given time— and a connectivity vector—the set of PNs that each KC connects to. With a large number of KCs (50,000 in a locust), a mushroom body can realize many different connection patterns and thus recognize many different PN activity patterns (R Jortner, SS Farivar, and G Laurent, in prep). Because each KC contacts about 50% of the PN population, differences between connectivity vectors can be maximized across the population (R Jortner, SS Farivar, and G Laurent, in prep), generating very different input specificities.

For high specificity to arise, however, this pattern matching between input and connectivity vectors must occur over limited time windows: indeed, if KCs were allowed to summate their input over long periods of time, they would eventually reach spike threshold even when stimulated with suboptimal PN activity vectors. Our present understanding is that the relevant KC integration window corresponds to about one half of one oscillation cycle (about 20ms) (Perez-Orive et al., 2002; Wehr and Laurent, 1996). Thus, each KC is given one chance to fire during each oscillation cycle and repeated chances over successive cycles as long as PN

output is synchronized: because PN activity vectors change from one oscillation cycle to the next (fast first, more slowly later) (Laurent et al., 1996; Mazor and Laurent, 2005; Stopfer and Laurent, 1999; Wehr and Laurent, 1996), each KC carries out a new pattern matching at each oscillation cycle. In other words, each KC action potential at a given time represents a specific instantaneous state of a large percentage of the PN population at that time. If this is true, the response of a KC should be very sensitive to the instantaneous variations of its input vector (instantaneous state of the PN population). Under conditions of overlapping stimuli, for example, one would predict that a KC that responds to odor *A* at time *t* would fail to fire if odor *B* were added to *A* a short time before *t*. Conversely, if a KC were found to respond at time *t* to a particular pattern of *A*-*B* stimulation, we predict that its response probability should drop as the relative timings of the *A* and *B* stimuli are changed. The stimulation paradigms we will explore here are therefore a means to explore the sensitivity of KCs to the instantaneous state of the PN population and to test our understanding of the decoding of PN activity by Kenyon cells.

2.2 Results

2.2.1 PN Responses to Overlapping Odor Patterns

PNs respond to odors (singular or mixtures) by producing both fast and slow temporally patterned responses. For each PN these responses are both highly reproducible and odor specific. We examine here the responses of PNs in conditions of staggered stimulations with two odors. As previously described (Stopfer et al. 2003; Mazor and Laurent, 2005) we performed extra-cellular simultaneous multi-single-unit recordings from groups of PNs (n = 87, avg. group size = 9, see Methods) while presenting 30 different stimulus conditions (10 to 15 trials each) composed of 6 pure odor conditions (citral x 2, geraniol x 2, no odor, paraffin oil) and 24 2-odor-pulse stimuli (Fig. 2.1A) in pseudo-random order. All stimuli were presented or mixed in a dry air carrier

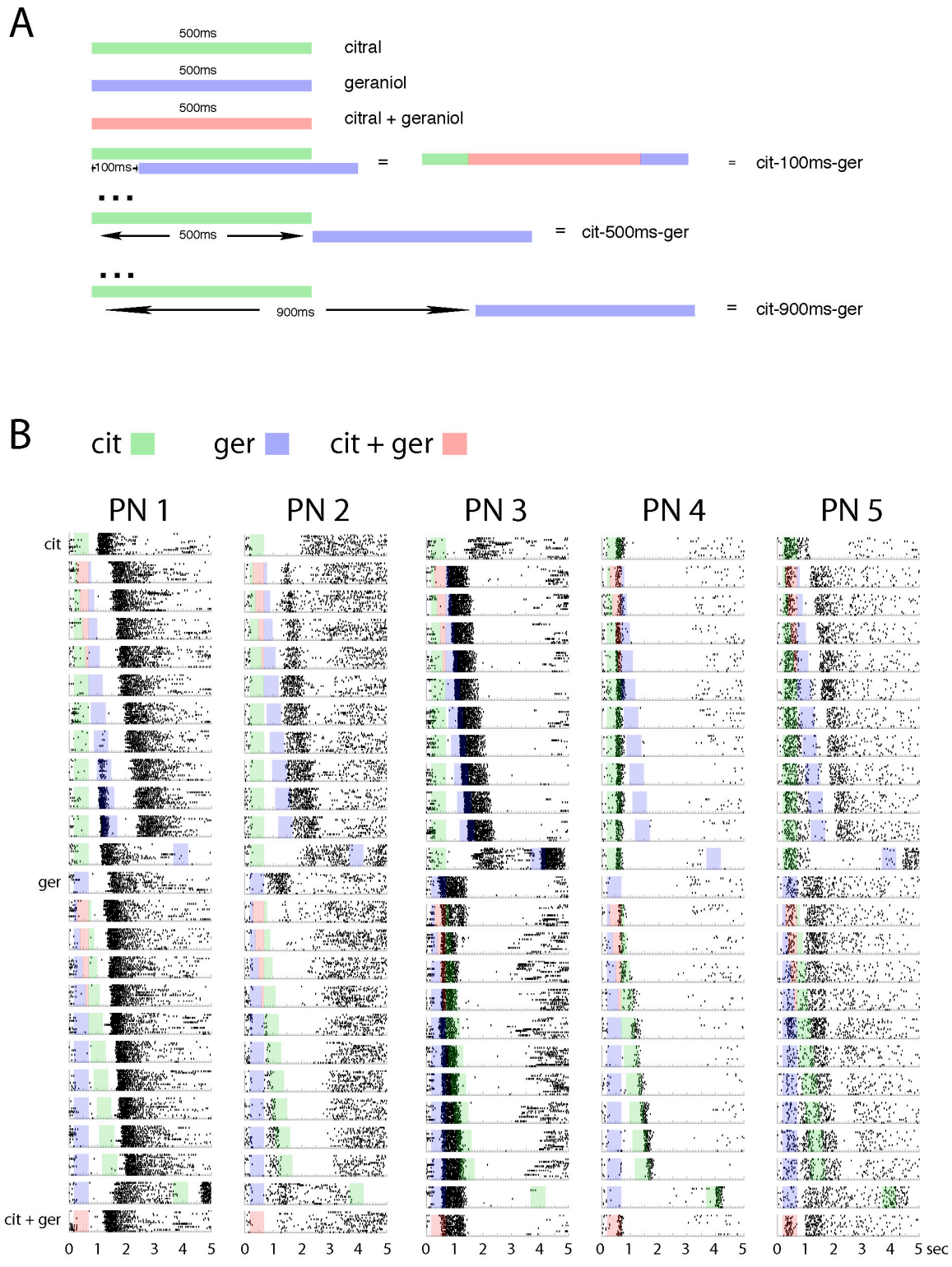

Figure 2.1, Stimulus Description and PN responses to Overlapping Stimuli
A: Description of stimuli. Two odors, citral (cit) and geraniol (ger), were presented either alone or with a staggered onset times. In all cases each individual odor was presented for 500ms. The start times of the two odors were staggered relative to one another using the notation shown. The

separation in odor start times ranged from 0ms (overlapping presentation, cit+ger) to 1s in steps of 100ms. An additional trial at 3.5s staggered onset was also included. **B:** Representative PNs displaying olfactory masking. Raster plots of 5 in vivo tetrode recordings from odor responsive locust PNs. Cells shown were not recorded simultaneously. Shaded areas correspond to pure and mixed odors indicated in legend and described in A. 15 consecutive trials per odor condition. Condition order was randomized within a given experiment.

stream (2 l/min). In all cases the responses of a given PN to an odor were highly reproducible across a block of 15 trials and across the course of an experiment (Fig. 2.1B). In locusts, PNs are the only antennal lobe neurons that produce sodium action potentials (Laurent and Davidowitz, 1994). Thus, all spikes reported here can be unambiguously attributed to PNs. PN responses to the two odors (citral, geraniol) or their mixture (citral + geraniol) contained excitatory and/or inhibitory epochs with odor- and PN- specific onset times and durations.

2.2.2 Single PN Responses to Overlapping Odor Pulses

Given the complex nature of PN responses to odors, we first examined whether the firing profiles of individual PNs to overlapping odor pulses could be predicted from the knowledge of their responses to each odor presented alone. Qualitative examples to each odor are shown for five PNs (Fig. 2.1B). While these five representative examples show different combinations of response types, the main interactions between overlapping pulses can be described as various forms of masking. When excitation by one of the two odors overlapped with inhibition caused by the other odor, excitation was generally reduced and sometimes totally suppressed. Consequently, one would predict that the detection of a component within a mixture from PN patterns alone should be compromised. We estimated the predictability of the interactions between firing rates (for each PN) by comparing observed and calculated firing rate profiles (Fig. 2.2A). These sums were calculated assuming that all cessation of firing, often caused by inhibition (Leitch and Laurent, 1996; MacLeod and Laurent, 1996), should be represented by the negative of the mean baseline-firing rate (see Methods). While this assumption may not be the best one, these

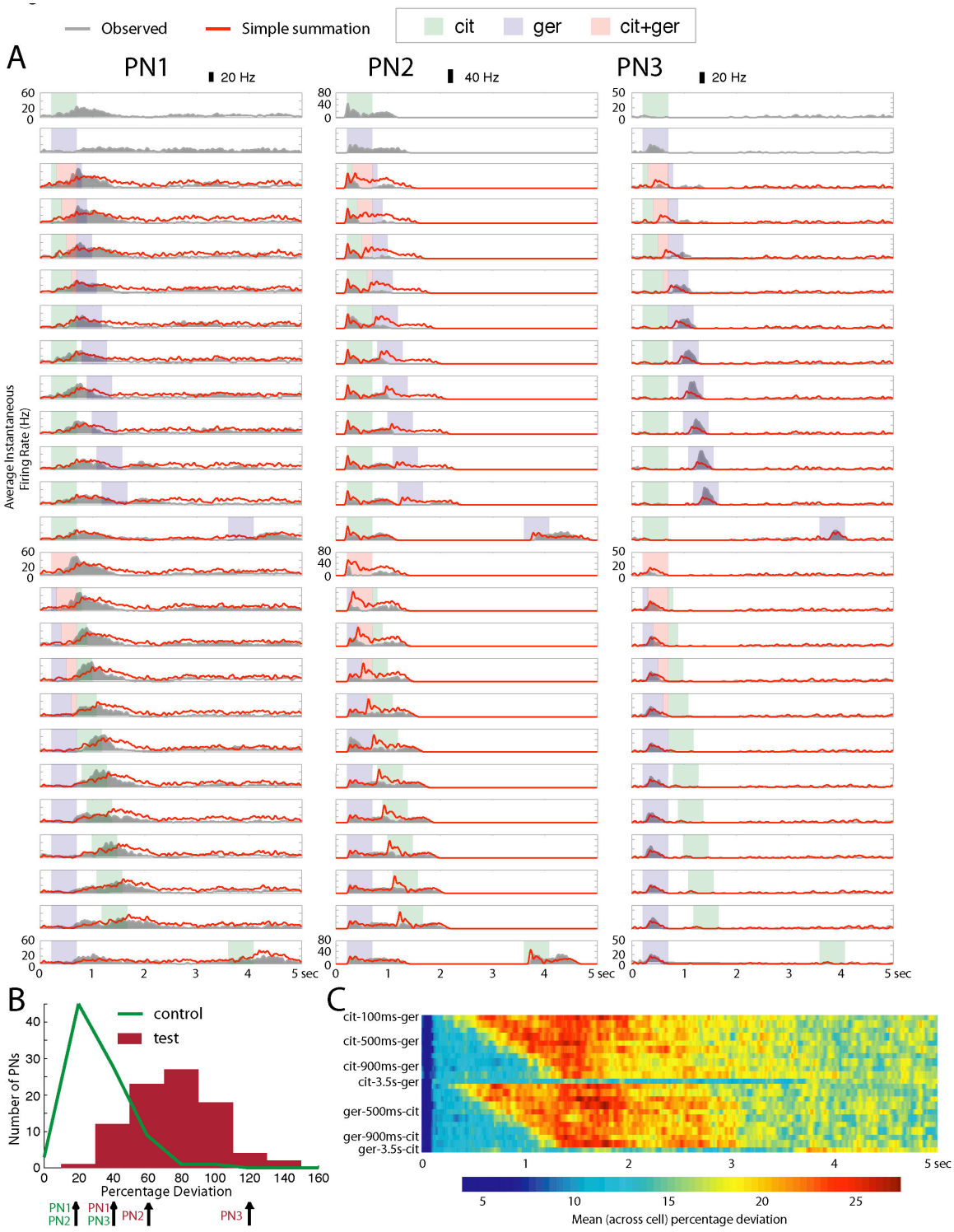

Figure 2.2, Individual PN responses to overlap conditions are not simple summations of their responses to pure odor conditions.

A: Three PNs responding to the various overlap conditions (gray) compared to the simple linear summation of their responses to pure odor conditions (red lines), with responses to the second odor shifted by the appropriate delay. Overlap conditions indicated by blue, green, and pale red bars in the background. Simple summation of pure condition responses matches PN1's actual

response fairly well for all overlap conditions. PN2 responds to most overlap conditions differently than might be expected from simple linear summation of its responses to the pure conditions. PN3 shows unexpectedly strong responses to geraniol when it is presented with a delay after citral. The response to geraniol in these cases is significantly stronger than both the linear summation and the response to either odor singly or the mixture (in the cit-900msec-ger condition, for example, the peak response to geraniol is twice as strong as when geraniol is presented by itself). **B**: The bar plot (test) shows the distribution of percentage deviations of estimated from measured firing rate (see Methods for an explanation of the computation) for all 87 recorded PNs (mean = 75%, SD = 22%). The green curve (control) shows the distribution of percent deviations calculated for all PNs (mean = 31%, SD = 17%) using only times of zero overlap (first 600ms following presentation of the first of two odors in conditions with 100ms or greater delays between pulses). Brown and green labels to the left of the arrows indicate difference ranges for PNs 1, 2, and 3 for overlap and non-overlap times respectively. **C**: Mean (over all PNs) percentage deviations for all overlap conditions plotted for each time bin (see Methods). Times of high deviation from summation-based estimates begin with the presentation of the second odor. Non-zero differences are seen even in the 3.5s delay condition, indicating that some PN responses at least are affected by history going back 3s.

comparisons were informative. They revealed, for example, that the response of a PN could match reasonably well (PN1, Fig. 2.2A), undershoot (PN2, Fig. 2.2A), or exceed (PN3, Fig. 2.2A) the simple sum of the component responses. Many of these more complex interactions could not be explained by an inadequate scoring of inhibition: the excess activity of PN3 (rows 8-12, Fig 2.2A) or the under-activity of PN2, (rows 3-8, Fig. 2.2A) for example, must be explained by other types of interactions, possibly involving receptor responses to mixtures, local circuit interactions within the antennal lobes, or likely, both. We then estimated the extent of these nonlinear interactions over all the recorded PNs. The distribution of differences between estimated (simple summation) and measured firing rate profiles during odor overlap conditions varied between 20 and 150%, with a mean of ~75% (Fig. 2.2B; also see Methods). PN1, PN2, and PN3 were -1.7, -0.9 and 1.55 SDs from the mean, respectively (brown labels next to arrows, Fig. 2.2B). As a control, we measured the distribution of differences measured between different trials of the same condition (green curve, Fig. 2.2B): for this we used the first 600ms of all odor overlap conditions with inter-pulse delays >100ms (i.e., cit-600ms-ger/ger-600ms-cit through cit-3.5s-ger/ger-3.5s-cit). For 75 out of the 87 PNs, deviations were significantly higher during overlap conditions than in controls (Wilcoxon rank sum test, $p<0.0001$; see Methods and Fig.

2.2B). Large deviations between estimated (sums) and measured rates occurred at most times during and for some time after the presentation of the second odor (Fig. 2.2C) and could, in some PNs, be observed as late as 3s after the second pulse (yellow and orange pixels at ~4s in cit-3.5s-ger and ger-3.5s-cit rows in Fig. 2.2C).

2.2.3 PN Population Responses to Overlapping Odor Pulses

PNs were recorded from physically distributed areas across the AL in 10 animals. The number of simultaneously sampled PNs varied between 5 and 25. A recording site was chosen if at least some multi-unit activity could be recorded in response to each of the two odors and to a static mixture of the two odors at the beginning of each experiment. Only PNs that exceeded a set of equally applied inclusion criteria (see Methods) were selected (n = 87 PNs). In aggregate, this group represents more than 10% of the PN population in the antennal lobe. The spiking responses of each PN were analyzed in 50ms bins locked to the trial start time. 50ms bins corresponding to the mean duration of individual LFP oscillation cycles were chosen because they include the effective integration period of the PNs' main target, the mushroom body Kenyon cells (Perez-Orive et al., 2002).

Recent experiments indicate that Kenyon cells each connect, on average, to 50 ±13% of the PN population and that their firing threshold corresponds to 100-200 coincident PN spikes (R Jortner, SS Farivar, and G Laurent, in prep). We also know that odor–evoked PN activity is composed of successive PN spike volleys (Laurent and Davidowitz, 1994), where each oscillation cycle contains the spikes of 80-240 PNs on average (Mazor and Laurent, 2005). We analyzed the representations of the odors and stimulus conditions as time series of PN population vectors (87 PNs, 50ms resolution, 30s trials, 15 trials per condition), as successfully applied previously to the encoding and decoding of odor concentrations (Stopfer et al., 2003).

Figure 2.3 provides a pictorial representation of this population activity using locally-linear embedding (Roweis and Saul, 2000), a nonlinear dimensionality reduction technique useful for uncovering structure in high-dimensional space (Stopfer et al., 2003). These plots should be

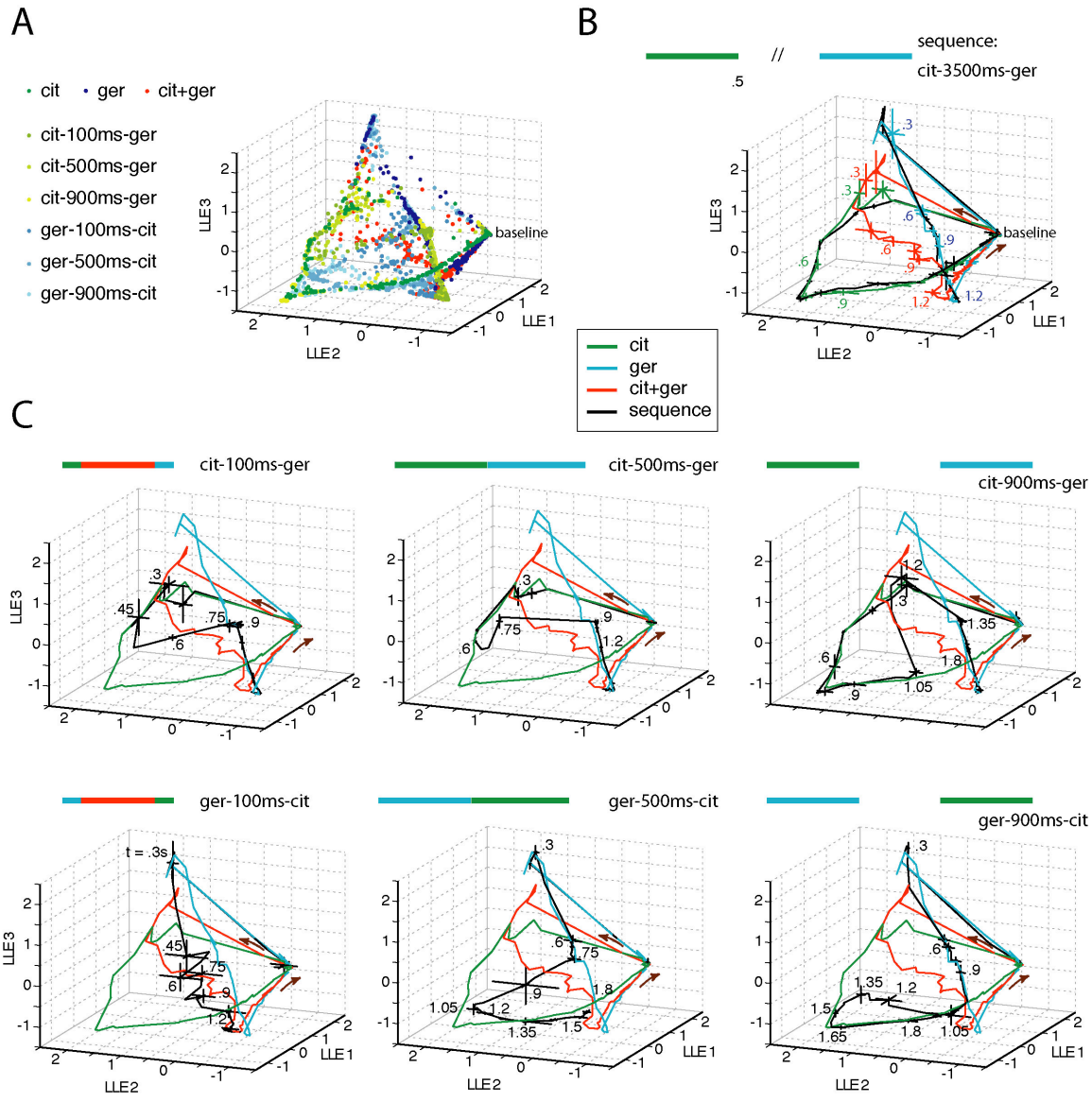

Figure 2.3, PN ensemble responses track odor sequences.
A: Time-slice points calculated from 87-PN responses to overlap sequences reduced to three dimensions using locally linear embedding. A subset of the original 5850 points embedded – only those for sequences shown in Fig. 2.3A,C – are shown here. Time slice points (50ms bins averaged over 3 trials) for the overlap sequences were taken beginning 0.5s before stimulus onset and ending 1 second after the end of the second stimulus. Correlations between 87-PN time slice vectors for these conditions are shown in Figures 2.4 and 2.5. **B**: Time-slice points in Fig. 2.3A

were connected in sequence to visualize trajectories. Initially in a resting state (labeled "baseline"), the system responds with stimulus-specific trajectories. Shown as a control with trajectories for all pure conditions is the ensemble response to citral and geraniol presented with a gap of 3s between them – the trajectory for this sequence first follows the response to pure citral and then the response to pure geraniol. Five-trial averages for each condition; lines at vertices indicate S.D.; arrows indicate direction of motion. Time relative to odor onset indicated every 300ms. Color bars above plots in Fig. 2.3B,C indicate sequence presented. **C**: Trajectories in black show responses to 6 different overlap sequences with increasing delays in the presentation of the second odor (first row, citral followed by geraniol; second row, geraniol followed by citral). When switching from the first odor to the next, the system does not reset (return to baseline) and instead jumps to a later part of the second odor's response. Ensemble responses to the second odor can be very different based on the duration of overlap (compare ger-100ms-cit sequence with ger-500ms- and ger-900ms-cit sequences).

read as qualitative indices of PN population state; quantitative analysis, carried out in the original high dimensional space, will be shown later. Figure 2.3A represents all the points (each point represents the state of the 87 PNs during one 50ms bin averaged over 3 trials) corresponding to six stimulus conditions in the space defined by the first three LLE dimensions. Baseline represents the state of the population prior to each stimulus (30s inter-trial interval). The points corresponding to successive time bins in the same trials were then joined together to generate stimulus specific trajectories (Fig. 2.3B&C). Figure 2.3B overlays the trajectories corresponding to four simple stimulus conditions: citral alone (green); geraniol alone (cyan); citral mixed with geraniol (red); citral followed 3.5s later by geraniol (black). We can see that the two odor pulses separated by 3.5s generated PN trajectories nearly identical to those generated by the same odors presented separately (i.e., with 30s interval or more). By contrast, the two odors presented simultaneously generated a hybrid response trajectory (red, Fig. 2.3B) that overlapped little with those of either odor alone, except well after termination of the stimulus pulse (at 0.5s). We will now examine several partial overlap conditions (Fig. 2.3C). In each case, the sequence trajectory is shown in black, overlaid on the three single trajectories shown in Fig 2.3B (green, cyan and red). In the top row citral was presented first; in the bottom row, the order was reversed.

First we observed that the masking present in some single-PN responses is visible in these PN trajectories. In the ger-*x* ms-cit cases (bottom row, Fig. 2.3C), the trajectories process

farther into the citral trajectory as the delay between pulses (*x*) increases from 100 to 900ms. This observation corresponds well with the increasing duration of some single-PN responses (PN1, Fig. 2.1B) under similarly varying conditions. Second, we noticed that the state of the PN

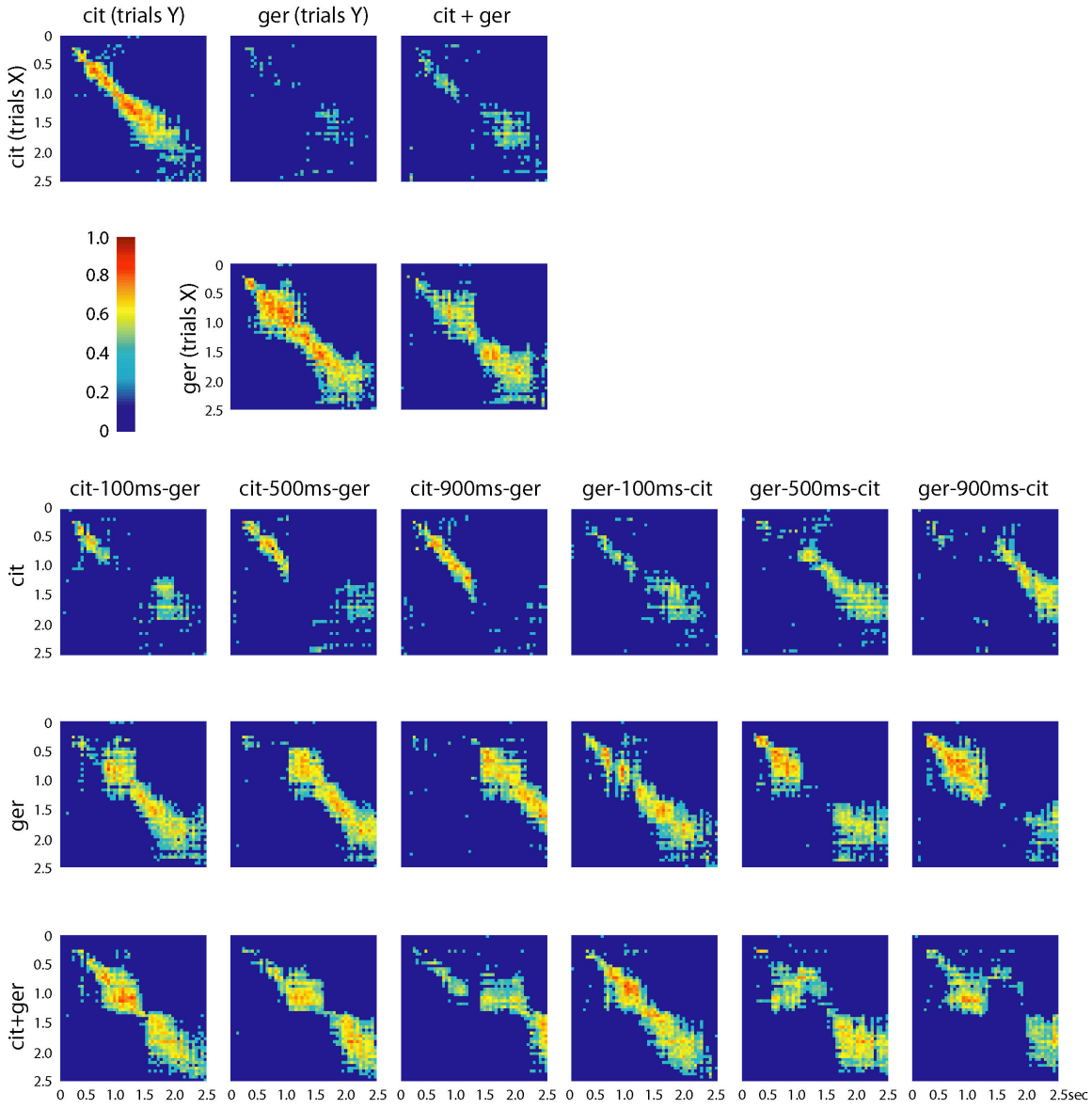

Figure 2.4 Correlation matrices for 87-PN time-slice vectors
In the top two rows time slices from PN responses to the pure conditions are correlated with each other and with those of the odor mixture. The mixture response is different from both pure odor responses early and similar to the ger response late. In the lower three rows time slices from PN

responses to these conditions are correlated with some of the conditions shown in Fig. 2.3B,C and Fig. 2.6. In correspondence with what is seen in the LLE plots (Fig. 2.3C), responses for the overlap conditions are first strongly correlated to the first odor presented and then switch, with a lag, to being correlated to the second or the mixture. Each pixel, $C_{r,c}$, represents the correlation of one 3-trial-averaged 87-PN time slice vector, r, with another, c, from either the same condition (but different 3-trial-averaged set) or a different condition, as indicated. Thus, a pixel $C_{t1,t2}$ represents the correlation of the time slice of trajectory A at time t_1 to the time slice of trajectory B at time t_2. All correlations shown are significant ($p<0.001$).

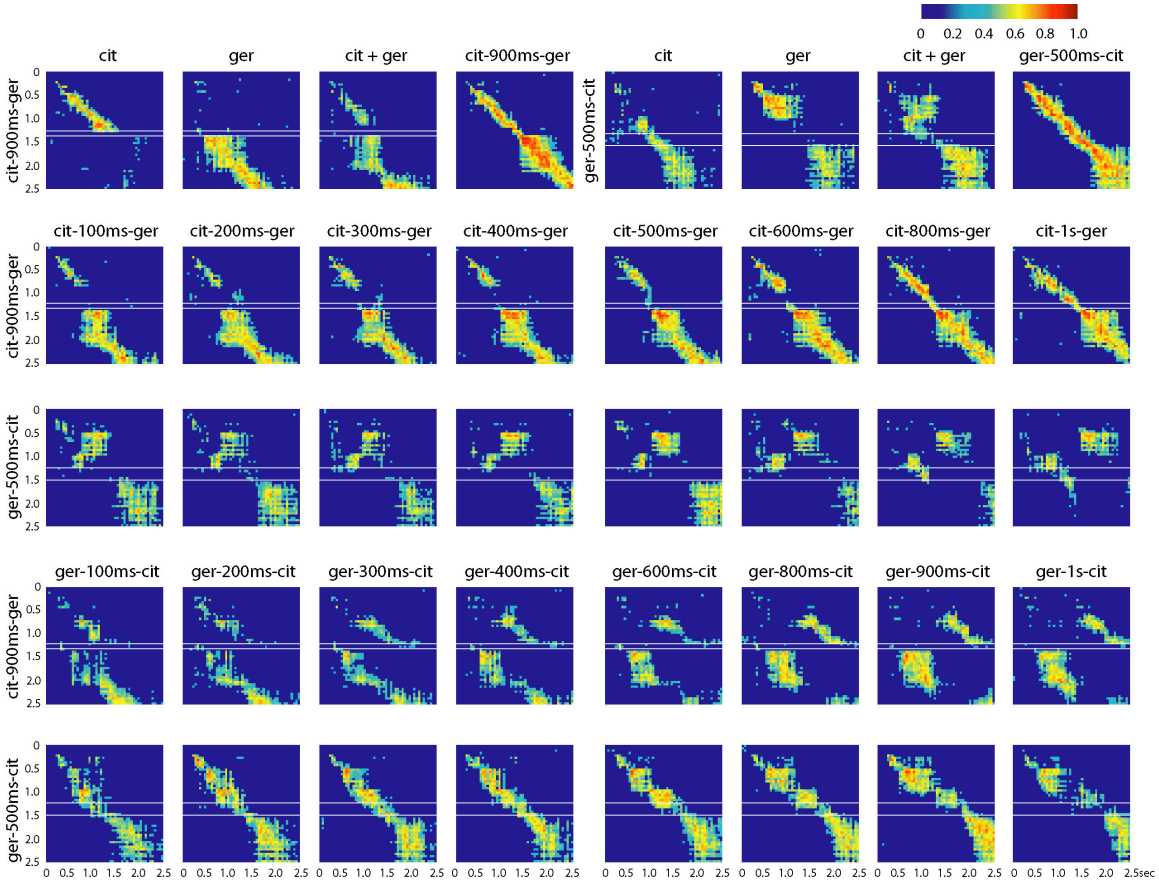

Figure 2.5 Correlation matrices for 87-PN time-slice vectors
Correlations between time slices for different overlap responses. White rectangles highlight regions (times) where overlap responses show decreased or zero correlation with time slices from the pure conditions and with the mixture. These times and conditions match those revealed by MDA as being distant from both pure conditions and the mixture and for which unique KC responses were found. Note that the across-condition correlation levels at these times are not always zero; in some cases (see especially the last row for ger-500ms-cit) they are merely lower than at other times. Whether or not they are significant for the KCs (and ultimately for the animal) depends on the KCs' sensitivities.

populations during an overlap condition depends on past history. For example, the cit-100ms-ger and ger-100ms-cit conditions produced 400ms of identical stimulus conditions (Fig 2.3C, left

panels), yet the corresponding PN trajectories differed from each other and from that generated by the mixture (red, Fig. 2.3C). Third, for inter-pulse intervals of up to one second, the response of the PNs to the second pulse did not, even for an instant, pass through the baseline state. The trajectory corresponding to a sequence started as that for the first odor before moving towards the second. The sequence trajectory rejoined the second odor in segments corresponding to late phases of the second odor trajectory as if the second odor had been presented alone. This result suggests that, at least for epochs corresponding to the slow return to baseline after odor offset, the same PN population states can be reached through different paths or past histories. The cit-500ms-ger trajectories (top row, middle graph, Fig. 2.3C) provide another illustration of this general observation, as the black and blue trajectories rejoin at $t \approx 0.9$s. These results were not visible from inspection of single-PN activity profiles.

This population vector analysis proved useful as a potential predictor of Kenyon cell responses. If our present understanding of PN activity decoding by Kenyon cells is correct (Mazor and Laurent, 2005; Perez-Orive et al., 2002; Stopfer et al., 2003), the orbits traced by the PN populations should define a variety of KC response conditions. For example, if the PN trajectories corresponding to an odor sequence move far away from the trajectories corresponding to either odor alone or to their mixture, we predict that some Kenyon cells should respond only to such sequence conditions and at particular times correspond to the structure of these trajectories. This hypothesis will be tested below. To identify these conditions, however, we needed to quantify the qualitative impression generated by the LLE projections in Fig. 2.3. Thus, we examined the PN population in the original 87-D space (using the same time bins and durations), one trial at a time, using multiple-discriminant-analysis (Fig. 2.6), a technique similar to multivariate analysis of variance (Duda et al., 2000). Our goal was to classify all the trajectories corresponding to overlapping stimuli on the basis of their similarity to single stimulus trajectories (citral alone, geraniol alone, citral + geraniol). This classification was done piecewise (time bin

by time bin), against sixteen templates taken from the single-stimulus conditions (baseline + 3 odors x 5 time bins; Fig 2.6A, see Methods). 87-PN vectors from these sixteen

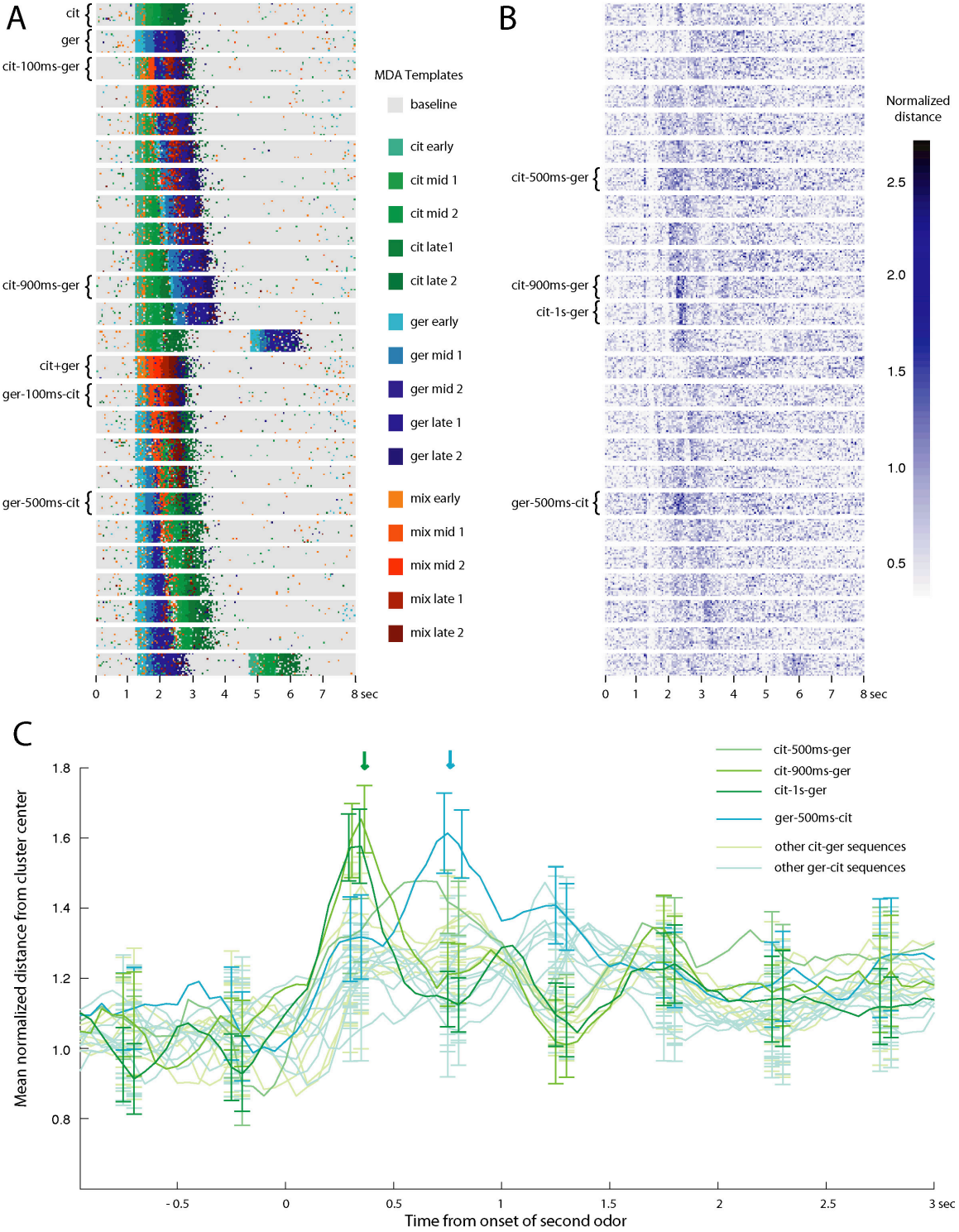

Figure 2.6, MDA and Euclidean-distance-based classification of single trial ensemble time slices from all conditions into clusters of time slices taken from responses to pure conditions (cit, ger, cit+ger).
A: Sixteen groups of time slices representing baseline and five different phases of ensemble responses to pure conditions were chosen as templates based on correlation widths over the course of the responses (see Figure 2.4 and Methods). These 87-dimensional time slices were used for MDA, and the 15 discriminant functions calculated (all significant; MANOVA: Wilk's Lambda = 0.0063; $F = 1.6124*10^3$) were then used on all time slices. The reduced-dimensional time slices for all sequences were then classified as belonging to one of the clusters defined by the pure condition templates (colors representing the clusters shown at right) using Euclidean distance from cluster centers. **B**: Distance from cluster centers for all time slice points normalized by intra-cluster distances for template time slices. Bands of time slices that are far away from their centers (darker blue) are prominently clustered together during times of overlap (see, for example, the 4 labeled overlap sequences). **C**: Running 5-time-point averages of mean distances for all overlap conditions (vertical lines at selected vertices indicate S.D.) aligned to the arrival of the second odor. Conditions that feature time slice points farthest from the centers of clusters they were classified as belonging to are colored darker (for example, curves representing ger-500ms-cit, cit-900ms-ger, cit-1s-ger; indicated by arrows to show times in question).

conditions were used to calculate discriminant functions that were subsequently applied to all other PN vectors. For any test trial each PN vector measured at time *t* was transformed and then classified on the basis of its similarity to the sixteen templates. Figure 2.6A plots the results of this classification. We note that using such measures very good reconstructions of stimulus histories can be made purely on the basis of the PN population activity. For example, for cit-100ms-ger (third row, Fig 2.6A) the initial PN vectors were classified as cit-early and cit-mid, the later ones as mix-early, ger-mid, mix-late again, and finally as ger-late (dark blue). This approach creates linear decoders that maximally separate each of the training template groups and then applies the decoders to all other PN vectors. By design, the transformed test vectors are classified as "most similar" to one of the templates, although similarly classified vectors may be at a range of distances from their templates. To quantify this we measured the Euclidean distances between each test vector and the template vector to which it was closest (Fig 2.6B). Those distances have been normalized by the mean intra-cluster distance of the closest training template. We note that across all conditions some time bins correspond to vectors that, although often correctly classified, were nevertheless quite different from their template: the darkest pixels represent vectors that are more than twice the average intra-cluster distance from their closest templates.

These epochs (dark bands, Fig 2.6B) occur when the test trajectories (overlapping conditions) diverged the furthest from the templates. The twenty-five conditions in Fig. 2.6B have been collapsed and averaged over all trials/conditions in Fig. 2.6C. This identifies two time periods (arrows, Fig. 2.6C) and three stimulus conditions when deviations were the greatest. These times and conditions identify the PN vectors whose composition was the most different from those generated by the single stimulus conditions and, given the degree of PN synchrony at these times and conditions (Fig. 2.7), those for which one might expect to find specific Kenyon cell responses. This hypothesis was tested next.

2.2.4 Decoding of PN Trajectories by Kenyon Cells

Kenyon cells (there are 50,000 KCs in each mushroom body in the locust) are the main decoders of PN output. PNs are their sole source of olfactory input and receive no feedback from Kenyon cells. Our current understanding of Kenyon cell physiology is that they act as pattern classifiers on PN population activity (Laurent, 2002; Perez-Orive et al., 2002). Each KC receives input from approximately 50% of the PN population and fires an action potential when a sufficiently large number of pre-synaptic PNs are co-activated during the same half of one oscillation cycle. We estimate that the KC spike threshold corresponds to between 100 and 200 PN inputs (R Jortner, SS Farivar, and G Laurent, in prep). This number matches well the measured average number of co-active PNs per oscillation cycle (Mazor and Laurent, 2005). Because this pattern matching occurs once per oscillation cycle, individual KCs get repeated opportunities to “recognize” a pattern as antennal lobe activity evolves along its odor-specific PN trajectory. Consistent with this, KC responses are also time-specific (Perez-Orive et al., 2004; Stopfer et al., 2003).

Our results on PN population behavior during overlapping odor stimuli (above) lead to specific predictions about KC responses. If each KC acts as a piecewise PN pattern classifier (once per oscillation cycle as PN activity proceeds along its trajectory), deviations of a PN

trajectory from a path that normally generates a response in a KC should suppress that response (masking). Conversely, deviations of a trajectory to new regions of PN phase space should generate new responses in some specific KCs.

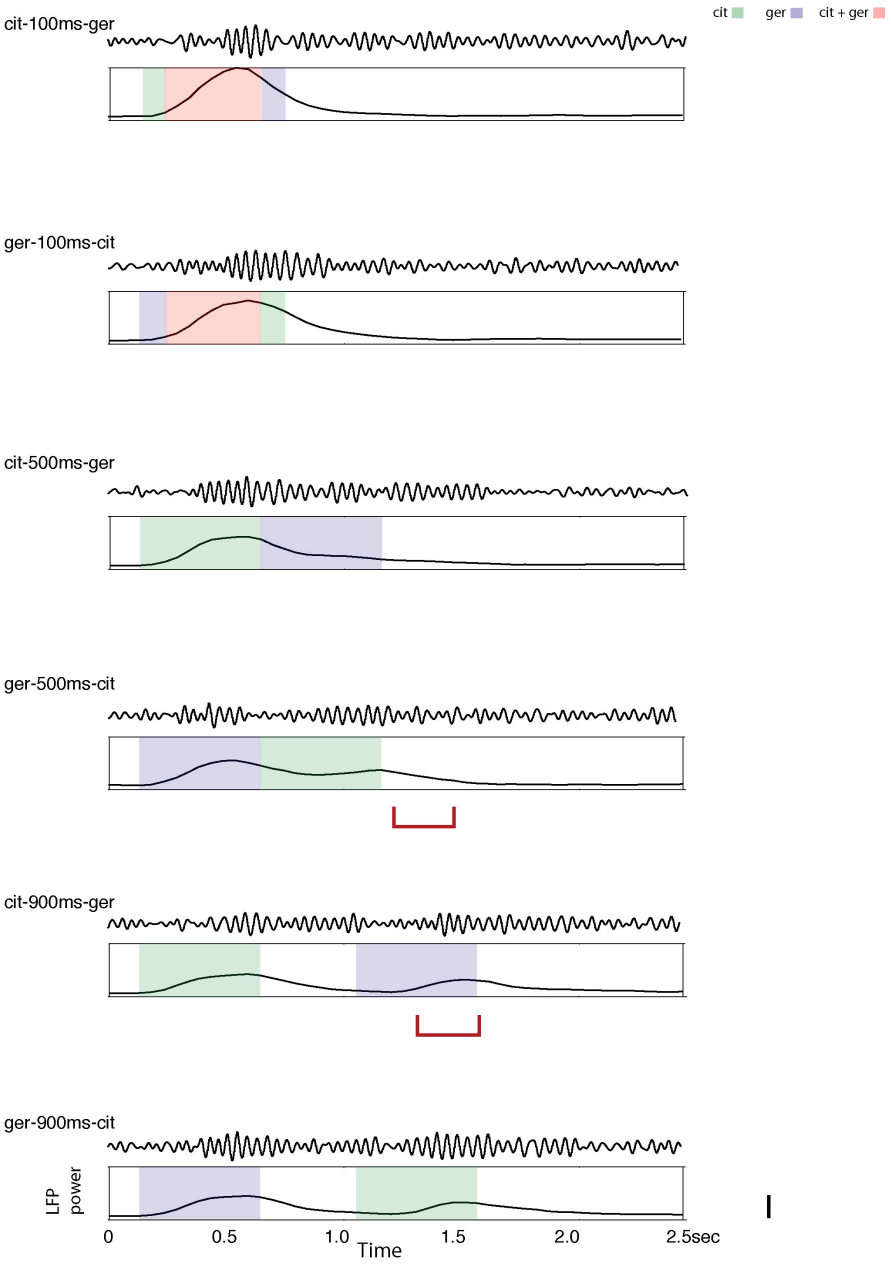

Figure 2.7, PN synchrony during overlapping odor pulses, as measured by local field potential power in the 5-55 Hz band

Shown for six overlap conditions are sample LFP traces recorded over the course of one experiment and mean power in the LFP (see Methods for details on computation). Shaded areas

correspond to pure and mixed odors indicated in legend and described in Fig. 2.1A. Red lines span times and conditions when PN ensemble trajectories are furthest away from trajectories of the pure conditions. The significant power in the LFP at these times indicates that PNs are synchronized at these times and should thus generate KC responses.

We examined the responses of 203 KCs, recorded over 24 experiments (see Methods), using odors, delivery apparatus, and pulse protocols identical to those used with PNs. While most PNs exhibit a substantial change in firing rate when challenged with an odor, KCs do not. To qualify as "responding," a KC had to pass the following criteria: respond with a minimum of one spike during the odor presentation or within 500ms after the odor presentation in at least 5/10 trials, excluding the first trial (Stopfer and Laurent, 1999). KCs whose basal firing rate did not remain constant throughout the duration of the experiment were excluded. These criteria are identical to ones used previously to classify KC responses to odors (Perez-Orive et al., 2002). Several response windows were examined, all yielding similar results. (Note: KCs 1-5 in Fig. 2.8 were classified as responding. KC6, typical of the great majority, was classified as not responding.)

From the 203 KCs recorded, we found 10 that responded uniquely to geraniol, 3 that responded uniquely to citral, and 6 that responded with equal strength to both odors, including some that responded to the static binary mixture of the two odors. (Note: KC recording sites were selected on the basis of there being detectable activity upon presentation of these odors. Therefore, these response probabilities are biased towards high values, by experimental design.) All of the remaining KCs either did not respond to any odor condition (n = 83) or did not respond in a consistent way to either a pure odor or a specific odor pattern. (For KC group selection criteria see Methods.) KCs that responded specifically to one odor frequently showed masking when the second odor pulse overlapped with the first. This is shown for two KCs (KC1 and KC2) in Figure 2.8A: both were activated by geraniol alone (representing 5% of selected Kenyon cells), but this response was suppressed if citral presentations overlapped with or preceded geraniol. The PN trajectory corresponding to one masking condition (cit-100ms-ger) is shown in Fig. 2.8B,

together with the spread of KC2 spike times for the pure geraniol condition overlaid (purple segment and *). KC2 does not respond when the cit-100ms-ger trajectory does not traverse the early part of the pure geraniol trajectory – the region to which KC2 appears to be tuned – due to the preceding and partially overlapping presence of citral. In the ger-100ms-cit condition, the duration of KC2's response is reduced when the corresponding PN trajectory deviates away from the geraniol trajectory due to the addition of citral. Masking was observed independently of odor pulse order (see cit-100ms-ger condition) for the odors tested, but one pulse order could have more pronounced effects than the other. KC3 (representing 1.5% of recorded KCs) showed a similar suppression (though less pronounced) of its response to citral by the addition of geraniol. KC4 (representing 5% of KCs) was the counterpart of the preceding three. This KC responded best to the static mixture conditions and responded less and less as the overlap between the two odors was reduced. Once again this result is consistent with the hypothesis that each KC listens to "preferred regions" of PN phase space and that their response probability depends sensitively on whether the trajectory defined by the PN population traverses that region during an odor stimulus. KC5 (representing 4% of KCs) belongs to the most interesting category of KCs encountered in these experiments. KC5 remained silent over most stimulation conditions, except when a citral pulse followed a geraniol pulse onset with some non-zero delay. The most reliable responses occurred for the ger-500ms-cit condition (Fig. 2.8A). The spread of spike times for KC5 is shown overlaid on the ger-500ms-cit PN trajectory in Fig. 2.8C (purple segment and *). We then noted that the time of KC5's response during this stimulus corresponded to the time at which the PN population trajectory was maximally different from the template trajectories (pure cit, pure ger, or static cit+ger mixture, Figs. 2.6A,B,C). Thus, this KC appeared to recognize this particular state of the PN population activity, supporting the hypothesis that KCs act as classifiers of PN activity vectors over a large fraction of the PN population. Over all 203 KCs analyzed, we found only 8 KCs with such specific responses, each corresponding to a particular region of PN phase space

visited only during these specific stimulation conditions. Note that such KCs were not looked for at the time of the experiment. In addition, all were subsequently confirmed to remain stable

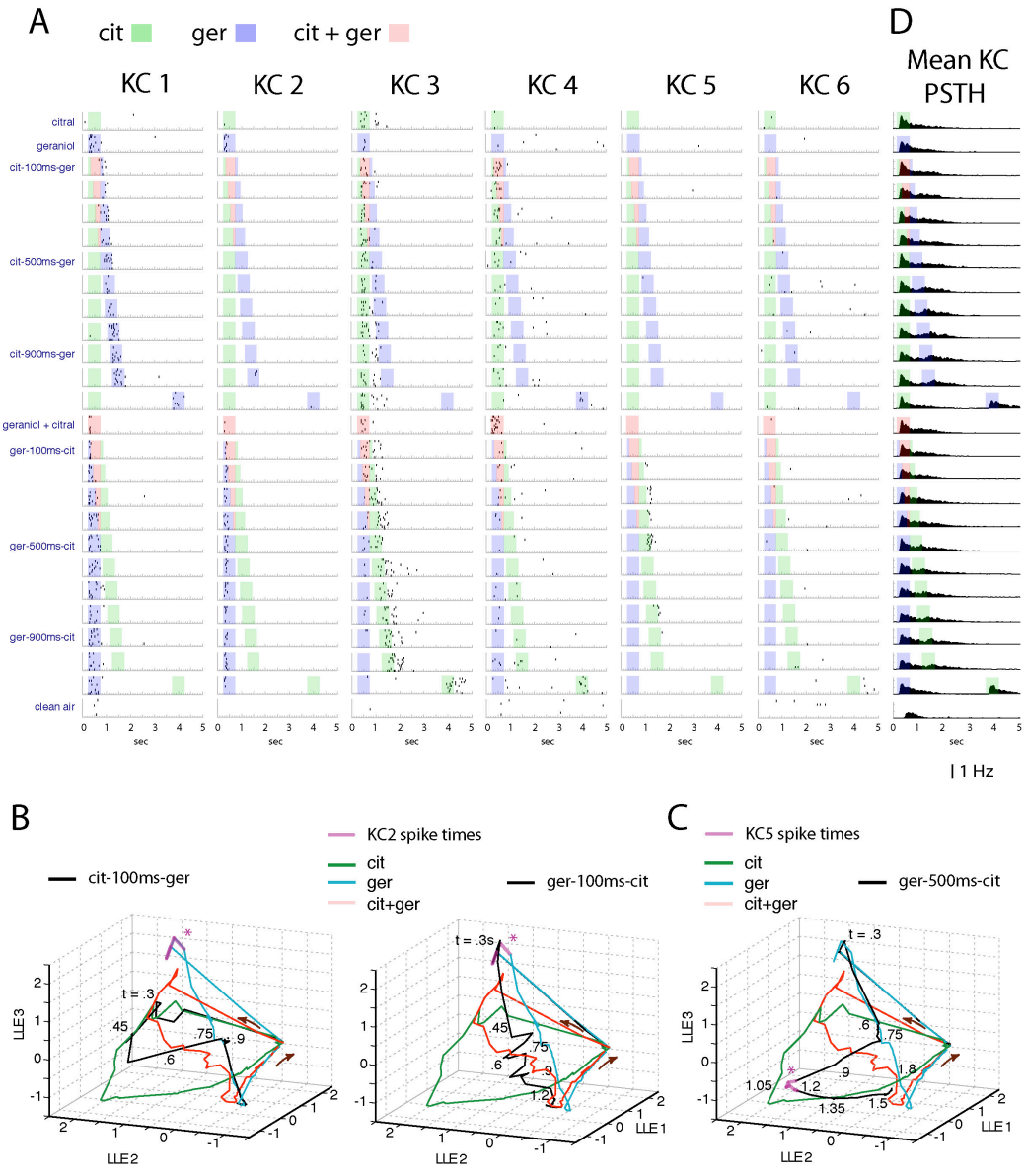

Figure 2.8, KC responses to overlapping stimuli
A: Representative KCs displaying odor and condition specific responses (see text for details of distribution of responses). Raster plots of 6 *in vivo* tetrode recordings from odor responsive KCs. Cells shown were not recorded simultaneously. Shaded areas correspond to pure and mixed odors indicated in legend and described in Fig. 2.1A. 10 consecutive trials per odor condition. Condition order was randomized within a given experiment. **B**: Spread of KC2 spike times in response to geraniol shown overlaid (in transparent orange; see legend) on PN ensemble responses as represented by LLE (from Fig. 2.3C). PN ensemble responses are shown for the pure

conditions as well as two overlap conditions: cit-100ms-ger, for which KC2's response is masked, and ger-100ms-cit, for which KC2 does respond, but with a more restricted spread of spike times than for the pure ger case (see Fig. 2.8A). **C**: Spread of KC5 spike times in response to the ger-500ms-cit condition shown overlaid on PN ensemble responses to pure conditions and the ger-500ms-cit overlap condition. KC5 responds preferentially during a particular period of the overlap condition when the PN ensemble trajectories are distant from those of the pure conditions (shown quantitatively in Fig. 2.6B,C). **D**: Mean PSTH for all 203 KCs that satisfied inclusion criteria. Plot shows strong initial response in all odor conditions with a second response that is initially masked, but increases in strength as the overlap decreases

throughout the course of the experiment (Fig. 2.9). Recording sites were chosen simply on the basis of there being some tetrode activity in response to cit, ger, or cit+ger. This explains the numerical bias toward KCs that responded to these particular odor conditions. KCs such as KC5 were discovered upon analyzing the data, and their paucity confirms the finding that odor representation by KCs is very sparse (Perez-Orive et al., 2004). KC6 was typical of the largest fraction of recorded KCs (41%) and did not respond to any of the stimulus conditions we offered during these experiments. Other examples of KC responses are described in supplementary information (Table 2.1).

Response Type	% Recorded KCs
Cit	2.0
Ger	5.0
Mix	4.5
Cit+Ger	4.5
Cit+Mix	3.5
Ger+Mix	7.0
Pattern-specific	3.5
All Stimuli	21.5
Paraffin oil/Clean air	4.5
Respond with Inhibition	2.5
No Response	41.5

Table 2.1, Classes of Recorded KCs
Each of the 207 recorded KCs was assigned to one of eleven classes based on the assignment criteria described in Methods.

Average KC responses are shown in the mean KC PSTH in Figure 2.8D. Most KCs fired in the early part of the response period, as reported previously (Stopfer et al., 2003). For overlap

conditions, PN ensemble trajectories did not pass through the early period of the pure responses of the odor that was presented second. As a result, we predicted that KCs with early responses to either odor presented alone – the majority of KC – would have reduced response rates when that odor was preceded by another. Consistent with this, we did not see peaks in the KC PSTHs for the second odor in any overlap conditions; these peaks only became apparent when the second odor was delivered with a >600ms delay (i.e., with a > 100ms gap between the odor presentations). Even with a large time lag between the odors, the masking effect of the first odor on the response second was obvious in the reduced height of the second peak. We found that of the 7% of KCs with pure-odor-specific responses, 43% did not fire when their odor came second. Also, for the 4.5% of KCs with responses to both odors (cit+ger), 22% did not fire during the second odor presentation. This is qualitatively similar to what Brown et al. observed in their experiments with repeated pulses of the same odor (Brown et al., 2005). An additional factor in the reduced number of KC responses during overlaps might be the bias inherent in our experimental design: we actively seek KCs with responses to the pure conditions and the mixture, but do not use the overlap conditions when searching for KCs. Therefore, we might have missed KCs – such as KC5 (Figure 2.8A) – that are recruited specifically during particular overlap conditions.

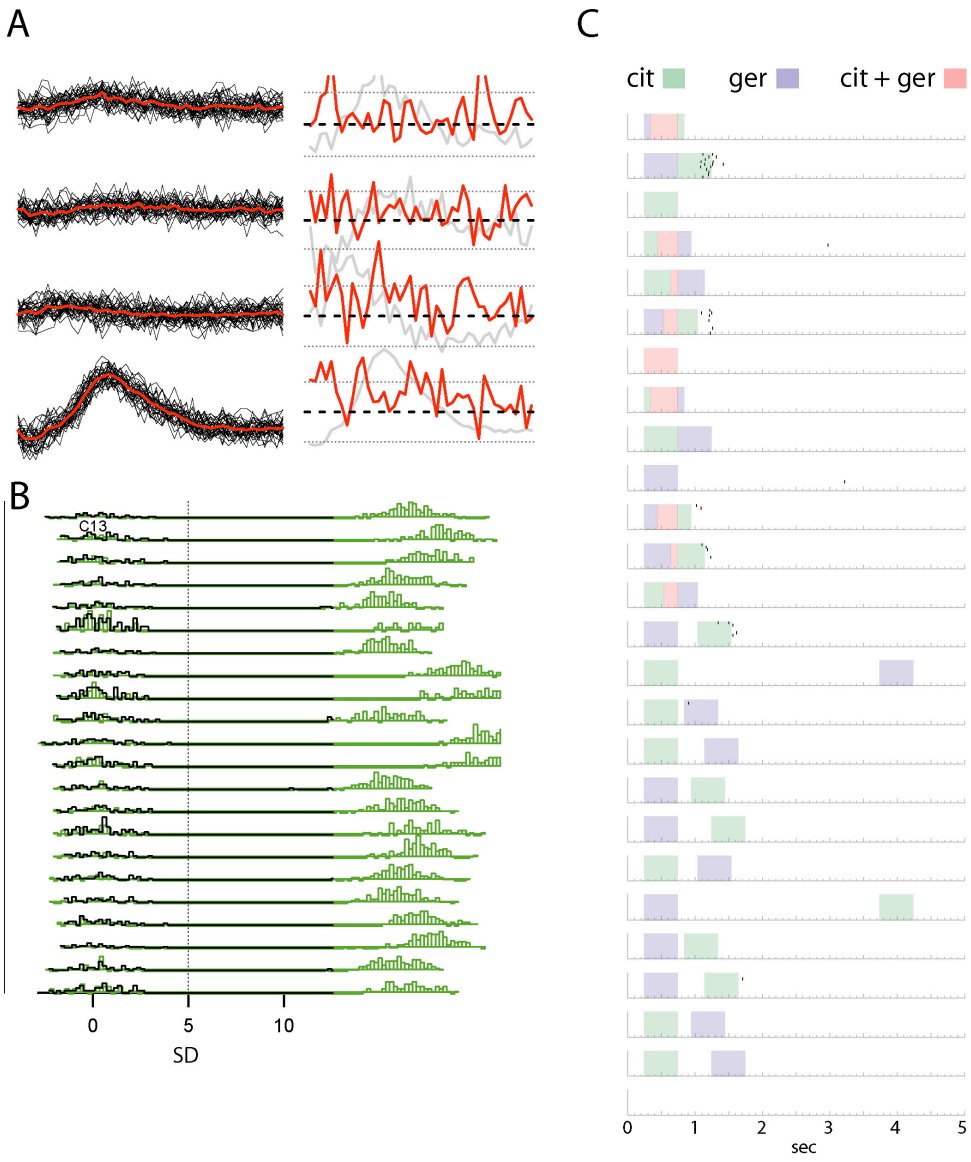

Figure 2.9, KC5 spike sorting
A. Example of cluster separation. On the left all of the events (black) that were classified as belonging to KC5 in Fig. 2.8 are shown superimposed with the other events recorded on the same channel of the four channel tetrode. Average waveform is in red. On the right is shown the variance around the mean for the each of the four channels (red) with the 95% confidence interval shown for each (dotted lines). The average event waveform is shown again in gray (scaled). **B**. The projection test for KC5 where each pair of clusters computed for this model in 180-D space is projected onto the line that connects the center of those two clusters. This plot shows the large distance (>10SD) between the cluster attributed to KC5 and all other cells. **C**. Raster plots for KC5 shown in the order that they were recorded. Shaded areas correspond to pure and mixed odors indicated in legend and described in Fig. 2.1A.

2.3 Discussion

Our odor stimuli included two single odors, one odor-mixture, pulse-overlap and consecutive-pulse conditions: odor-mixture describes a condition in which both odors were pulsed together from stimulus beginning to end. In all cases, single pulses were 500ms long. Pulse-overlap describes conditions in which one odor pulse was started before the other odor pulse had ended; during some time, therefore, both odors were present together. We also used consecutive-pulse conditions with intervals up to 3.5s. The rationale for these consecutive pulses is that PN population activity generally outlasts the stimulus that caused it (Laurent et al., 1996); with inter-pulse delays of up to 3s, overlaps between the responses of the PN population could indeed be seen, even though the stimulus pulses themselves did not overlap. With inter-pulse intervals greater than 3.5s, the effects of the two consecutive pulses on PN responses were nearly independent. In other words, consecutive-pulse conditions with intervals between 0 and 3s generated what we will call overlapping responses.

We recorded the responses of eighty-seven PNs (recorded in groups of 8 to 25) to twenty-four odor stimulus conditions (single, mixed, overlapping, and consecutive). We examined the responses of the PNs to these stimuli one PN at a time and analyzed the 87-PN response dataset as time-series of instantaneous vectors of activity across all 87 PNs, as previously described for simpler stimulus conditions (Mazor and Laurent, 2005; Stopfer et al., 2003). This group of 87 PNs represents over 10% of the entire PN population in the locust. PN sampling was broad in that our tetrodes covered, over all experiments, most regions of the antennal lobe. Our results add to previous results on identity and concentration coding (Stopfer et al., 2003) and single odor pulses (Brown et al., 2005), that spatio-temporal patterns of PN activity also depend, in ways that we did not predict, on the history of stimulation.

Generally speaking, odor-evoked spatio-temporal patterns of PN activity can be pictured as sequences of instantaneous PN vectors, or trajectories, in PN phase space (see below). We

updated each PN vector every 50ms, a duration corresponding to the average period of the 20-Hz odor-evoked oscillations in this system (Laurent and Naraghi, 1994; Wehr and Laurent, 1996). The relevance of this time scale in locust is determined by the integrative properties of Kenyon cells, the PNs' targets in the mushroom bodies (Laurent and Naraghi, 1994; Perez-Orive et al., 2002). We determined previously that, upon stimulation with a single odor, PN vectors leave a noisy baseline state, defined by uncorrelated, 2-4 spikes/s baseline firing (Mazor and Laurent, 2005; Perez-Orive et al., 2002). Following termination of stimulation, the trajectories return to baseline over several hundred milliseconds (Mazor and Laurent, 2005; Stopfer et al., 2003). During stimulation, the trajectories evolve in a stimulus-dependent manner at a velocity that is highest at onset and decreases monotonically to 0 (thus defining a fixed point) if the stimulus is sustained for 1.5s or more (Mazor and Laurent, 2005). When the odor pulse is turned off, velocity peaks up again and progressively returns to 0 as the system relaxes back to baseline in a few hundred ms (Mazor and Laurent, 2005). For 0.5s long stimuli (as used here) the system never reaches fixed points: the odor-evoked PN patterns we analyzed in this paper can thus be described as loops, consisting of one segment (on-transient) away from baseline and a second (off-transient) corresponding to the return to baseline (Mazor and Laurent, 2005; Stopfer et al., 2003). A recent study examined PN and KC odor representations for a single odor presented in 100ms pulses at different frequencies and suggested that information about individual odors (as measured by classification performance) was not significantly affected by pulse frequency and preceding temporal pattern (Brown et al., 2005). In the present experiments we examined how odor representations by PNs and by KCs change as different stimuli coincide within a 3.5s window.

2.3.1 Temporal and Spatial Scales of Analysis

Our interpretation of high-dimensional, instantaneous PN vectors as a functionally-relevant scale of representation rests on the assumption that the decoding of PN activity by KCs — their targets in the mushroom bodies — follows similar rules: that is, that individual KCs fire

or do not fire on the basis of an interpretation of high-dimensional, instantaneous PN vectors of activity. Recent observations from this laboratory indicate that individual KCs sample 50% of all PNs on average (R Jortner, SS Farivar, and G Laurent, in prep) and that each oscillation cycle contains spikes from 80-240 PNs over the entire PN population (Mazor and Laurent, 2005): the dimensionality of PN vectors analyzed here (87) is thus less than that of those experienced and decoded by individual KCs (~400); yet, our interpretation of those 87-D vectors and of the trajectories they define is in good agreement with the KC responses we observed. This supports our assumption that interpreting PN population vectors and trajectories, as done here, approximates the decoding conditions for KCs reasonably well. For example, a consistent effect of overlapping odor stimuli was a masking (sometimes complete) of the responses of KCs activated by either odor alone: this observation is in excellent agreement with our synthetic interpretation of PN trajectories. While this result may begin to explain the "binding" nature of odor perception or recognition (Jinks and Laing, 1999), more exhaustive experiments must now be carried out using more complex mixture conditions. This is particularly important because natural odors often contain tens to hundreds of volatile components.

2.3.2 Importance of Stimulation History

We hypothesized that the stimulation of a PN population already activated by one odor with a second odor (odor overlap) might either cause a transient reset of the system — transient return to baseline followed by the development of the trajectory corresponding to the second odor — or alternatively, cause the first trajectory to deviate from its ongoing course to the path corresponding to the mixture of the two odors. Our results rule out the first hypothesis and support the second, with notable differences. When the PN vectors evoked during an overlap condition were compared to those caused by either odor alone or by their binary mixture, distances to the mixture vectors were nearly always shorter. When we measured these distances in absolute terms, however, we observed that they were often large (i.e., that matches with the

mixture response were poor). These measures of inter-PN-vector distances were consistent with the responses of KCs (the PN decoders) to the same stimuli: Kenyon cells that responded to a mixture stimulus did not always respond to an overlap condition, even though the stimuli were, for some time, instantaneously identical; conversely, some KCs responded transiently to a particular overlap condition and yet did not respond when the two odors were presented as a mixture. These transient overlap KC responses occurred at times when the PN-vectors corresponding to the overlap deviated the most from those corresponding to the mixture and there was significant PN synchrony. Both measures (inter PN-vector distances and the responses of the PNs' natural decoders) thus indicate that odor overlaps cause antennal lobe dynamics related to, but not identical to, those caused by binary mixture conditions; KCs could thus, by this specificity, encode some aspect of the history of stimulation. Because some overlap conditions create such unique responses — as seen both in the PN population and in single KCs — we predict that these overlaps could also be memorized and/or perceived as different from either odor alone or from their binary mixture. The specificity of these representations may extend to mixtures of particular ratios of these odors. This remains to be tested behaviorally.

Our results may also shed some light on interesting behavioral experiments on odor discrimination with mixtures. Jessica Hopfield and Alan Gelperin (1989) examined the ability of the terrestrial mollusk Limax to segment a binary odor mixture when classical conditioning had been done in either of two conditions: in the first, an *AB* odor mixture was paired with an aversive unconditioned stimulus (US), and animals were later tested with *AB* and either odor (*A* or *B*) alone. In the second, the freely behaving animals were trained in conditions where odors *A* and *B* were located on alternating strips; in this condition, the US could, in principle, be associated by the animal with either odor alone or with the representation of some (undefined) mixture of them. Again, the animals were tested some time later with odors *A*, *B*, and *AB*. With the first training condition, Hopfield and Gelperin observed that the conditioned response (aversion) was specific to the mixture: the animals failed to show aversion to the mixture components alone. This is

consistent with our physiological results: the representation of a binary mixture (assessed as a family of PN vectors) differs from those of the components, and the sets of KCs that responds to a mixture and to its components are not the same. With the second training condition the behavioral results were different: the animals avoided the mixture and also its components. Assuming that Hopfield and Gelperin's training paradigm contained stimulus conditions similar to those we used in our study (i.e., periods of partial overlap between the two stimuli or between the responses to these stimuli), these behavioral results are again consistent with our observations: in conditions of stimulus (or response) overlap, some fragments of the PN responses (and correspondingly, the KCs that fire) match those evoked by each odor component alone and sometimes those evoked by the mixture. What these behavioral experiments do not address, however, is whether conditioned aversion was expressed also towards stimuli that were neither a component nor the binary mixture, but some particular overlapping sequence of the two components (as we would predict from the physiological results on PNs and KCs). As we indicated above, this remains to be tested.

2.3.3 Possible Mechanisms

Our results indicate that the antennal lobe is a dynamical system whose responses to stimulation depend, to a significant extent, on initial conditions. For example, the response of the PN population to an odor was usually delayed if that odor pulse followed or overlapped with an earlier one. Also, the path followed by the PN population during an odor overlap condition depended on the precise nature (order, duration) of this overlap. History dependence or hysteresis has also been noted in other systems, such as the oculomotor system, where neuronal activity during the same eye-fixation position can be different depending on preceding saccade history (Aksay et al., 2003). In our system, the origins of the sensitivity to history are probably multiple

First, the responses of receptor neurons, to the extent that many odorant receptors are broadly tuned (Hallem et al., 2004; Wilson et al., 2004), must depend on past history of

stimulation, due to the biophysics of receptor occupancy and to G-protein activation and inactivation kinetics (Kurahashi and Menini, 1997; Zufall and Leinders-Zufall, 1998; Zufall and Leinders-Zufall, 2000).

Second, the locust antennal lobe itself is a recurrent network with widely branched local inhibitory neurons causing rhythmic negative feedback (MacLeod and Laurent, 1996) as well as slow inhibitory patterning (Laurent et al., 1996). How randomly connected recurrent networks can process time-varying continuous input is the subject of recent theoretical work on "liquid state machines" (Maass et al., 2002). It was suggested that to perform complex computations on time-varying input such networks need to operate at the edge of dynamical regimes where behavior becomes chaotic (Bertschinger and Natschlager, 2004). Building on this work, Latham and colleagues have recently investigated the response trajectories of such networks when placed under different initial conditions (Maei and Latham, 2004) but driven by the same input for some time – a situation very similar to our experiments. They examined three cases: convergence, divergence, and neutral. Convergence, after a delay, matches our experimental results for most overlaps and pulse conditions. Divergence is a behavior we did not observe. The ger-100ms-cit condition came closest to what Maei and Latham (2004) call a neutral condition, which allows the network to remember input history but is, according to that study, difficult to sustain beyond the time constants of neurons in the network. In a different theoretical study, Knusel et al. found that for information encoded over time to be reliably decoded, a reset of the network was desirable (Knusel et al., 2004). This does not match our experimental observations (trajectories move from one pure condition's trajectory to a later part of the next without going through baseline). While this may place theoretical limits on how much information about an input pattern can be reliably decoded, it may equally indicate that antennal lobe circuits are designed to identify instantaneous odor conditions reliably rather than recognize particular temporal patterns of odor input. A more complete investigation of the sensitivity of PN ensembles to different odor patterns will be the subject of future work (B Broome, M Meister, & G Laurent, in prep).

2.3.4 Consequences for Natural Odor Plume Conditions

We observed that trajectories evoked by one odor could be influenced by an earlier pulse of another odor presented up to 3s before. Conversely, the return paths to baseline upon the termination of related stimulus conditions (*A* then *B*, with different delays between the onsets of *A* and *B*) generally converged before (sometimes well before) reaching baseline. These observations identify the interval 0-3s as the time over which different stimuli (of 0.5s duration) may generally interfere with one another; they also indicate that the degree of interference between odor pulses decreases quite rapidly as the pulse interval increases. Only in limited conditions of close pulse overlap did the PN population response deviate significantly from what could be predicted, knowing the trajectories corresponding to either odor alone or to their binary mixture. For such conditions of close overlap, new KCs were recruited, consistent with large deviations of the PN population vectors. For conditions of limited overlap, masking of KC responses was the main effect. Together, these results suggest that in conditions of chaotic overlapping odor plumes, the dominant effects (on KC activation at least) should be ones of masking and mixture encoding with occasional recruitment of other KCs detecting particular conditions of overlap (sequences). Naturally, the distribution of such conditions would depend entirely on the statistics of inter-pulse intervals and on their temporal correlation. It will be interesting to examine behavior, learning, and recognition in such increasingly complex stimulation conditions.

2.4 Methods

Two odors at 12 different time delays relative to one another while recording summated output from olfactory receptor neurons, extracellular multi-single-unit activity from groups of up to 25 PNs, the LFP elicited by PNs in the MB, and multi-single-unit activity from groups of up to 20 KCs.

2.4.1 Odorants

For all experiments, two odorants (citral and geraniol, Sigma) were diluted 1/100 in mineral oil (J.T. Baker) and stored in separate 60ml scintillation vials. This concentration is comparable to those used in prior studies. Odor vials were prepared fresh each day. The vials were arranged in parallel, and 0.5s puffs of desiccated and filtered air (460 ml/nim) carried the headspace of each vial into an odor nozzle and then past the antenna. The odor nozzle (1cm diameter, teflon) was placed 1cm from the antenna and supplied a constant 900 ml/min carrier stream of desiccated, filtered air. The odors were injected into the carrier stream 6.5cm from the output end of the odor nozzle to ensure complete mixing by the time the odors exited the tube. A large vacuum hose placed behind the antenna assured the quick removal of odorants from the space surrounding the antenna. Odor puffs were triggered automatically using a custom computer interface (LabView).

2.4.2 Electrophysiology

Experiments were carried out on 34 male locusts (*Schistocerca americana*) raised in a crowded colony. Young adults (prior to reproduction) were immobilized in a wax cup with their antenna exposed. The cuticle over the brain was removed, the brain was exposed, and later desheathed while the head of the animal was bathed in locust saline, as previously described (Laurent and Naraghi, 1994; Stopfer and Laurent, 1999). PN data were acquired using silicon

tetrodes obtained from the Center for Neural Communication Technology (Drake et al., 1988). Our multi-single-unit extracellular recordings only detected events attributable to PNs, as LNs do not produce sodium action potentials (Laurent and Davidowitz, 1994). KC data were obtained using twisted wire tetrodes obtained from FMC (#CE4B75). Electrode tips were re-plated with gold prior to each experiment. KCs were recorded in a region containing only KC somata. All KC recordings were performed using extra-cellular wire tetrodes due to the unique recording requirements of these neurons. Recording locations were tested randomly across the MB and selected if activity could be elicited by either pure odor or their static mixture. PN and KC spikes were sorted offline using custom designed algorithms (Pouzat et al., 2002) implemented in Igor (WaveMetrics). Clusters were selected for inclusion in the final data set based on their successful completion of several statistical tests. These included waveform SD variation of <0.05 throughout the length of the stimulus, distance between cluster centers (>4SD), low numbers (<2%) of spikes with <5ms inter-spike-intervals, and no significant drop in the SD trace during the spike peak. Identical stimuli were presented at the beginning and end of the experiment to confirm that clusters did not drift significantly over the course of the experiment. Drift was measured qualitatively by determining if a given cell's response to pure odors at the beginning of the experiment were similar to the responses of each odor in the cit-3.5s-ger and cit-3.5s-ger trials. cit-3.5s-ger and ger-3.5s-cit were always presented near the end of an experiment.

The KC data was sorted using the first 11 conditions of the experiment (10 trials each) as the basis for the sorting model. The condition that occurs in the middle of the set was used for the noise covariance matrix. The threshold was set so that the total number of events was approximately 2000. The model generated by this method was refined using criteria identical to those used on the PN data. Stability over the course of the experiment was assessed after sorting and was based on a stable baseline firing rate over the course of the experiment.

2.4.3 Data Analysis

MATLAB and the Statistics Toolbox (The MathWorks, Inc.) were used for data analysis and modeling.

To test whether a PN response to an odor overlap (with a t_d msec delay between presentations of the first and second odors) was a simple summation of its responses to the odors presented individually, we convolved spikes from the responses with a Gaussian of width 20 msec, averaged the smoothed spike counts across trials, and subtracted mean baseline spike counts (calculated from data preceding stimulus onset). We then compared the response to the overlap condition with the response of the first odor added to the response to the second odor shifted by the appropriate delay (t_d-ms). We quantified the deviation of summation-based estimates (*sum*) from the firing rate profiles measured during overlapping stimuli (*recorded*) as follows: First, for each cell, condition, and time bin, we calculated the absolute difference (*absdiff*) of *sum* from *recorded* as a percentage of the recorded maximum firing rate of the given PN (across all times and conditions). To identify PNs that showed significantly greater deviation in overlap than in non-overlap conditions, we used a Wilcoxon rank sum test (with $p<0.0001$) to compare *absdiffs* for time bins from 0-1s after presentation of the second odor in overlap/pulse conditions (except the 3.5s case) with those of the first 600ms after presentation of the first of two odors in conditions from cit/ger-600ms-ger/cit up to cit/ger-3.5s-ger/cit. To characterize each PN by a single number representing percentage deviation (distribution shown in Fig. 2.2B), we used the following procedure: (i) We defined the percentage difference for a particular condition (*conddiff*) to be the maximum of *absdiff* over time for that condition. The percentage deviation for a given PN was then calculated as its mean *conddiff* over all overlap conditions (and, as a control, also for all times of zero-overlap). (ii) We also computed mean percentage differences for each condition and time bin by simply averaging *absdiff* across all PNs. This is shown in Fig. 2.2C.

For nonlinear dimensionality reduction with Locally Linear Embedding (Roweis and Saul, 2000), we used code from Sam Roweis (http://www.cs.toronto.edu/~roweis/lle/) with

Gerard Sleijpen's code for the JDQR eigensolver (http://www.math.uu.nl/people/vorst/JDQR.html). In the figures shown for nonlinear dimensionality reduction with LLE, we used as input 87-D time slices, each 50ms wide and averaged over 3 trials. Other details are as described in Stopfer et al., 2003.

For multiple discriminant analysis we used functions from Richard Strauss's MATLAB-based statistics library (http://www.biol.ttu.edu/Strauss/Matlab/Matlab.htm). Training data consisted of 16 groups of time slices from single trial responses to pure conditions (5 groups from the citral response, 5 from geraniol, 5 from the citral+geraniol mixture, and 1 baseline group). 42 time slices – 3 per trial, 14 trials – were used to represent each group. Time slice correlation analysis (Fig. 2.4) and trial-averaged hierarchical clustering were used to guide the choice of groups so as to adequately represent different periods of the population response. We used 672 time slice vectors as training data to compute 15 discriminant functions that were then used to transform the 55,328 sample data vectors. For classification we used Euclidean distances of individual 15-D points from group centroids (means of the remaining points in a group). Classification with other metrics such as Mahalanobis distance produced similar results. Group centroids were computed using only training data, and distances were normalized by mean intra-cluster distance for training data.

KCs were grouped into the categories shown in Table 2.1 based on the following criteria. Condition 1: more than half of all trials with pure odors (i.e., cit, ger, or cit+ger) contain at least one spike during a response window lasting from odor onset to 500ms after odor offset. Condition 2: condition 1 is satisfied for the first odor in a consecutive-pulse trial (i.e. cit-≥600ms-ger or ger-≥600ms-cit). Cells were then classified as follows: Cit, Ger, and Mix: satisfy Condition 1 for odors of this type only, and do not satisfy Condition 1 or Condition 2 for any of the other two. Cit+Ger, Cit+Mix, Ger+Mix: satisfy Condition 1 for two odors, and do not satisfy Condition 1 or Condition 2 for the third odor. Pattern-specific: satisfy Condition 1 during overlap periods when applied to overlap trials, and do not satisfy Condition 1 or Condition 2 for any odor. All Stimuli:

do not satisfy Condition 1 or 2 for any pure odor but respond to all stimuli with at least one spike in ≥ 2 trials/condition. Paraffin oil/clean air: satisfy Condition 1 for these conditions, and do not satisfy Condition 1 or 2 for any other conditions. Respond with Inhibition: no response to the first odor presented regardless of the condition and then response to all conditions ≥ 500ms after odor offset. No Response: do not satisfy Condition 1 or 2 for any stimulus, and have no response in >75% of conditions.

To construct the KC mean PSTH we convolved KC spikes with a Gaussian of width 20ms and averaged the smoothed spike counts across trials and across cells for each condition.

2.5 Acknowledgements

The work was described in this chapter was a collaborative effort between Vivek Jarayaman and myself. I formulated the original idea and performed all the experiments while the extensive data analysis was performed jointly.

This chapter has been submitted for publication as: BM Broome, V Jayaraman, and G Laurent. Encoding and decoding of overlapping odor sequences. Vivek and I are listed as co-first authors.

Chapter 3

Encoding and Reconstructing Rapidly Varying Odor Stimuli

3.1 Introduction

In natural environments animals must navigate through complex odor landscapes. These landscapes consist of many different odor filaments (originating from, for example, food sources, mates, and predators) that fluctuate rapidly due to wind currents or an animal's movements (Koehl et al., 2001). In fact, even strong odor sources are not solid clouds of odorant; rather, once a short distance from the source, they rapidly become clusters of individual odor filaments encountered in series by the olfactory system (Murlis, 1982). This is particularly true for insects, which lack an enclosed structure around their odor receptors to trap odors (Murlis et al., 1992). However, despite the irregular character of natural stimuli, much of our knowledge about the olfactory system concerns its responses to regularly pulsed odors presented within long periods without odor, with a few exceptions (Brown et al., 2005; Vickers et al., 2001). We explore here how the olfactory system responds to rapidly varying odor plumes, similar to those that an animal might experience in nature, and how those responses differ from those elicited by pulsed stimuli.

In this context it is important to consider the effects that stimulus history may have on olfactory processing. Our current model of olfactory processing proposes that many odors are not

encoded at the level of the AL by a single pattern of PN activation, but rather by the ordered progression of several distinct PN patterns, each during a different oscillation cycle (Laurent et al., 1996; MacLeod and Laurent, 1996; Stopfer et al., 1999; Wehr and Laurent, 1996). Furthermore, previous work suggests that antennal lobe odor representations evolve over several hundred milliseconds, with the maximum decorrelation (ability to discriminate between patterns) occurring in the first 200-300ms following either the onset or offset of an odor pulse (Friedrich and Laurent, 2001). However, in nature insects and other animals encounter streams of stimuli whose cross section may be even shorter (Murlis, 1982). How then can an incoming odor be processed in situations where the olfactory system is already actively engaged in processing the same or another odor? Are animals capable of following the temporal dynamics of rapidly varying odor stimuli? If so, what is their maximum temporal resolution? The answers to these questions require that we explore further the coding mechanisms that operate in the AL.

A test of our understanding of neural coding mechanisms sometimes relies on the ability of observers to reconstruct the original spatiotemporal features of a stimulus from neuronal activity recorded when the stimulus was presented (Rieke et al., 1997). Whereas this approach has limitations — non-selective reconstruction of the sensory world does not appear to be the goal of sensory systems — it has the merit to identify minimal rules to recover the information present in spike patterns. While reconstruction has been employed with success in the visual system (Bialek et al., 1991; Warland et al., 1997), to date there have not been any significant attempts at reconstructing olfactory stimuli. There are several reasons for this. First, the distributed nature of coding in the antennal lobe and mushroom body requires that one record from large groups of neurons simultaneously (Mazor and Laurent, 2005). Second, it has been difficult to carefully measure the time course of an olfactory stimulus, as few sensors are capable of tracking an odor stimulus in a manner that is compatible with simultaneous electrophysiological recording (Park and Hardie, 1998; Park et al., 2002; Smith and Spanel, 2005; Smith et al., 2002; van Ruth, 2001; van Ruth, 2004). Third, PNs and KCs respond in ways

difficult to describe accurately with traditional tuning curves, and the high-level representations present in the AL are not optimally suited to certain decoding methods (e.g. Bayesian inference, population vector) (Dayan and Abbott, 2001; Laurent et al., 2001).

We examine here the ability of the antennal lobe, the insect analog of the olfactory bulb, to respond to rapidly varying, naturalistic odor stimuli. We presented one or two natural odors while simultaneously recording from large groups of neurons in the AL. In addition, we adapted a new device developed by organic chemists (Freund and Lewis, 1995; Matzger et al., 2000), here called the "electronic nose," to record the dynamics of the stimulus. The signals recorded from this device enabled us to compare a virtual stimulus reconstructed from the activity of AL neuron ensembles to the real one and thereby test several hypotheses about the optimal composition of these neural ensembles and about the information content of spike trains. We asked: Do PNs respond differently to rapidly varying odors than they do to sustained isolated pulses? How are individual and ensemble PN responses affected by stimulus history and complexity? Can we reconstruct an odor stimulus based on the activity of individual cells or groups of cells? Can we infer anything about the functional organization of the system by our ability to reconstruct stimuli?

3.2 Results

3.2.1 Electronic Nose

Odor stimuli rarely occur as square waves, either in nature or in an experimental setting (Murlis, 1982). This problem complicates attempts to reconstruct stimuli from downstream neuronal activity, as most methods require detailed knowledge of the stimulus (Dayan and Abbott, 2001; Rieke et al., 1997). One solution is to record the stimulus instead of trying to perfectly control its structure. However, most techniques for measuring the course of an odor

stimulus, i.e. mass spectrometry and gas chromatography, do not have the temporal resolution necessary for recording rapidly varying stimuli (Smith and Spanel, 2005; Smith et al., 2002; van Ruth, 2001; van Ruth, 2004). When studying insects, electroantennograms (EAGs), differential recordings from both ends of an antenna (probably representing the combined receptor potentials of all neurons located in between the two recording electrodes) can be used (Park and Hardie, 1998; Park et al., 2002; Vickers et al., 2001); these techniques are sensitive but problematic in two main respects: reproducibility and stability over time.

We delivered precisely controlled sequences of odor pulses using an electro-mechanical olfactometer (Laurent and Davidowitz, 1994; Laurent and Naraghi, 1994) and measured actual odor delivery using a fast electronic sensor, thus generating continuous recordings of the odor stimulus. Electronic noses (ENs), polymers whose resistivity varies with the adsorption of odor molecules (Freund and Lewis, 1995; Matzger et al., 2000), were manufactured in the laboratory of Professor Nathan Lewis following published protocols and tested against the odors selected for use in this experiment (Fig 3.1). All odors used in this experiment affected the detector with similar temporal characteristics despite their different chemical structures (the sensor and the odors were selected so as to enable this). Figure 3.2A illustrates the similarity between the signals recorded simultaneously using an EN and an EAG. EN and EAG signals are comparable both in time course and amplitude. Furthermore, a linear transformation can be made from the EAG signal to the EN signal using a simple kernel (Fig. 3.2B).

ENs have several distinct advantages over EAGs for monitoring odor stimuli. First, a single sensor can be used for hours at a time and over several experiments without its response properties changing significantly. Preliminary tests showed that ENs responding to repeated 100ms pulses of hexanol did so with only 7ms of jitter. Individual ENs could also be used for several experiments over the span of weeks and displayed very similar responses over this period (Fig. 3.2C). In contrast, EAGs decay rapidly over time (Park et al., 2002). Second, the response properties of different ENs are very similar. Fig. 3.21C shows the responses of all the ENs used

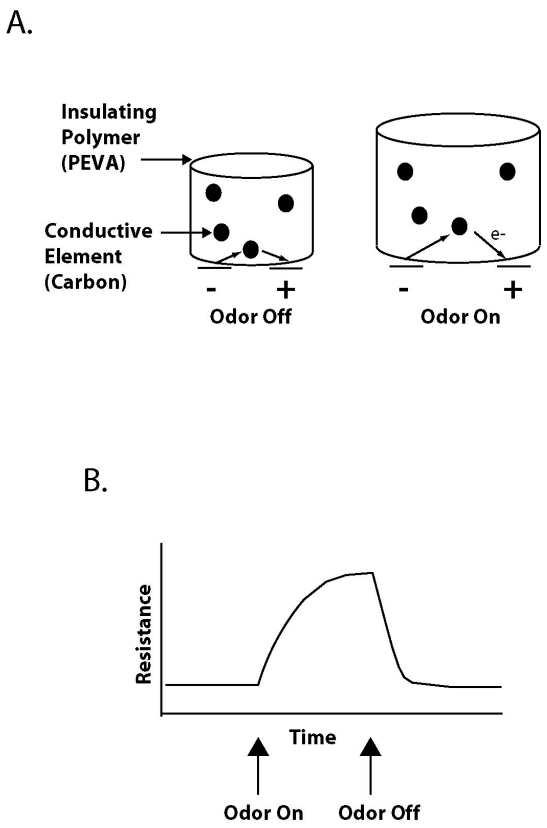

Figure 3.1, Electronic-nose.
A. Electronic nose polymer expands as it comes into contact with odor, moving the conducting elements embedded within the polymer farther from one another and increasing the resistance. **B**. An example of the change in resistance that accompanies odor presentation.

for these experiments. While there are some differences in the maximum values attained by the different sensors (~20%), response times varied at most by 10ms across all sensors. By contrast, EAGs are quite sensitive to preparation and can display wide variations in their response times (Park et al., 2002; Vickers et al., 2001). Third, ENs have fast response properties, enabling a very accurate recording of the stimulus over time. While it is possible that under rapidly varying odor conditions an EN might saturate, tests indicate that the sensors are capable of recording 100ms odor pulses and returning to baseline within 200ms (Fig. 3.2A).

We observed a delay of approximately 200ms between the odor valve opening command and sensor response (EAG or EN) (Fig. 3.2A). This delay was constant across all experiments and

is attributed to the time necessary for the odorized airwave to propagate through the tubing of the odor delivery apparatus. This delay was kept constant by positioning the antenna in the same

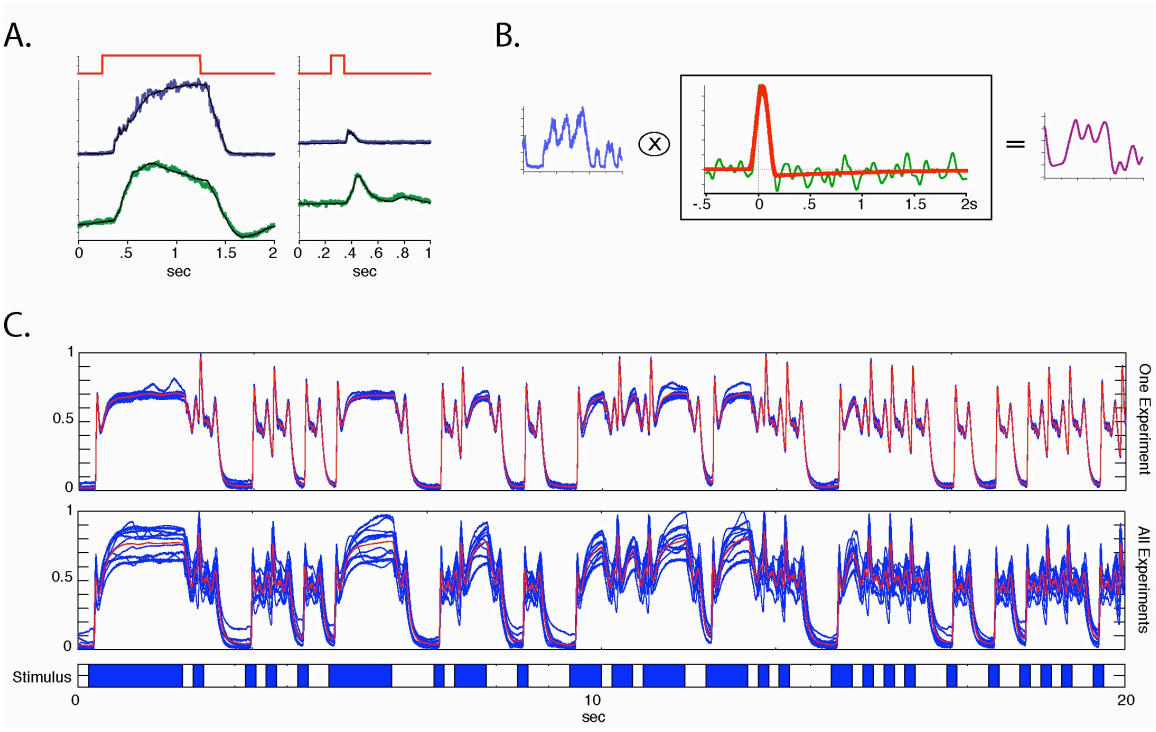

Figure 3.2, **EN recordings closely approximate EAG responses and are highly reproducible** **A**. Simultaneous valve (red), electronic nose (blue), and electroantennogram (green) recordings to a hex stimulus (left, 500ms; right, 100ms). Recordings presented without temporal adjustment. **B**. Kernel calculated to match EAG recordings (left, blue) and simultaneous EN recordings (right, magenta). Undershoot in kernel demonstrates adaptation in EAG response. **C**. EN responses to a 20s window within the 105s rapidly varying odor stimulus for oct (50-70s, see Fig. 3.9). Top: 9 individual trials from a single experiment (blue) and average EN response (red). Bottom: average responses from 12 experiments (blue), average of those experiments (red). 3 different ENs used over 8 experiments (3 months). The responses from each experiment were normalized for display.

position in all experiments (using antenna-sized holes in the tubing), and is accounted for in all subsequent analysis.

3.2.2 Single PN Responses

Previous work has demonstrated that a locust antenna placed in a turbulent odor plume about 1m away from the odor source receives odor filaments with skewed hit-duration and inter-

hit-interval distributions (Stopfer and Laurent, in prep). The median of each one of these distributions was close to 200ms (Stopfer and Laurent, in prep). Using this information we constructed intermittent odor stimuli that approximate these characteristics. To maximize the number of pulse histories in each intermittent sequence, we used M-sequence protocols (Sutter, 1987) with 200ms pulse durations and inter-pulse intervals in 200ms increments. We generated long stimuli with either 2-octanone (oct) or 1-hexanol (hex) that included all possible combinations of on or off "letters" within 1.8s long "words" (Fig. 3.3A). We used 1.8s words because pilot experiments showed that PNs responses, measured as spike-triggered stimulus averages, to rapidly varying stimuli seemed only minimally affected by events 1.5 to 2s prior to a spike (see below, Figure 3.5A). These results were confirmed by the experiments described and discussed below. We included all possible combinations of 9 letter words (2^9 = 512) in our stimuli. Such stimuli would in principle last 922s (512 words * 9-letters-word * 0.2 s/letter = 922s). Using a simple optimization technique that exploits overlapping concatenation of sequences (M-sequences) and that is routinely used in visual neuroscience (Bernardete and Victor, 1994; Reid et al., 1997), the stimuli were compressed to 105s (Fig 3.3A). To our knowledge such stimuli have never before been used to study olfaction.

M-sequences present a number of mathematical features that are advantageous for analysis. They enable the generation of all possible combinations of n-bit binary sequences in a format that is both maximally compact and random with respect to bit-to-bit transitions. In addition, the auto-correlation of an M-sequence is 0. The patterns for each pure odor were constructed separately. These sequences were also combined to yield a mixed stimulus (oct+hex). The mixed odor stimulus was a straight superposition of the two single-odor stimuli and produced a mixture that varied randomly between the two odors and the mixture, over 105s. Yet, this mixture stimulus was not itself an M-sequence of mixed pulses, for it did not include all possible combinations of 9 oct+hex-letter words (see Methods).

PNs responded to these rapidly varying odor stimuli with fast temporally patterned responses (Fig. 3.3B, left). We examined in detail the responses of 97 PNs, recorded extra-cellularly in groups of 9 to 23 neurons (see Methods), while presenting separately the two pure

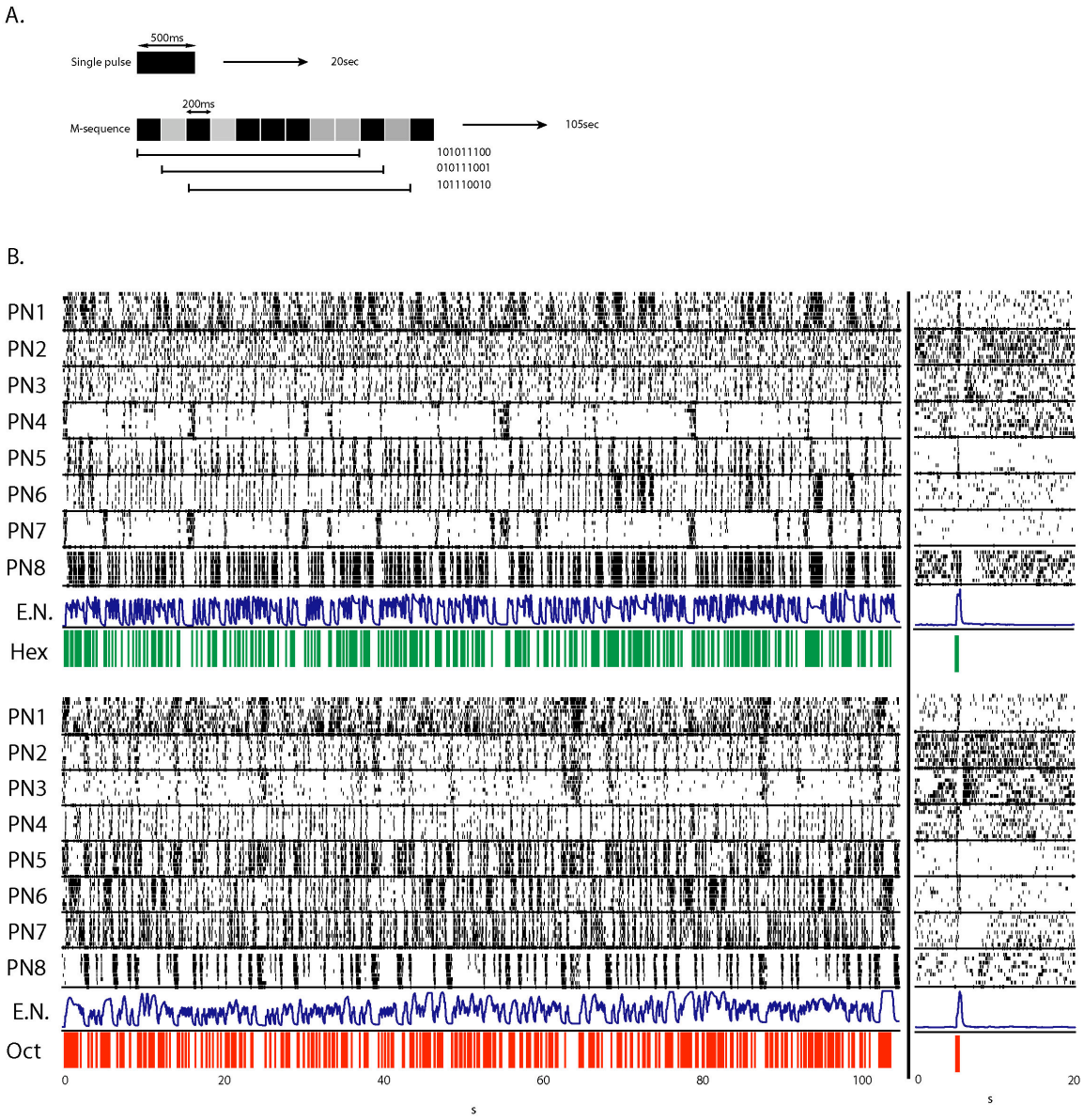

Figure 3.3, Individual PN responses to rapidly varying and pulse stimuli.
A. Structure of single pulse and M-sequence stimuli. Single 500ms pulses of either oct, hex, or oct+hex presented against clean air background in 20s trial. M-sequence stimuli constructed from patterned 200ms periods when the odor was on or off (1 or 0, respectively). Collectively, nine 200ms odor "letters" formed a 1.8s odor "word." All combinatorial 1.8s words included in the 105s stimulus. Individual 1.8s words overlapped as shown. For more information on the manner in which pure oct and hex stimuli were combined to yield multi-odor oct+hex see Methods. **B**. Responses of 8 simultaneously recorded PNs to either single pulse or M-sequence stimuli. 9

consecutive trials (numbered consecutively from the top down) shown with simultaneously recorded EN. All data collected from the same animal over the course of a single experiment.

odors, oct and hex, and one mixture, oct+hex. These stimuli were 105s long M-sequences, as described above. For comparison, "pulse stimuli" of oct, hex, and oct+hex were presented as single 500ms long pulses in 20s trials (Fig 3.3B, right). All stimuli were mixed in a dry air carrier stream (2 l/min). PNs are the only neurons in the locust AL that produce sodium action potentials, and therefore all spikes were unambiguously attributed to PN activity (Laurent and Davidowitz, 1994).

PN responses to the time varying odor stimuli (oct, hex, or oct+hex) contained excitatory and/or inhibitory epochs with onset times and durations that were odor and PN specific. The responses of an individual PN were very reproducible across trials, as noted previously for simple pulse stimuli (Mazor and Laurent, 2005; Stopfer et al., 2003). Given the stability of the M-sequence odor stimulus (Fig 3.2), this reproducibility of PN responses suggests that PNs may be quite reliable, even under complex stimulation conditions. Many PNs produced action potentials with an accuracy of less than 50ms (e.g. PN5, PN6 & PN8 Fig 3.3B), the average period of the PN population's synchronized activity, across all 10 trials. On a gross level, individual PN responses to both pulse and rapidly varying stimuli were similar; those neurons that responded with inhibition to the presence/absence of an odor did so irrespective of the stimulus structure. While there appear to be differences in the baseline activity between the two conditions, it is important to remember that no real baseline existed during the M-sequence stimulation condition: the frequency of on/off pulsing during such stimuli was too high to allow any recovery and stabilization of the system (the longest off period was 2s). In a few PNs (<10, e.g. PN8-oct, Fig 3.3B) the response to a particular odor waned as the number of trials increased; however, these neurons responded at full strength again when a new stimulus was presented. This change was PN- and odor-specific, as it did not apply equally to all PNs recorded simultaneously (e.g., PN7-hex or PN3-oct, Fig 3.3B). The significance of and mechanisms underlying this slow adaptation

are not known, and because it was observed in a small minority of cases only, it will not be examined further in this study. While some of the PNs followed the M-sequence stimulus quite faithfully (PN8, Fig 3.3B), others did not (PN1, Fig. 3.3B). This was true for both long and short odor pulses and did not seem to be related to the complexity or modulation of the PN's response to a simple pulse. We observed a few complementary on/off responses from simultaneously recorded pairs, as reported previously (Laurent and Davidowitz, 1994). These antagonistic response patterns were not always stable across odors for the same neuron pairs, suggesting that the underlying mechanisms may be distributed across many neurons in the AL circuitry.

We observed that in the rapidly varying odor condition (M-sequence) many PNs responded strongly and precisely to the odor being turned off (Fig. 3.4). Summed over the 97 PNs included in our data set, PN firing rates were often strongest in the epochs following pulse offsets. This is consistent with results obtained with single odor pulses (Mazor and Laurent, 2005), where PN firing rates during off phases (as the odor is being turned off) often rise well above those following odor onset. Analysis of the simultaneously recorded LFPs indicated that power in the 5-50 Hz band was also greatest following pulse offset (Fig. 3.4B). This result, by contrast, is different from what has been observed with pulsed stimuli, where oscillatory power is greatest following pulse onset (Mazor and Laurent, 2005). Because PN oscillatory synchronization is due to fast inhibitory feedback from local neurons (MacLeod and Laurent, 1996), this result suggests that LN recruitment, synaptic release, or postsynaptic efficacy may be different in static and fast-changing stimulation conditions.

3.2.3 Functional Subdivisions within the PN Population

We next examined the tuning of the 97 PNs, with particular attention to the correlation between the responses of each PN to the two odors tested. For example, if a PN spike indicated the presence of odor *A* x-ms in the past, would it also reliably indicate the presence (or absence) of odor *B* y-ms in the past? More importantly, if a particular property was identified in a PN (e.g.,

odor A predicts a spike in 200ms), would it reliably predict another relationship for that PN (e.g., odor B predicts an absence of spike in 200ms)? In other words, we wished to establish whether

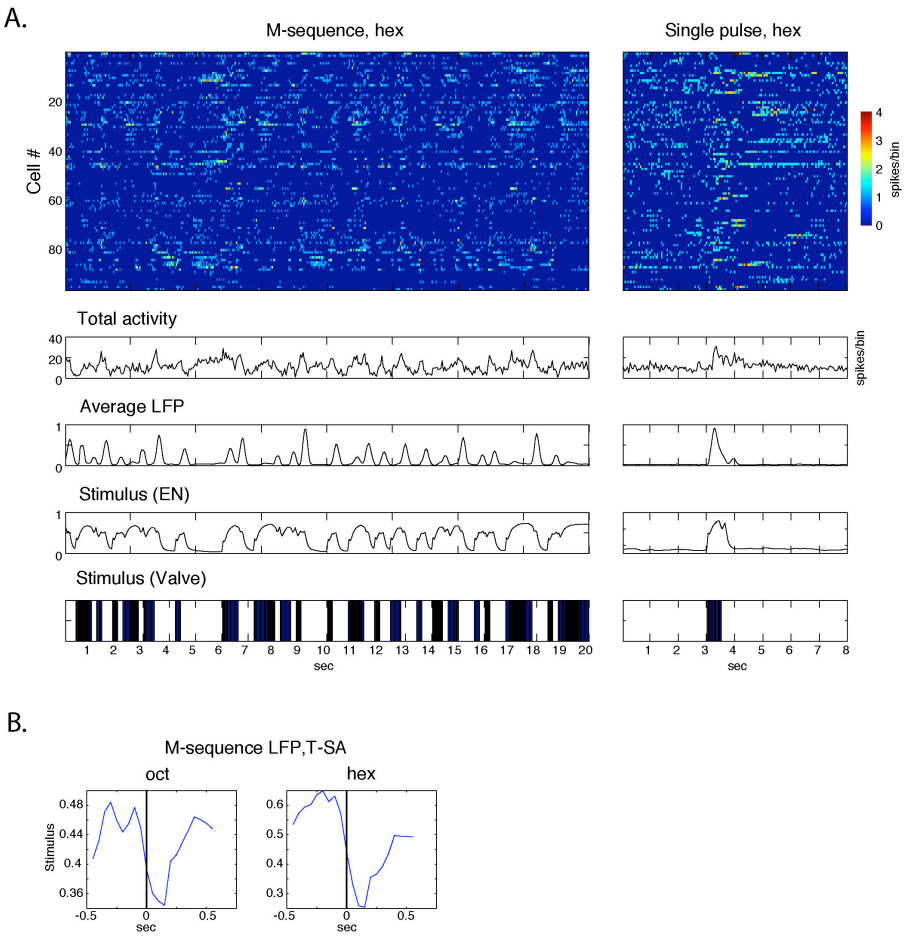

Figure 3.4, LFP power is highest at odor offset for rapidly varying stimuli.
A. Top, individual cell firing rates for one single pulse and M-sequence oct trial. Bottom, average firing rate across cells vs. LFP (averaged over 9 trials and 4 experiments) vs. odor concentration (averaged over 9 trials and 4 experiments) vs. stimulus valve times. Graphs time corrected to account for known, fixed mechanical delay in odor delivery system. **B**. LFP-peak triggered stimulus average calculated from EN recording for the LFP shown above.

PNs could be classified and grouped in simple and/or consistent ways. M-sequence stimuli are particularly well suited to address this kind of question since they probe the space of stimulus conditions (here timing) optimally. Spike-triggered stimulus averages (STSAs) were calculated for all odor-cell pairs using the simultaneously recorded EN data (see Methods). Using these STSAs, we confirmed our preliminary observations that the period relevant for a PN in an M-

sequence stimulation condition is mostly contained within the 2s preceding a spike (Fig. 3.5A). Figure 3.5A (red: oct; dark blue; hex) shows a representative sample of STSAs taken from the 97 PNs (t = 0 at spike time). These average waveforms illustrate that a spike in a given PN can indicate the presence of an odor (upward deflections), its absence (downward deflections), or a succession of both at specific times preceding it. Importantly, these waveforms can be different across odors in one PN (consistent with the knowledge we have about PN responses to odors; (Laurent et al., 1996)) and occur in different combinations across PNs. As seen in this selected sample (Fig 5A), many pairs of STSAs were found independently of whether the PNs had been recorded from the same electrode or not. We also calculated the STSAs using the trials in which the two odors had been presented together (using different but overlapping M-sequences). Not surprisingly (Broome et al., (submitted)), the stimulus averages often differed from what they were in single-odor conditions (Fig. 3.5A).

To further assess the possible existence of PN or response classes, we described each STSA as a vector of amplitudes (time bins = 0.5ms) and used simple quantitative tests on all vectors so described to search for possible clusters (Fig 5B-D). Using PCA we found that 90% of the variance could be accounted for by the first two components. A plot of all 97 STSAs for the oct condition in the space defined by these components (1 and 2) is shown in Figure 3.5B. On each axis we also plotted a frequency distribution of each value. Similar distributions were observed for either odor. We noted that the distribution of STSAs did not suggest obvious groupings. Hierarchical clustering applied to this data-set (see Methods) confirmed this impression (Fig. 3.5D). We thus conclude that PNs do not fall neatly into clusters of neurons with predictable responses to odors.

The fact that such a large fraction of the variance across STSAs could be captured by only two principal components suggested that the nature of PN responses can be described by a small number of variables. By plotting the two PCs (Fig. 3.5C) and examining their structure, we observed that PCs 1 and 2 approximate a summation and a difference (derivative) operation,

respectively. A simple interpretation of this observation is that PNs might be distinguished by the

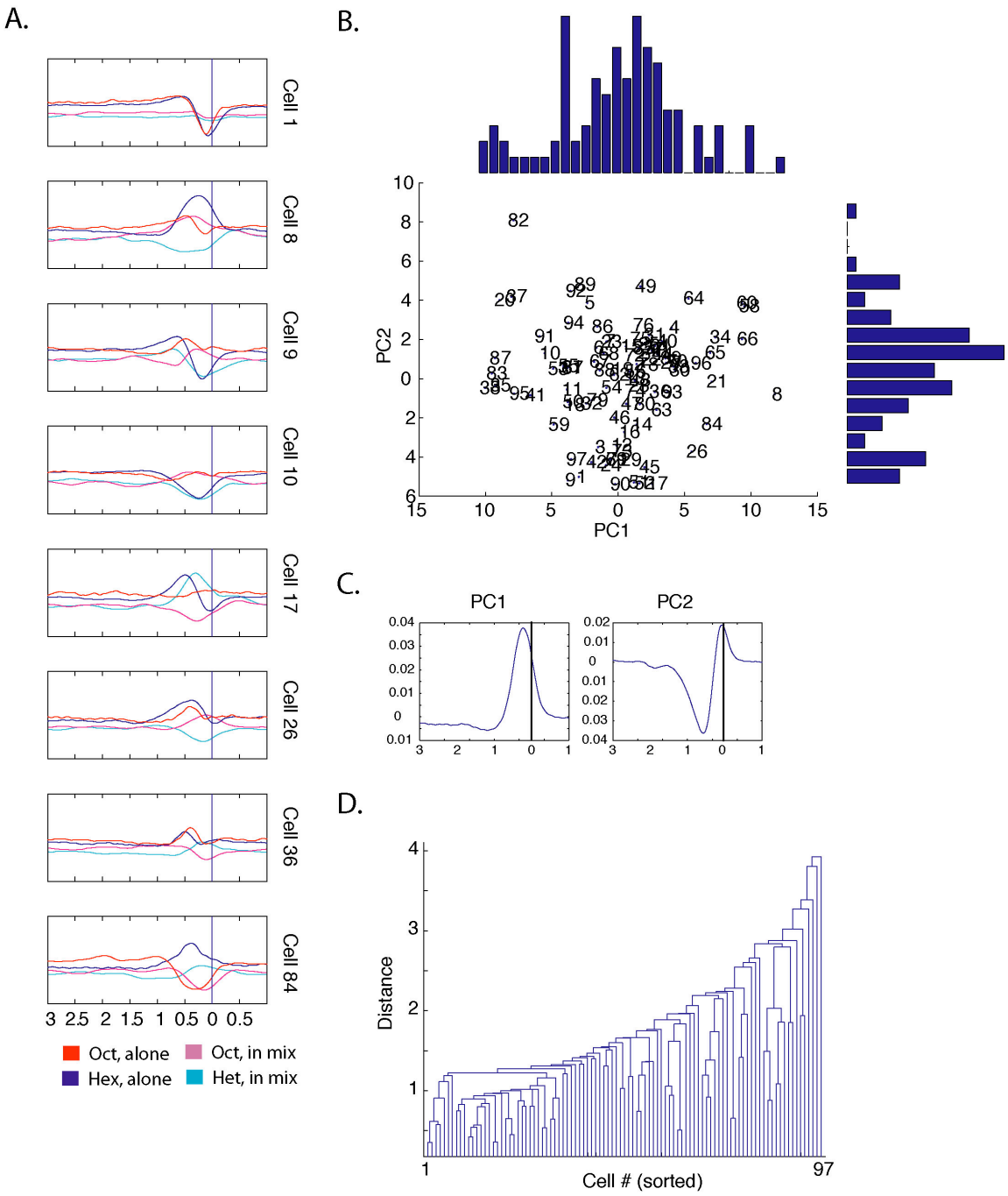

Figure 3.5, PNs have odor specific responses that are distinguished by a limited number of factors.

A. 9 representative PNs highlight the diversity in a single PN's response to two different odors. For more information on data collection and STSA generation see Methods. **B**. STSAs of all 97 cells analyzed in 6000-D (time bin=0.5ms) space to identify groups of clustered STSAs. PCA applied to reduce dimensionality and visualize the data. A large fraction of the variance can be accounted for by only 2 PCs: PC1= 62.9%, PC2=23.6%. The results were binned along the x or

y-axes into 30 or 16 bins, respectively. **C**. PCA waveforms that correspond to the first (left) and second (right) principal coefficients in B. **D**. Results of hierarchical clustering using same STSA data set.

relative degrees to which they measure the average odor concentration (PC1) or sense transitions between different odor states (PC2). Yet, because the coefficients corresponding to each PC differ across odors for each PN, these properties appear not to be PN specific. Rather, we can say that for each odor (in the set we tested) there exist some PNs with static properties, some with sensitivity to change, and yet others with combined properties, but that the precise distribution of these properties across the PN population changes with each odor. While apparently complex and inefficient (and incompatible with the traditional notion of cell classes), this non-static distribution of information may not be of any functional consequence if the PNs' targets receive convergent input from sufficiently large subsets of PNs: for each stimulus, there will always be some PNs to provide the relevant features about it.

3.2.4 PN Trajectories Corresponding to Rapidly Varying Stimuli

Whereas our ability to record simultaneously from numerous PNs continues to improve, we still cannot record all of the 830 AL PNs at once. Yet, by analyzing the activity of reasonably large sets of PNs selected randomly (~10% of the entire population) recorded under identical conditions, we can get qualitative and quantitative insights about the nature of odor representations by PNs in this system. Sets of 9 to 23 PNs were sampled from all regions of the AL at recording sites selected during each experiment for the quality of baseline activity, responsiveness to odor presentations, and stability. PNs were included in the analysis only if they exceeded a set of equally applied inclusion criteria (see Methods). 97 PNs met these criteria. We analyzed the PNs' responses as time series of population vectors (single trials or averaged over nine trials) using non-overlapping time bins locked to the start of the trial (Stopfer et al., 2003) and plotted the trajectories they defined after dimensionality reduction (using principal

components analysis, PCA) (Fig. 3.6A). The first 3 principal components (PCs) captured between 30 and 40% of the variance in the data, similar to results on single pulses with a different dataset (25-40% of variance in first 3 PCs, (Mazor and Laurent, 2005)). Prior work has shown that the downstream decoders of PN output in the mushroom bodies, the Kenyon cells

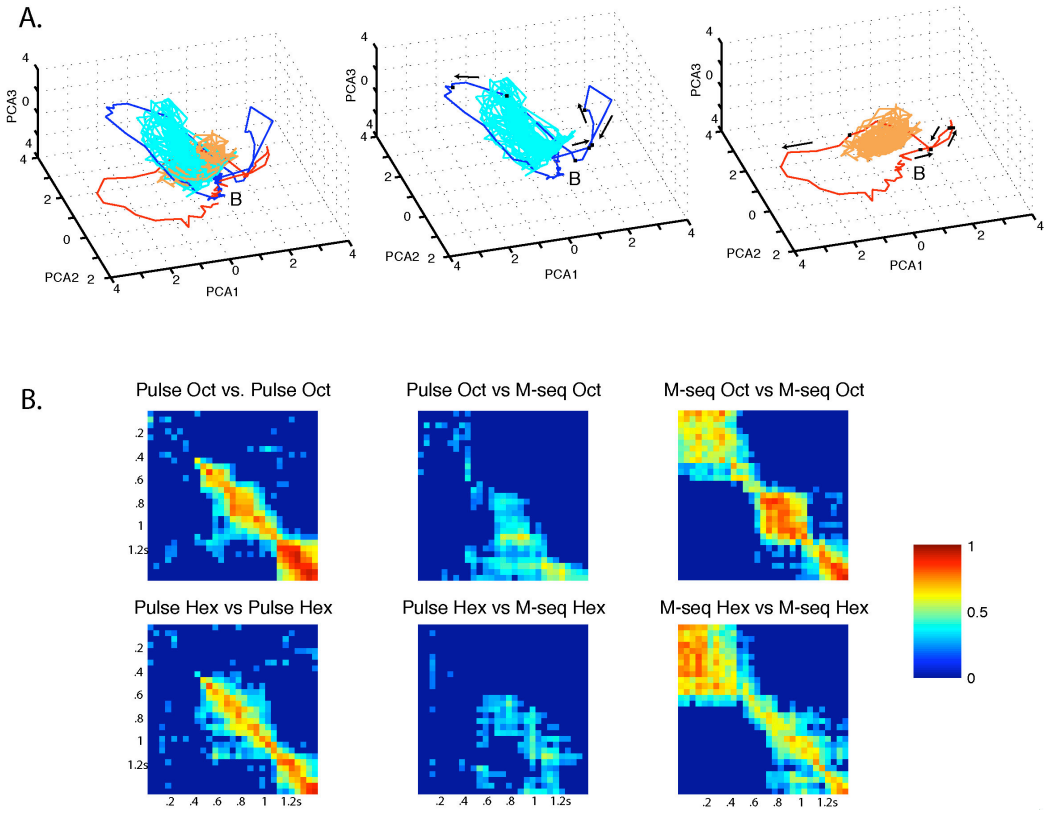

Figure 3.6, PN ensemble responses to rapidly varying and pulsed stimuli.
A. Ensemble trajectories for 97 PNs to single pulse (oct = dark blue, hex = red) and M-sequence (oct=light blue, hex = orange) stimuli. Trajectories computed in 97-D space, and PCA performed to reduce dimensionality for display. PCA axes calculated using 2.4s of data from single pulse stimuli (oct and hex conditions) starting 200ms before any PN response was detected (from 5 to 7.4 s). 50s (from 50 to 100s) of M-sequence data was subsequently plotted into that coordinate system. The following variance was accounted for by first three PCs: PC1= 12.47%, PC2 = 9.51%, PC3 = 6.79%. **B**. Correlation plots between ensemble responses of different odor stimuli. 97-D ensemble vectors are compared in 50ms increments. The 1.4s of data shown corresponds to 400ms pre-odor→500ms odor→500ms post-odor for single pulse conditions and 400ms pre-odor→600ms odor→400ms post-odor for M-sequence stimuli. All vectors are 3-trial averages. Correlations between identical stimuli are between different 3-trial averages (i.e. trials 2-4 vs. trials 5-7).

(KCs), integrate PN output over periods corresponding to about 1/2 of an oscillation cycle (oscillation cycle period is approximately 50ms) (Perez-Orive et al., 2002). Our time step was thus chosen to be 50ms, as previously chosen (Broome et al., (submitted); Mazor and Laurent, 2005; Stopfer et al., 2003). Quantitative analysis (Euclidian distances, correlations) was always carried out in the full 97-D space.

Figure 3.6A plots the trajectories corresponding to each odor in the two conditions (single pulse and M-sequence). The trajectories for both odors are overlaid in the leftmost panel. The trajectories corresponding to each odor are represented alone in the other two. PCA was carried out on the single-pulse data; both pulse and M-sequence data were then projected in the space of the first 3 PCs so calculated. We observed that the trajectories corresponding to M-sequence stimuli were both qualitatively related to and yet different from those evoked by single pulses of the same odor (Fig 3.6A). Note first that the long initial and terminal looping segments of the pulse trajectories are absent from the trajectories corresponding to M-sequences. This is a consequence of the fact that initial conditions were different in both cases: single pulses were delivered at 20s inter-trial intervals, allowing recovery of PN activity to baseline after the end of each pulse. We know from previous work that complete recovery can take many seconds (Mazor and Laurent, 2005). M-sequences, by contrast, lasted 105s, had inter-pulse intervals that lasted 2s at most—all intervals were distributed between 0 and 2s, with most much too short to allow recovery. In addition, successive trials (ten repeats of the same M-sequence) were delivered with no significant recovery period between them; the system (i.e., the AL) was thus activated intermittently at a rate too high to allow recovery. Fig 3.6A plots 50s (interval 50-100s) of the 105s in each M-sequence, and thus represent the evolution of the PN vector during these intermittent stimuli.

Second, and more importantly, the trajectories corresponding to the M-sequences were confined to some odor-specific volume, traversed by the single-pulse trajectories corresponding to the same odor. Thus, rather than looping from and back to baseline state, the M-sequence

trajectory remained off baseline and moved around some mean position, different from baseline and different for each one of the two odors. Previous work on the encoding of odor concentrations showed that different concentrations of the same odors evoke related PN trajectories that together, form low-dimensional, odor-specific manifolds (Stopfer et al., 2003). Whether and how the complex trajectories observed in response to M-sequence stimuli (Fig 3.6A) correspond to those concentration manifolds is as yet unknown, but it is reasonable to hypothesize that they are related. Indeed, electronic nose profiles (Fig. 1) clearly show that odor concentration profiles during M-sequence stimulation are far richer and contain more modes than those that correspond to single pulses. In summary, PN vector trajectories defined during rapidly intermittent stimuli move in a self-contained volume of PN space, (i) away from baseline, (ii) consistent with (i.e., overlapping with) single-pulse trajectories (Fig 3.6A), and (iii) consistent with our knowledge of concentration coding in this system (Stopfer et al., 2003).

Figure 3.6B attempts to quantify, in the original 97-D space, the qualitative differences illustrated in Figure 3.6A. We performed cross-correlations between 3-trial averages of the single pulse period displayed in Figure 3.6A and segments of equal length, taken from the M-sequence with the same odor. The M-sequence segments were selected to contain an odor pulse of 600ms, bounded by two odor-off epochs of at least 400ms each. (The selected single pulse segments contained a 500ms odor pulse preceded by 400ms without odor and followed by 500ms without odor.) The traces on which cross-correlations were computed thus differed in two main respects: (i) the odor pulse lasted 500ms in the single pulse condition and 600ms in the M-sequence; (ii) more importantly, the past history (before t = 0) differed across the two conditions: for single pulses, the odor had been off for 20s; for M-sequences, the odor had been pulsed on and off many times. These cross-correlations thus illustrate the differences (of PN population behavior) that result from different past histories. These differences are expressed in the fact that correlations were significantly lower for the [pulse x M-sequence] correlations (central matrices, Fig 3.6B) than for the [pulse x pulse] or [M-sequence x M-sequence] correlations (left and right matrices,

Fig 3.6B). This low correlation reflects the fact that baseline is not reached during the short inter-pulse intervals found in an M-sequence, as seen qualitatively in the trajectories in Fig 3.6A. However, while [pulse x pulse] correlations are low in the period preceding odor onset, as shown previously (Stopfer et al., 2003), [M-Sequence x M-sequence] correlations are high and

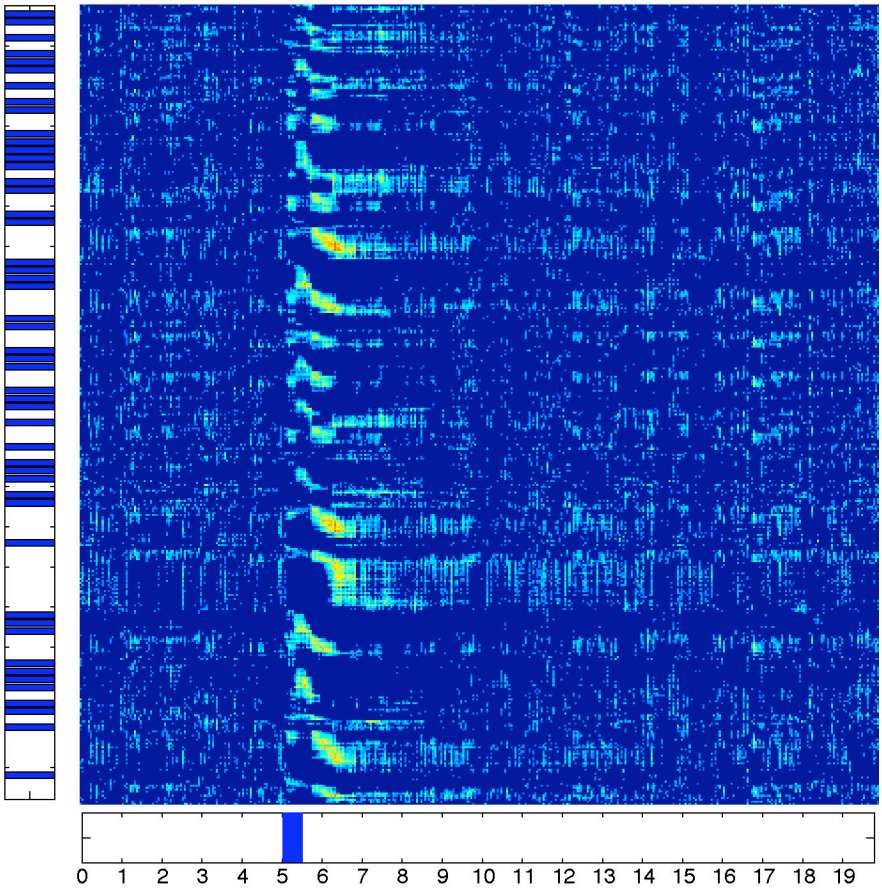

Figure 3.7, PN ensemble responses to rapidly varying and pulsed stimuli across a large window.
A. Cross-correlation between 20s oct M-sequence (boxed region Fig. 3.9A) and 20s single pulse. Odor presentation patterns for M-sequence and single pulse are shown on left and at bottom, respectively.

the correlation width is broad (~400ms), indicating that these trajectories occupy a similar state between odor pulses, but one which is distinct from pulse conditions. During the common odor pulse (t = 400 to 900ms interval), the difference between these two conditions [pulse x M-sequence] is the most pronounced, indicating that PN vector trajectories following odor onset

depend on past history to beyond -400ms. A correlation of the entire M-sequence with the single pulse stimulus did not yield any region that was more similar than the one used (Fig. 3.7).

3.2.5 Reconstructing Odor Concentration Profiles

We next studied the effect of PN number on an observer's ability to reconstruct a rapidly varying odor stimulus (M-sequence or combination of M-sequences). Our goal was to reconstruct the electronic nose profile (related to odor concentration profile and to the EAG; Fig. 3.2) caused by intermittent delivery of one odor from the activity of subsets of PNs (of varying sizes) and the knowledge of their STSAs to that odor. We used PN responses as input to a spike-train decoding method, as described previously with visual stimuli (Bialek et al., 1991; Warland et al., 1997). Reconstruction is carried out by (i) convolving each neuron's single-trial raster response (to a given M-sequence stimulus) with its neuron/odor specific STSA and (ii) subsequently summating the resulting waveforms across all neurons (Fig 3.8A). This "reconstructed stimulus" was then correlated with the corresponding actual stimulus (EN recording) to quantify the quality of the reconstruction (see Methods). Given our observations about PN tuning reported above (i.e., the absence of apparent response classes), we made no assumption about PN tuning and constructed subsets of 10, 25, and 50 PNs (1,000 subsets for each size), with random selection of PNs among our set of 97 PNs. Our results are divided into two groups: (1) single odor and (2) multi-odor reconstructions. The STSAs used in the single- and multi-odor cases were calculated separately with each corresponding stimulus type to account for our finding that individual PNs' STSAs can differ when odors are presented alone or interwoven with another.

Figure 3.8B illustrates three randomly selected reconstructions of the M-sequence with the odor oct using 10, 25, and 50 PNs. We found that we could create reconstructions that closely matched the EN recording using relatively few PNs (as low as 10), that the best reconstructions

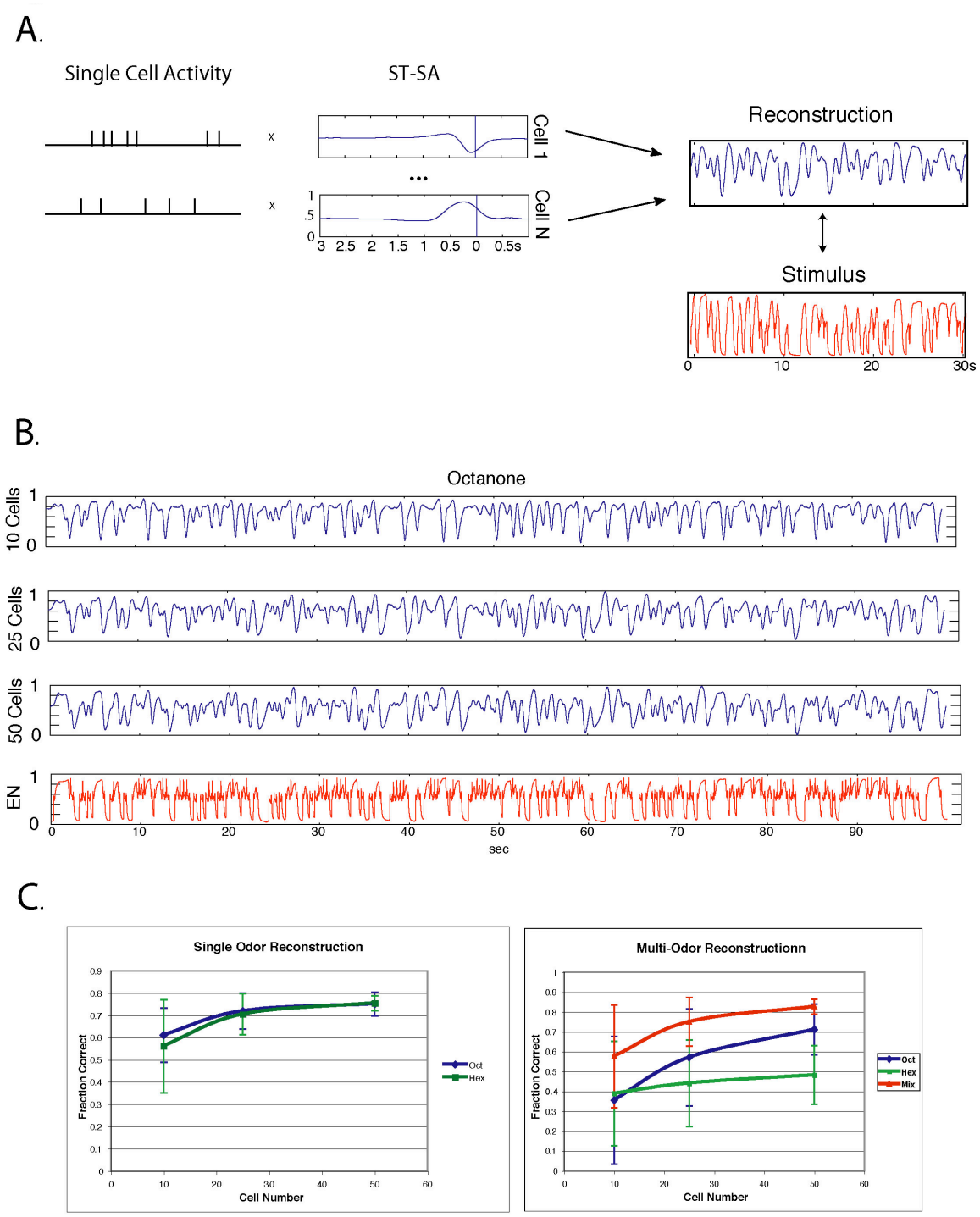

Figure 3.8, A reconstruction of odor concentration over time.
A. A summary of the spike-decoding method adapted from Bialek et al., 1991. The spike trains from all cells (or random subsets of the 97 cell set) for each odor condition in a given trial were convolved with the corresponding cell/odor STSAs and summed together. This procedure was repeated for each trial and the result was averaged. **B**. Representative examples of 10, 25, and 50 cell random subset reconstructions for oct M-sequence. Actual odor concentration variation (EN) is shown below. **C**. Summary figure of 1000 random subsets for reconstructions of different sizes.

Single odor condition applies to oct and hex conditions. Multi-odor condition applies to oct+hex. Mean value is plotted; error bars are at 2SDs from the mean.

(peak of each set of 1,000) for the 10, 25, and 50-PN subsets were comparable, but that the mean quality of the reconstruction increased and the variability decreased across the 1,000 random subsets as the number of PNs used was increased (Fig. 3.8C). We then examined the components of those sets that produced the best reconstructions from 10 PNs and discovered that the primary shared characteristic was a diversity of STSA waveforms (both on and off), in agreement with results in other systems (Warland et al., 1997). Thus, combining more PNs increases the probability that a set with diverse properties will be selected. Because STSAs are not stable across odors for each PN, the selection of one particular set of 10 PNs to reconstruct a pulse profile with one odor is not optimal for the reconstruction of a stimulus with a different odor. We conclude that large PN sets are therefore highly advantageous.

With two-odor stimuli, the average quality of the reconstruction across all subsets increased and variability decreased as we increased the number of PNs used for the reconstruction. Reconstruction quality of the two-odor profiles in a combined-odor stimulus, however, varied over the length of the time series; when analyzed piecewise, reconstruction was best for the epochs of combined odor pulses (and worst for the periods of single-odor stimulation). This can probably be ascribed to the aforementioned dependence of STSAs on the conditions in which they are initially calculated (single- vs. multi-odor conditions); better reconstructions would require adaptive STSAs matched to recent history.

3.2.6 Reconstructing Odor Identity Profiles

While the spike–decoding method described above allowed us to reconstruct odor concentration profiles over time, it is based on prior knowledge of the odor identity and on the appropriate choice of the corresponding STSAs. This method is obviously unsuitable to identify the different chemical identities in an unknown, potentially composite stimulus. Here we used a

different method (described below) to reconstruct odor identity profiles in single- and multi-odor stimuli from PN ensemble activity. This method relies on the assumption that each sampled instantaneous PN vector (measured, as above, over a 50ms time bin) can be assigned to a particular odor identity on the basis of its distance to a set of reference vectors. Biologically, such reference vectors can be thought of as the normal set of PNs that provide inputs to individual odor classifiers, the Kenyon cells of the mushroom bodies (Laurent, 2002; Perez-Orive et al., 2002). Again, we evaluated the quality of reconstruction using small to large subsets of PNs (10, 25, 50, and 75 PNs, chosen randomly, 1,000 sets per set size) and the complete 97-PN set. We used a clustering algorithm (see Methods) based on multiple-discriminant analysis (MDA), a technique similar to multivariate analysis of variance (Duda et al., 2000). MDA acts to minimize the distance within user-defined clusters of template points while maximizing the distance between these sets and has been used previously to discriminate odor vectors (Broome et al., (submitted)). Each PN's single-trial responses were divided into 50ms bins, for reasons explained above, and aligned with the start of the trial. Fifteen templates, each composed of 3 individual time bins, of "pure-odor" activity (oct, n=5; hex, n=5; oct+hex, n=4; baseline, n=1) were constructed across time periods when each odor was known to be present—the same periods used for the correlation plots shown in Fig. 3.6B. These templates were used to calculate the discriminant functions that were then applied to the test vectors. Collectively, these training/template/reference vectors made up <1 percent of all vectors recorded in each M-sequence trial.

Test vectors were then classified piecewise, time bin by time bin, and assigned to the pure odor closest to it based on Euclidean distances between each test vector and the 4 template cluster centers. Because each test vector was forcibly assigned to one of the 4 templates, some members of a similarly classified set could be closer to their template center than others. To assess the quality of our reconstructions, we compared the "consensus activity" profile (see below) to the time series of valve openings and closings corresponding to each odor. (We could not use the EN recording to assess the quality of the reconstructions because our sensors are not

sufficiently odor selective and record only the total odor concentration.) “Consensus activity” was a simple assignment of odor on the basis of observation frequency: if the test vector in a given time bin was classified as odor *A* in 6 or more of 9 trials, it was classified as *A*. Consensus activity values could be: oct, hex, oct+hex, no odor, and unclassified.

Figure 3.9 shows our classification results using all 97 PNs to reconstruct two single-odor M-sequences (hex and oct) and one combined (superimposed M-sequences: mix) condition. The entire trial duration is shown in panel A (Fig 3.9), and short segments are zoomed in in panel B. Each vertical tick mark represents, by its color, the assignment of a single-trial, 50ms PN vector to one template; 9 successive trials are analyzed, and the results for all 9 trials are displayed as a vertical stack (1st trial at bottom) forming a multi-color band. Individual trial assignments are visible in B. These classifications are to be compared to the corresponding stimulus, indicating valve opening and closing times for each odor (oct=blue; hex=green; mix=red).

The quality and variability of these reconstructions can be best assessed in Fig 3.9B. For single odor sequences, for example, it is clear that odor assignments become increasingly accurate as pulse length increases. For odor oct, classification was best with late response vectors (dark blue, explaining the delay between stimulus and classification), while for hex, early and late classifications seemed equally likely. For mixture conditions, early classification was excellent, provided that the overlap lasted long enough. These discrepancies may be due in part to the particular PN identities in our recorded set and to its relatively small size (<15% of all PNs). We next examined the effect of PN set size on the reconstruction.

Figure 3.10A illustrates the importance of PN set size on reconstruction quality (measured by comparing consensus, as defined above, with valve opening sequence). Panel A shows representative examples (short segments for illustration purposes) using one 10-, 25-, and 50-PN set (out of 1,000 analyzed for each set size) for the reconstruction. As observed with the spike-decoding method and concentration profile reconstruction (Fig. 3.8), increasing the number

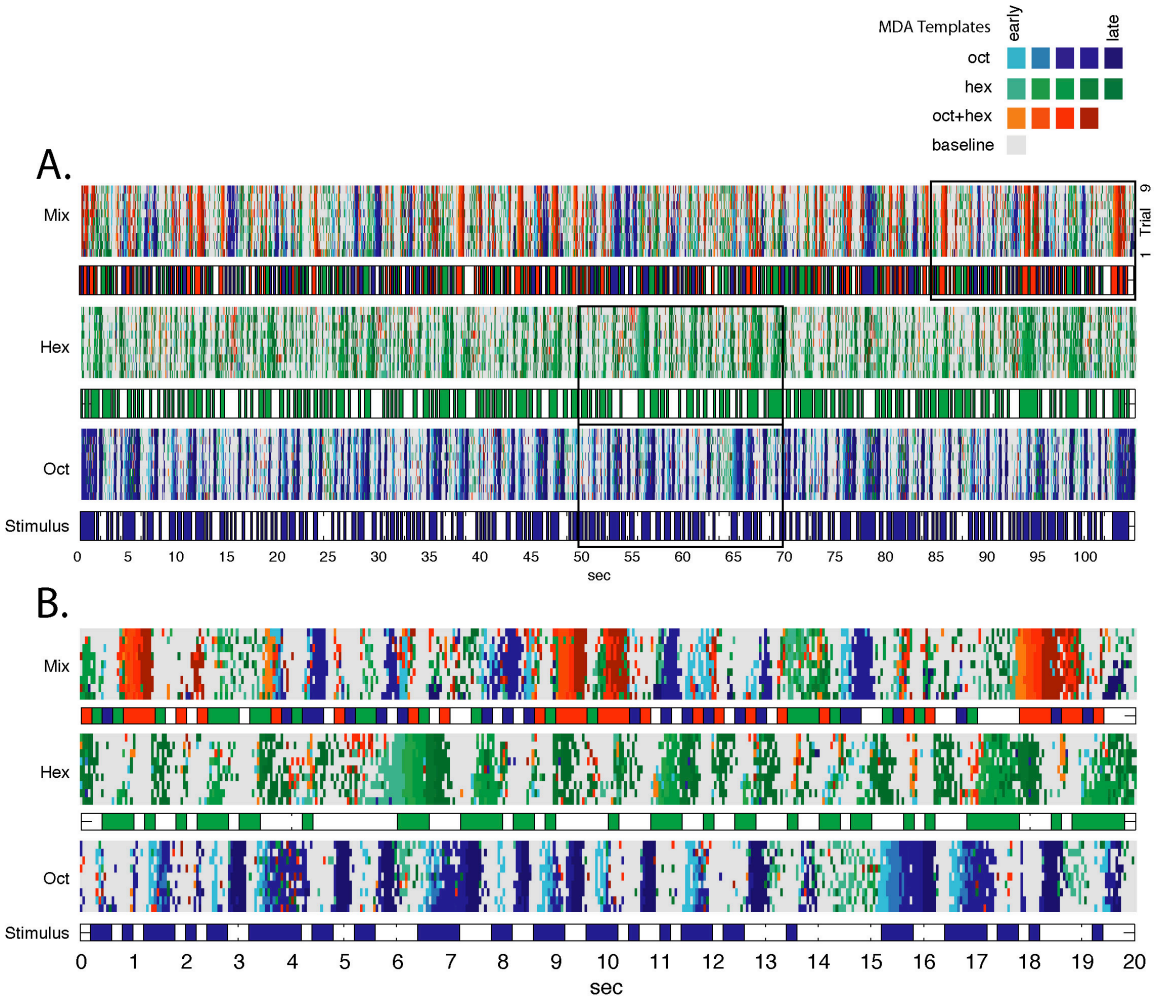

Figure 3.9, Template matching method for reconstructing of odor identity in a rapidly varying stimulus.

A. 97-D 50ms time slices for individual trials were assigned to one of four categories (oct→blue, hex→green, oct+hex→orange, and no odor→gray) based on their proximity in Euclidean distance to the center of template clusters. Template clusters contained time slices from periods during the 105s rapidly varying stimuli (<1% of total) when long bursts of a specific odor were known to be present. The distance within these clusters was minimized and the distance between these clusters was maximized using MDA prior to classification (see Methods). The actual stimulus, represented by valve opening times, is shown underneath 9 reconstructed trials. **B**. An expansion of the boxed regions from A.

of PNs used for the reconstruction increased the average quality among the 1,000 random subsets (Fig. 3.10B). Again, the very best sets in each size group were less different (though to a lesser degree than with concentration profile reconstructions) across size groups than their means.

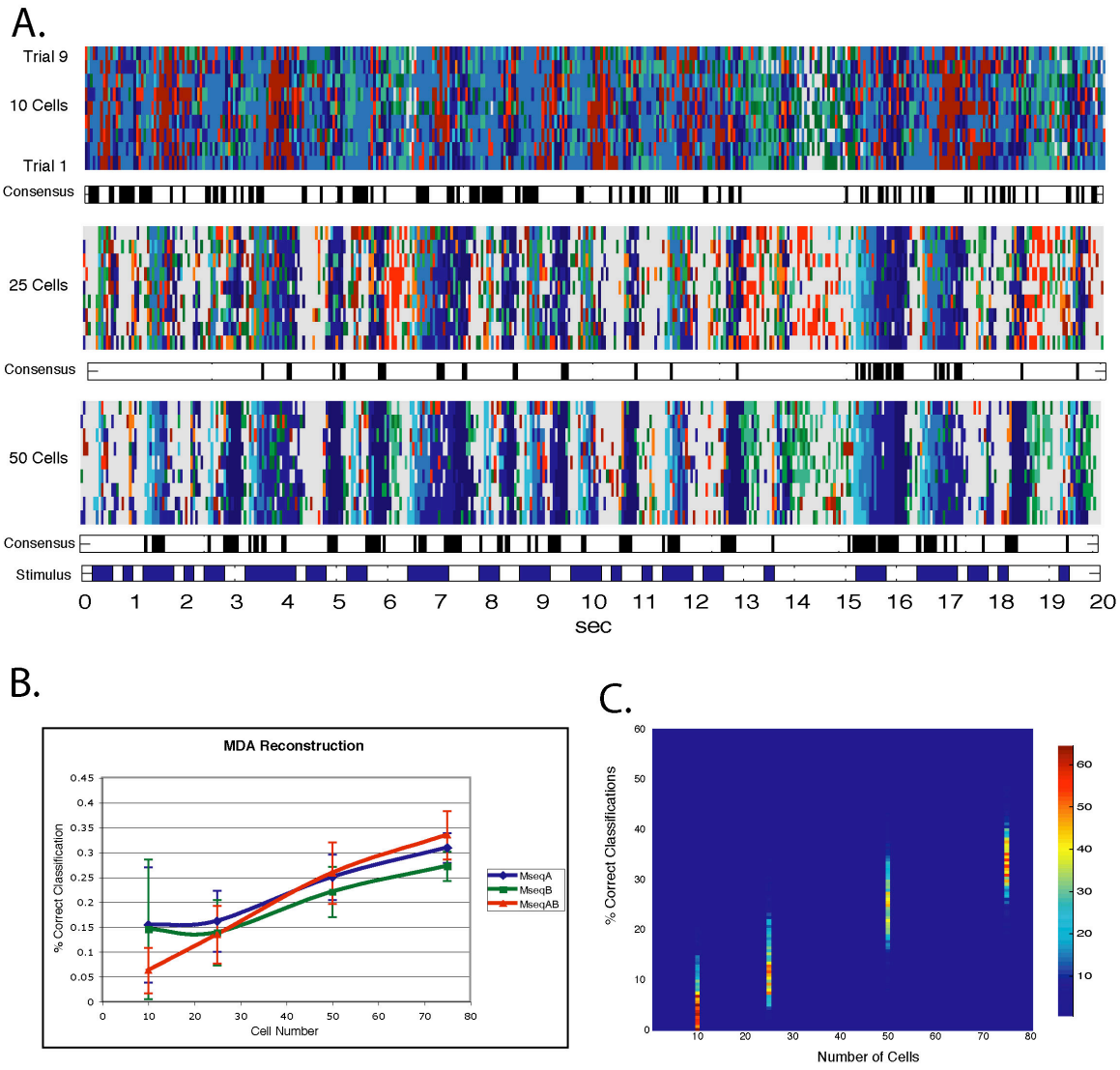

Figure 3.10, Effect of varying cell number of reconstructions of odor identity
A. Representative examples of oct M-sequence odor identity reconstruction involving 10, 25, and 50 cells. Consensus values represent the activity in 6/9 trials classified 5 ways (oct, hex, oct+hex, no odor, not classified). Color values correspond to those of Figure 3.9. **B**. Summary results for 1000 random 10, 25, 50, and 75-cell subsets from the 97-cell set. Average value is displayed with 2SDs from the mean indicated by error bars. **C**. A color plot showing how the quality of the reconstructions is distributed among the various 1000 random subsets. Color bar indicating the number of reconstructions at each quality level is shown at right.

Nevertheless, the average trend was a consistent improvement of the reconstruction with set size. The frequency distributions of reconstruction quality scores, binned by set size, are plotted in Figure 3.10C. Both plots (B and C) also indicate that classification success failed to saturate at n=75 PNs, our largest set size. Note, however, that the correct-classification rates are, even for the

larger PN set size, lower (35%, Fig 3.10C) than when our task was to reconstruct the stimulus concentration profiles (often as high as 80% with similar set size, Fig 3.8). This suggests that sampling larger numbers of PNs, if those are chosen randomly, should further improve classification in this odor identification task. Independent data on PN-Kenyon cell connectivity in locust (Kenyon cells are the decoders of PN output) indicate that individual Kenyon cells contact 400 PNs on average (R Jortner, SS Farivar, & G Laurent, in prep).

Finally, we evaluated the composition of the top ten 10-PN identity reconstructions to see if specific PNs were overrepresented (Table 3.1). While the random sets that we chose from the 97-PN data set represent only a very small fraction [1,000/(97choose10)] of the possible sets, we observed that no PN was overrepresented in the best 10, suggesting that the ability of a decoder to extract information about odor identity from the PN population is contained within the distributed and cooperative activity of many PNs across the AL and not by a few highly tuned cells.

Odor identity reconstruction, oct+hex, Top 10 Sets

Rank	Value	Set Components
1	0.3019	8 13 21 24 28 43 60 62 67 81
2	0.2288	10 11 13 29 35 48 50 60 86 91
3	0.2274	7 17 35 44 47 49 51 67 77 91
4	0.2053	5 6 11 15 16 22 31 51 57 59
5	0.2029	6 8 16 42 68 74 76 80 82 84
6	0.2029	38 44 47 55 62 73 74 83 93 94
7	0.201	4 16 27 42 45 51 58 67 87 90
8	0.1981	3 6 9 10 31 61 86 87 91 93
9	0.1971	1 16 21 32 41 45 46 51 59 79
10	0.1952	21 24 29 42 52 61 71 82 90 93

Table 3.1, Composition of the top ten odor identity reconstructions for oct+hex.
Rank, Quality score (0 to 1), and set components for the top ten odor identity reconstructions. Set component number indicates cell number in 97-cell data set.

3.3 Discussion

We compared PN responses between single pulse and rapidly varying odor stimuli; paradigms that were either similar to or more complex than those used previously by us (Mazor and Laurent, 2005; Perez-Orive et al., 2002; Stopfer et al., 2003; Stopfer and Laurent, 1999) or other laboratories (Brown et al., 2005; Christensen, 1988; Vickers et al., 2001). In designing our rapidly varying stimuli we sought to create naturalistic patterns that could test a complete range of responses. Accordingly, we compressed 512 1.8s odor "words" composed of 200ms on/off pulses using M-sequences; these constructs produce trains of binary patterns that are both random and maximally compressed.

We recorded responses from 97 PNs, sampled from all regions of the AL, in sets of 9-23 over the course of 8 experiments. All of the experiments were conducted under rigidly controlled conditions so that the results might be pooled together, creating a data set that collectively represented the activity of about 12% of the AL. In all experiments we simultaneously monitored the odor stimulus using an electronic nose sensor (Freund and Lewis, 1995; Matzger et al., 2000). We then analyzed the data both with individual PNs and collectively as a time series of PN activity vectors sampled every 50ms across all 97 PNs.

3.3.1 Stimulus Structure and PN Properties

Single cell PN responses were qualitatively similar for both single pulse and M-sequence stimuli; cells responded with periods of inhibition or excitation, relative to basal firing rate, in an odor specific manner, regardless of how rapidly the stimulus was presented. High precision PN responses, demonstrated previously for single pulse stimuli (Perez-Orive et al., 2002; Stopfer et al., 2003), were also seen with M-sequence stimuli where some cells exhibited <50ms jitter across 9 trials. This precision is consistent with our knowledge of activity and response precision in the downstream decoders of PN activity, the KCs (Perez-Orive et al., 2002). For example,

previous work has demonstrated that the jitter of some KC responses (to simple odor pulses) is commensurate with our present observations (Perez-Orive et al., 2002).

Patterned and intermittent stimulus sequences proved very useful in revealing PN properties previously poorly characterized. First, single PN spike-triggered stimulus averages contained significant modulation to about 2s prior to spike time. However, some effects of past history on PNs probably extend well beyond this: for example, experiments using overlapping odor pulses identified interactions up to about 3s interval between pulses (Broome et al., (submitted)). The conditions of these two-pulse experiments were different, however, from those described here in important respects: pulses were short (500ms) and were presented only once per odor and trial. Interactions between odors could thus be observed during the off-transient phases—relaxation of PN trajectories to baseline (Mazor and Laurent, 2005). In the present (M-sequence) experiments, by contrast, the PN system was not allowed to relax after each odor pulse and spent most of its time in an activated state. This difference is seen clearly, for example, in the PN trajectories corresponding to single and M-sequence pulses (Fig. 3.4A).

Second, we observed that PN global synchronization as assessed by LFP power profiles (5-50 Hz band) was greatest at times corresponding to pulse offset during M-sequence stimuli. During single-pulse stimulation, oscillatory power is higher following pulse onset than offset (Mazor and Laurent, 2005). Again, these differences are probably explained by the fact that, under M-sequence stimulation, the system spends little time in "relaxation state." Indeed, relaxation is the mode during which mean PN firing rates are the highest and often well exceed the 20 Hz of oscillatory coherence measured during an odor pulse (Mazor and Laurent, 2005). In most PNs where fast off-transient activity is observed, it is associated with apparent rebound from inhibition: the highest PN firing rates are unsynchronized across PNs and are generally observed following a phase of deep and sustained inhibition after odor offset (Laurent et al., 1996; Mazor and Laurent, 2005). The reasons for this behavior are as yet unknown; it could be, for example, that fast inhibition by LNs — the negative feedback elements underlying PN oscillatory

synchronization (MacLeod and Laurent, 1996) is less effective during off- than during on-transients. Yet, these observations may explain why pulse offset times are associated with high synchronization during M-sequences: during such stimulation, PNs were, by experimental design, not allowed to spend much time in relaxation mode and were thus prevented from firing in the asynchronous and high-frequency modes associated with slow relaxation. Given the importance of PN synchronization for decoding by Kenyon cells, the PNs' mushroom body targets (Laurent and Naraghi, 1994; Perez-Orive et al., 2002), we predict that KC responses should be highly correlated with off-phases during rapidly varying intermittent stimuli. This remains to be tested experimentally. In conclusion, we observe that the response properties of PNs are qualitatively similar when examined with single pulse or M-sequence stimuli, but that some aspects of their properties are revealed, or masked, by using only one stimulus set. These differences are explained by the relative time scales of the stimulus variation and the response kernels of the PNs: a PN's response depends, to a significant extent, on about 3s of past history.

3.3.2 Are There PN Classes?

First, PN responses are low dimensional. Most PN spike-triggered stimulus-averages could be reconstructed with good accuracy using a simple weighted combination of two component waveforms. This can be taken to suggest that a PN's response to an odor is shaped by relatively simple circuits, comprising excitatory and inhibitory arms, and that these basic circuits are similar across the PN population. It is known that PNs receive direct excitatory inputs from odorant receptor afferents (Wehr and Laurent, 1999) and inhibitory input from local interneurons (MacLeod and Laurent, 1996). These two sources constitute the shortest paths from receptors to PNs. We also know, however, that PNs can be affected by odor stimuli through more complex pathways: although PNs do not seem to be directly interconnected with one another within the antennal lobe (R Jortner, SS Farivar, & G Laurent, in prep), they are heavily interconnected with LNs (R Jortner, SS Farivar & G Laurent, in prep), and LNs are interconnected among themselves

through extensive dendritic arborizations (Leitch and Laurent, 1996). Because locust local neurons do not produce sodium action potentials and assuming that they are like other well-studied locust nonspiking local neurons, they may release neurotransmitter tonically (Burrows, 1979; Laurent, 1993); if so, simple pathways through two LNs in series can, in principle, also easily mediate excitation by disinhibition. Unfortunately, nothing in the STSA waveforms allows one to weigh the different contributions of these potential mechanisms.

Second, the weight parameters used to model the STSAs of one PN were generally different from one odor to the other and they were not correlated across PNs. Hence, predicting the response of one PN to one odor from the knowledge of its response to the other is not possible. Conversely, knowing that two PNs have (for example) antagonistic responses to one odor says nothing about whether their responses to a second odor are likely to be also antagonistic. This suggests that the functional paths linking the elements of this antennal lobe network vary with each stimulus, an observation consistent with rich interconnectivity.

Third, our results failed to reveal particular functional classes of PNs. Quantitative analysis of their responses and STSAs revealed that most PNs are, in a statistical sense, like most others. What makes each PN unique is its own particular set of responses to a set of odor stimuli. Studies with other sensory systems (Bialek et al., 1991; Warland et al., 1997) have shown that sampling from sets of complementary response types is beneficial to stimulus reconstruction (by an observer). Our present observations with PNs, however, indicate that such strategic sampling (by their natural decoders, the Kenyon cells) is not possible here. They suggest an alternative, and possibly simpler strategy: that a Kenyon cell connect to a subset of randomly chosen PNs, provided that this subset is sufficiently large to contain many complementary response types. This solution seems consistent with our separate estimations that each KC is connected to about 1/2 of the entire PN population (R Jortner, SS Farivar, & G Laurent, in prep). That these connection sets should be very large has at least two advantages: (i) If the distribution of connections between PNs and KCs is random (or pseudo random), it ensures that each KC samples a set of PNs that is,

on average (over all KCs), maximally different from all the others. This ensures specificity and, after choosing an appropriate spike threshold, sparseness (Perez-Orive et al., 2002). (ii) Given our observation that reconstruction quality increases monotonically with PN set size (Fig 3.8, this thesis) and that it fails to saturate at n=75 PNs, large connection sets should ensure that reconstruction quality improves further.

3.3.3 Rapidly Varying Stimuli vs. Single Pulses

Previous work has shown that odor representations can be described as odor- and concentration-specific trajectories, or time series of PN activity vectors (Broome et al., (submitted); Mazor and Laurent, 2005; Stopfer et al., 2003)); sampling frequency for these PN vectors is chosen so as to match the period of a 20-30 Hz oscillation evoked across PNs by odors. This period (50 ms) also corresponds to the maximum time over which the downstream decoders of PN activity, the Kenyon Cells (Perez-Orive et al., 2002), can summate their PN input. It is thus a functionally relevant time scale, given by the natural decoders of PN output. At odor onset, these trajectories rapidly proceed away from a noisy baseline state ("on transient"), reaching maximum distances (from baseline and from other odor trajectories) in ~100-300ms (Mazor and Laurent, 2005). If the odor is sustained for a sufficiently long time, odor trajectories eventually stabilize after 1-2s at a noisy fixed point, where they remain until the odor is switched off (Mazor and Laurent, 2005). At odor offset the PN trajectory follows a different odor-specific path ("off transient") whose evolution is fastest at the beginning (first 300ms after odor pulse offset) and slowest as the PN population relaxes back to baseline (Mazor and Laurent, 2005). When odor pulses are too short to enable the PN population to reach an odor-specific fixed point, trajectories consist of loops away from and back to baseline along odor-specific paths. The experiments that led to these results and descriptions generally consisted of single pulses interspersed with long delays (typically 20 to 30s). Such conditions allowed the system of PNs to relax back to baseline between successive pulses.

In the experiments described here, stimuli consisted of a very large number of short pulses (200ms) delivered over 105s at inter-pulse intervals varying systematically between 0 and 1,800ms. At no point did the system have an opportunity to relax back to baseline. The population behavior we describe here and the corresponding trajectories are thus probably much closer to those encountered naturally in a freely behaving animal. Under such conditions we observed that correlations between M-sequence segments and single-pulse trajectories (of similar durations) were sometimes very low; this was particularly true for epochs corresponding to the beginning or the end of a single odor pulse. These low correlations are obviously explained by the different initial conditions in which the system was placed in each paradigm; in an M-sequence stimulus, the system was never allowed to return to baseline: the early on- and late off-transients corresponding to an isolated pulse were thus never traced. By contrast, correlations were highest with segments corresponding to the early off-transients of an isolated pulse. These segments are generally excellent (as good as the rapidly evolving on-transients) for odor discrimination in single pulses, whether or not they originate from a fixed point (i.e., whether or not the preceding odor pulse had been sustained) (Mazor and Laurent, 2005). We also observed that during M-sequence stimulation off-transients were the periods of highest oscillatory synchronization, suggesting that they were the ones being decoded by KCs. These observations thus suggest that the off-transients, i.e., the short odor-specific "response" segments that occur during inter-odor pulse intervals, may be of great significance for odor classification, learning, or recognition in behaving animals.

Our observations do not fully agree with recent related work by Brown et al. (Brown et al., 2005). In that work, PN responses were recorded during and around one to five 100ms odor pulses presented at short and constant inter-pulse intervals, and followed by a long stimulus-free relaxation period (30s) (similar to our single-pulse condition). Brown et al. report that the trajectories constructed from the activity of 117 PNs (recorded and analyzed as we did here) depended only weakly on the pulsed-stimulus conditions (number of successive pulses). We note,

however, that the space of possible pulsed stimuli Brown et al. was sampled rather sparsely (Brown et al., 2005) and in conditions that allowed full relaxation between trials. Much of their results probably rest on the stable initial condition corresponding to baseline. By contrast, our approach sampled all possible histories of stimulation in conditions such that the system could not relax between stimuli.

3.3.4 How Many PNs Should Their Decoders Sample?

Given the nature of odor representations by PN populations, how should their output be decoded by their targets, and did nature choose an optimal strategy? Several opinions on this question have been voiced already. At one extreme lies a winner-take-all hypothesis in which the target population searches across the input and identifies the PN (or PNs) with the highest firing rate (Rabinovich et al., 2000; Yuille, 1989). At the other is a hypothesis of maximally distributed representation (across neurons and time) requiring broad sampling of PN output and coincidence detection (Laurent, 2002; Laurent et al., 2001). In between are hybrid hypotheses, such as selective sampling in the input neuron population for complementary response neuron types. From a simple analytical perspective, it seems obvious that a distributed code (broadly defined) is favorable if the space of stimuli to encode is large. From a chemical and biological perspective, it seems also that broad sampling should be favorable, for natural odors tend to be blends. A system (e.g., winner-take-all) that ignores non-maximal activity also ignores all but one information-bearing dimensions. Finally, our inability to identify PN functional classes (see above) cast doubt on across-classes selective pooling strategies.

Given these simple observations, do our results provide useful information on the decoding issue? We first note that we sampled only about 12% of the PN population. While this proportion is large when compared with typical datasets used in other studies, it is obvious that our sample might have been biased. We do not think so, for the response characteristics of the 97 PNs reported here match in all respects those of over 400 other PNs used in recent related studies

(Broome et al., (submitted); Mazor and Laurent, 2005; Perez-Orive et al., 2002; Stopfer et al., 2003). PNs are tuned broadly to odors and express odor-specific temporal response patterns. There is no evidence so far that there exist, among PNs, highly selective response profiles that differ in any way from those we described here. We thus assume that those PN response profiles are typical and representative.

We tested our ability to reconstruct complex odor stimuli from PN output using two main tasks. The first was to reconstruct a concentration profile, given prior knowledge of odor identity; this prior knowledge allowed us to select the appropriate STSAs for all PNs and test for the importance of PN numbers for reconstruction accuracy. The second was to reconstruct an odor identity profile by identifying periods of odor stimulation, periods of odor silence, and by identifying the odor using measures of similarity to three possible templates (odors 1, 2, and mixture). Our reconstruction techniques (different in each case) were chosen (i) for simplicity and (ii) to inform us on the possible size and composition of PN assemblies used for stimulus reconstruction. In this approach we implicitly assume that an animal's goal is to gain, through its senses, as accurate a "view" of its sensory world and that the neurons whose responses we studied are adapted to provide or enable such a faithful view. This, of course, is a reasonable but untested assumption. Yet, we consider it useful for three main reasons: First, it is simple and quantifiable. Second, it is applied to neurons in the early olfactory system, only one synapse away from the chemical transducer array. Selectivity for high-level features is thus reasonably unlikely. Third, it is eventually testable: we know the PNs' targets (the mushroom body KCs) and their responses to the same odor stimuli can be described and compared to our "ideal observer" reconstructions.

Given these caveats, what did we learn? We learned that for each of the two tasks there always exist small sets of PNs (10 neurons only for example) whose collective activity provides as much information (and sometimes more) than that which can be collected from many larger sets (e.g., 75 PNs) of randomly selected elements. The problem, however, is that the best sets have to be selected each time—PN responses do not fall into stable complementary types—and

that this selection cannot be done without prior knowledge of the stimulus. It is thus not realistic as a biological solution. An alternative, and simple, strategy is to sample across large PN sets. This ensures that, with both concentration- and identity-profile tasks most or all PN response types are combined and good reconstructions are achieved. For concentration profile reconstruction, performance as a function of PN number clearly saturated between 50 and 100 PNs. For identity reconstruction, no saturation was observed in the range studied (10-75 PNs). This indicates that better reconstructions would occur with large PN sets, an observation consistent with independent observations on PN-KC connectivity in locust: individual KCs seem to be connected to 400 PNs (1/2 of the PN population) on average.

In conclusion, we generated reliable trains of rapidly varying and arbitrarily complex odor stimuli. Our results on the processing of these intermittent stimuli are compatible with but more complex than our earlier results on single-pulse stimuli. We found that PN response types are varied and low dimensional and that individual PNs do not fall into stable functional classes. The ability of an observer to reconstruct a stimulus improves with PN number, and decoding-schemes that rest on small cell numbers rely also on prior knowledge of the stimulus to be reconstructed. These results thus add support to a growing body of evidence that Kenyon cells, the targets of PNs in the mushroom bodies, carry out a pattern classification on PN activity vectors sampled over large sets of PNs.

3.4 Methods

Two odors were presented as either rapidly varying M-sequence patterns or single pulses while simultaneously recording extra-cellular multi-single-unit activity from groups of PNs and the mushroom body LFP.

3.4.1 Odorants

For all experiments, the odors 1-hexanol and 2-octanone (Sigma) were diluted 1/100 in mineral oil (J.T. Baker) and stored separately in 60ml scintillation vials. The odor vials were produced fresh for each experiment. Desiccated, filtered air (460 ml/min) was passed over the headspace of the two vials, arranged in parallel, and carried the odor into a Teflon mixing tube into which the antenna and EN were placed. The input for the odor into the mixing tube was 0.7 cm from the antenna and 1.2cm from the EN, located at the end of the tube. An additional carrier air stream was passed through the mixing tube (900 ml/min). A large vacuum hose was placed behind the animal to ensure that excess odor was removed from the animal's antenna. Odors were delivered by triggers sent from a custom computer interface (LabView) using odor sequences predetermined using a custom computer program (Matlab).

3.4.2 Electronic Nose

Electronic noses were produced by spraying a mixture of carbon black, polyethylene vinyl di-acetate, and resin onto glass micropipette tubes (Warner Instrument Corp.) using an airbrush following established protocols (Freund and Lewis, 1995; Matzger et al., 2000). The thickness of the polymer varied depending on the individual application. Electrical contacts were made on either side of a 3mm exposed patch of polymer by attaching 0.5mm copper wires to the glass with silver paint. ENs were checked for their resistance using a multi-meter, and only those ENs with resistances between 50k and 500k Ohms were used.

3.4.3 Electrophysiology

Experiments were performed on 8 young (<14 days post 5th-instar) male locusts (*Schistocerca americana*) that were raised in our breeding colony. The locusts were immobilized in wax cups atop Plexiglas holders with their antennae protruding from the cup. The brain was exposed by removing the cuticle and sheath while the head was submerged in locust saline, as

previously described (Laurent and Naraghi, 1994; Stopfer and Laurent, 1999). Silicon tetrodes obtained from the Center for Neural Communication Technology were used to record PN activity (Drake et al., 1988). Silicon probes were placed into the antennal lobe at different locations for each experiment, and recording sites were chosen based on regions where high levels of PN activity could be detected. LFP activity was recorded using twisted wire tetrodes, model #CE4B75, obtained from FMC. Wire electrode tips were re-plated with gold before each experiment. LFP recording locations were chosen by placing a wire electrode into the mushroom body calyx and checking for activity in response to an odor. LFP data was collected at 3 kHz and subsequently filtered offline between 5 and 50 Hz.

PN spikes were sorted offline using custom designed algorithms (Pouzat et al., 2002) implemented in Igor (WaveMetrics). Individual clusters were included in the final data set only if they exceeded several statistical thresholds. These included distance between the cluster centers >5 SDs, <2% of spikes with <5 msec inter-spike-intervals, and <5% variation in SD waveform during the stimulus presentation period. The cells were evaluated individually for drift, determined by comparing responses to identical odors at different points in the experiment. Only those cells with minimal drift were included.

3.4.4 Data analysis

Matlab (Mathworks) was used for all offline data analysis.

For dimensionality reduction we employed principal component analysis using custom Matlab scripts. As input we used 97-D time slices, each 50ms in duration, and averaged the resulting trajectories over 9 trials.

For multiple discriminant analysis we employed custom Matlab scripts with included functions from Richard Strauss's statistics library (http://www.biol.ttu.edu/Strauss/Matlab /Matlab .htm). Training sets consisted of 15 groups (5 groups of hexanol, 5 of octanone, 4 of oct+hex, and 1 of baseline) of time slices that were taken from the ensemble (consisting of 97

cells or some subset thereof) single trial responses to a long pulse of odor from within the M-sequence odor patterns. This 0.6 s odor pulse was preceded by 1.2s without odor and followed by 0.5s without odor. 40 time slices – 4 per trial, 10 trials – represented each group. The time slice vectors were used to compute 10 discriminant functions, which in turn were used to transform the test vectors. Classification was performed by calculating the Euclidean distances of individual 10-D points from the centroid of each training group to a given test vector.

The individual trial reconstructions were combined to create a consensus reconstruction. Consensus was reached when 6 of 9 individual time bins across 9 trials were classified as belonging to the same odor; all odor sub-groups (i.e. oct early & late) were considered to be equivalent. Thus, for each time bin the reconstruction vector was assigned one of the following values: oct, hex, oct+hex, no odor or unclassified. This consensus reconstruction was compared to the valve patterns that elicited it (oct-M-sequence, hex-M-sequence, oct+hex-M-sequence) by matching the two vectors at all possible shifts and determining which shift had the greatest number of matches. This match number was reported as a percentage of the total number of time bins.

3.4.5 Calculating and Comparing ST-SAs

Raw EN recordings from individual trials of a given odor condition within a given experiment were loaded into Matlab, down-sampled by 10x, and normalized to values between 0 and 1. Depending of whether single- or multi-odor conditions were present, either the pure odor M-sequence EN or a separately recorded individual odor EN component from the multi-odor stimulus (described below) was used, respectively.

A = Time when oct is being presented alone
B = Time when hex is being presented alone
C = Time when both oct and hex are presented together
_ = Time when nothing is being presented

Given the following patterns for A and B:

```
AAA___AAA__AA_AAA_A_____ = A
BBB___B__BB__B_BBB_B___ = B
```

One can combine these two patterns to create a mixed pattern (i.e. oct+hex) that contains periods of pure A, pure B, pure A+B, and no odor. The corresponding mixed pattern is:

```
CCC___CAABBAABACCBAB___ = AB
```

AB can be broken up into 3 single odor specific components:

```
________AA__AA_A___A_____ = AB-B-C → A alone in mix
__________BB__B___B_B___ = AB-A-C → B alone in mix
CCC___C_________CC______ = AB-A-B → A+B alone in mix
```

Four seconds of EN data surrounding the occurrence of each spike (3s pre-, 1s post-stimulus) was extracted from the complete EN recording for each particular trial/odor condition/experiment. All of these EN segments for a given cell/odor combination were averaged to produce cell/odor condition specific STSAs.

Clustering was performed using standard hierarchical clustering algorithms contained in Matlab. Custom Matlab routines were used to calculate the Euclidean distance between ST-SAs.

3.5 Acknowledgements

We would like to thank Prof. Nathan Lewis and Anna Folinsky for their generous help with producing and adapting the electronic nose apparatus.

Chapter 4

Concluding Remarks

Chapters 2 and 3 describe in detail many of the results that I have accumulated while performing my dissertation research. In this chapter I will review the most significant findings, elaborate upon their importance, and suggest further experiments that could extend my conclusions.

4.1 Summary of Results

Considerable previous work has explored both the structure and function of the olfactory system in numerous animal models (Ache and Young, 2005; Firestein, 2001). However, this work has mostly focused on isolated odor pulses; stimuli that an animal is unlikely to experience in a nature (Koehl et al., 2001). The overall theme of my dissertation has been to resolve this disparity by using complex odor stimuli to test the applicability of our current models under these conditions.

In chapter 2 I explain how we presented two different odors at various overlaps and analyzed the results for both individual PNs and PN ensemble responses. This experiment

illustrates the complex activity sequences that are evoked by overlapping stimuli at two consecutive relays in the olfactory system; the antennal lobe and the mushroom body. Evaluating the responses of single neurons (PNs and KCs), we demonstrate that overlapping odors can mask individual responses. Subsequently, we demonstrate how groups of cells represent these unique stimuli. Using both qualitative and quantitative measures we show that PN ensembles were capable of tracking overlapping odors and quickly moving between individual odor representations as the odor changed. We establish how odor trajectories adjust when odors are switched on and off, making smooth transitions from one trajectory to another and following paths that were dependent upon prior history. Furthermore, we demonstrate the generation of PN representations that are very distant in high dimensional space from either of the two pure odors or their binary mixture. By looking at the activity of the KCs, which decode PN activity, we confirm many of the predictions based upon PN ensemble activity. Specifically, we show that specific stimulus conditions but not specific odors or odor combinations could excite a small unique population of KCs.

In chapter 3 I describe work that looked at another common situation in natural odor plumes, rapid variation, and compare how PNs respond when presented with frequent versus infrequent odor pulses. To have a quantitative measure of the stimulus for our analyses, we developed a sensor that was capable of recording concentration fluctuations in the odorant with high temporal resolution. To create stimuli that would allow us to comprehensively assess the effect of history on PN activity, we used M-sequences, mathematical constructs borrowed from work in the visual system (Reid et al., 1997). While grossly similar, we find several differences between individual PNs responses to the two stimuli. One notable example was that PNs tend to fire more strongly and are more synchronized at odor offset than onset. When we evaluate the activity across the entire PN population we find that the ensemble responses to rapidly varying odors were related to but different from those observed in pulse stimulus conditions; trajectories elicited by M-sequences occupied regions of PN space that straddled those evoked by single

pulses, but differed from them in at least two ways: First, M-sequence trajectories never returned to baseline because inter-pulse intervals in our intermittent protocols were never long enough to allow full relaxation. The M-sequence trajectories thus moved about some mean offset, different for each odor. Second, M-sequence trajectories occupied PN space more densely than single pulse sequences. These motions were reminiscent of the manifolds or families of trajectories evoked by different concentrations of single odors (Stopfer et al., 2003); they might indeed correspond to the different distributions of concentrations experienced in M-sequences and single pulse conditions. These results point to the need for new experiments combining concentration series and M-sequences.

Using STSAs derived from simultaneous EN recordings, we reconstructed the odor stimulus using two separate techniques. First, using spike-decoding (Bialek et al., 1991; Warland et al., 1997) we linearly reconstructed the time-varying odor concentration. We found that high quality reconstructions can be made with relatively few PNs; however, the overall quality increased and variability decreased as the number of PNs used in the reconstruction was increased. While this technique worked remarkably well, its success depended on prior knowledge of odor identity for selection of the appropriate reconstruction kernels. Second, using a clustering technique based on multiple discriminant analysis (Duda et al., 2000), we reconstructed the time varying odor identity of pure and mixed odor stimuli. We again found that increasing the number of PNs used for the reconstruction significantly improved average quality and decreased variability. Reconstruction accuracy, however, remained lower than for concentration profiles with the same number of PNs. The curve relating PN number to classification quality appeared to saturate quickly for concentration profile reconstruction, but showed no hint of saturation in the range studied (5-75 PNs) for identity profiles. This suggests that optimal decoding by the PNs' own targets may require pooling of larger numbers of PNs. This is consistent with independent results indicating that mean PN-KC convergence in locust is on the order of 400 (R Jortner, SS Farivar, & G Laurent, in prep).

4.2 Significance of Results

Overall, this work provides further support for the present hypothesis of olfactory coding and explains how the same framework applies in paradoxical conditions. Results of previous studies suggest that odors are represented in a distributed manner by evolving PN ensembles which synchronize their activity within 50ms windows and activate downstream KCs that respond very specifically (sparsely) due to a combination of feed-forward inhibition and high firing thresholds (Mazor and Laurent, 2005; Perez-Orive et al., 2002). However, given that odors are not processed instantaneously, it has been unclear how individual components are represented when two odors are introduced in close temporal proximity.

The work in chapter 2 provides definitive evidence to disprove dynamic resetting, which has been proposed based on both theoretical and experimental work, as a mechanism that would permit two odors to be perceived individually when presented in close temporal proximity (Brown et al., 2005). By demonstrating both quantitatively and qualitatively the exact transitions taken by PN ensembles when a new odor is presented, we show that this hypothesis is incorrect. Instead, we describe a model wherein stimulus history effects ensemble odor representations by continuously incorporating new information into evolving odor trajectories. Once new odor information is introduced, the system adjusts accordingly, moving towards the region of PN space that represents this new odor.

This work also raised the interesting possibility that “phantom-odors” could be caused by this process. We demonstrate how PN ensembles, in the process of moving from one odor trajectory to another in an overlap sequence, can move through regions that are highly dissimilar to either pure odor or the mixture. Given that KCs respond very specifically to regions of PN space, this movement could cause KCs that are unrelated to those odors presented or their mixture to be activated. An analogy of this occurrence would be presenting chocolate and vanilla to the animal, yet because of the order of presentation, its dynamics, and the identity of those two odors,

the animal would perceive cherry. In the process of confirming these hypotheses, matching PN predictions to KC responses, we also provided further evidence for our present model of olfactory coding (Perez-Orive et al., 2002), specifically, that PN ensembles represent odors and transfer this information to the downstream KCs which respond very sparsely.

The work in chapter 3 contains several important advances, both technical and theoretical. By using the electronic nose we demonstrate a necessary technical element for future olfactory experiments. This device will permit a more refined understanding of the transformation from stimulus to response in a way that was limited by prior technology either due to limited temporal resolution, e.g. mass spectroscopy (Smith and Spanel, 2005; Smith et al., 2002), or high response variability, e.g. electro-antennograms (Park et al., 2002; Vickers et al., 2001). Our electronic nose incorporates the best aspects of both mechanical sensors and biological systems; i.e. high sensitivity, reproducibility and temporal resolution. Making use of these new technical capabilities, our work is the first to apply M-sequences as olfactory stimuli and to present these highly complex, repeating odor patterns to an animal in order to record multiple-trial data (Reid et al., 1997). This stimulus paradigm allowed us to demonstrate significant differences between the PN odor representations for a single pulse and rapidly varying stimuli, which were not observed in previous work because of the limited stimuli used in those studies (Brown et al., 2005; Mazor and Laurent, 2005; Perez-Orive et al., 2002). Finally, we show - for the first time – that neuronal activity decoding methods can be applied to reconstruct both concentration and identity in single and multiple odor stimuli. While reconstruction techniques have long been applied to experiments in other sensory systems (particularly vision; (Bialek et al., 1991; Warland et al., 1997)), applications in the olfactory system have been conspicuously absent. Reasons for this include both the difficulty involved in faithfully recording the structure of an odor stimulus and our relatively new understanding of system level interactions in this sensory modality. The different technical advances of this study were necessary for us to reach the conclusions that the stimulus

frequency has a dramatic effect on the activity of PN ensembles and that increasing the ensemble size increases information representation for olfactory stimuli.

4.3 Future Directions

There several are technical and experimental advances that would greatly extend the impact of this work. While outside the scope of my dissertation research, it is my hope that these challenges will be taken up in the future.

1) While the electronic nose has been very useful in its present form, it could be improved by enabling it to detect odor identity. This could be achieved by grouping together multiple sensors, each with a different composition and therefore different odorant sensitivities. Lewis and colleagues have already developed such a sensor, but it remains to be adapted to electrophysiological experiments (Matzger et al., 2000). With this device one could follow the process of odor mixing and better quantify the quality of odor identity reconstructions.

2) Due to a variety of constraints, all of the experiments presented here involve only two odors. However, it is important that these results be repeated with more odors. This would address how generalizable these results are, given that the natural odor landscape contains an enormous number of diverse odorants.

3) Most of the experiments presented here involve the transformation of information from the PNs to the KCs. While these experiments recorded from both populations separately under identical conditions, much more information is likely to be gathered about PN to KC interactions if they are recorded simultaneously.

4) While much information was learned about PN representations of rapidly varying odors, it is important to extend this work to KCs. By recording the KC responses to the complex M-sequence stimuli, one will be able to test the predictions of this work and determine if the

differences in odor trajectories seen on the PN level between pulses and rapidly varying odors carry through as differences in the KC activity.

5) While the locust system provides a unique opportunity to simultaneously record from large groups of neurons, more can be done to advance our technical capability in this regard. As new technologies are developed, I look forward to the prospect of recording from a large fraction of both the AL and MB in a single experiment. The ability to monitor more KCs simultaneously will decrease the bias inherent in our sampling and allow us to begin performing some of the same analyses on the KC population that we currently do on the PNs, moving us from a qualitative to a quantitative assessment of KC function.

6) Finally, and most significantly, many of the results presented here should be confirmed with behavioral tests. While the locust is a good model for performing electrophysiological experiments, it is not a good model system for behavioral studies. By using other insects such as the honeybees or fruit flies (or larger animals like rats and mice) with well-documented learning paradigms one could test the perceptual significance of the hypotheses put forward by our work. Of specific importance to the work presented here, one must test if animals can be trained to distinguish “phantom-odors” from the overlapping odors that can create them and if animals can be trained to distinguish between rapidly varying and isolated pulses of the same odor as is suggested by our PN analysis.

REFERNCES

Ables, M. (1991). Corticonics: Neural circuits of the cerebral cortex (New York, Cambridge Univ. Press).

Ache, B., and Young, J. (2005). Olfaction: Diverse species, conserved principles. Neuron *48*, 417-430.

Adrian, E. (1942). Olfactory reactions in the brain of a hedgehog. J Physiol (Lond) *100*, 459-473.

Ahissar, E., and Arieli, A. (2001). Figuring space by time. Neuron *32*, 185-201.

Aksay, E., Major, G., Goldman, M. S., Baker, R., Seung, H. S., and Tank, D. W. (2003). History dependence of rate covariation between neurons during persistent activity in an oculomotor integrator. Cereb Cortex *13*, 1173-1184.

Amrein, H. (2004). Pheromone perception and behavior in Drosophila. Curr Opin Neurobiol *14*, 435-442.

Aviel, Y., Mehring, C., Abeles, M., Horn, D. (2003). On Embedding Synfire Chains in a Balanced Network. Neural Computation *15*, 1321-1340.

Bartos, M., Manor, Y., Nadim, F., Marder, E., and Nusbaum, M. P. (1999). Coordination of fast and slow rhythmic neuronal circuits. J Neurosci *19*, 6650-6660.

Bernardete, E., and Victor, J. (1994). An extension of the m-sequence technique for the analysis of multi-input nonlinear systems. In Advanced methods of physiological systems modeling, V. Z. Marmarelis, ed. (New York, Plenum), pp. 87-110.

Bernstein, J. (1902). Untersuchungen zur Termodynamik der bioelektrischen Ströme. Pflüger Arch ges Physiol *9*, 521-562.

Bertschinger, N., and Natschlager, T. (2004). Real-time computation at the edge of chaos in recurrent neural networks. Neural Comput *16*, 1413-1436.

Bialek, W., Rieke, F., de Ruyter van Steveninck, R. R., and Warland, D. (1991). Reading a neural code. Science *252*, 1854-1857.

Bitterman, M., Menzel, R., Fietz, A., Schaefer, S. (1983). Classical conditioning of proboscis extension in honeybees (Apis mellifera). J Comp Physiol *97*, 107-119.

Boekhoff, I., Strotmann, J., Raming, K., Tareilus, E., and Breer, H. (1990). Odorant-sensitive phospholipase C in insect antennae. Cell Signal *2*, 49-56.

Brennan, P. A., and Keverne, E. B. (2004). Something in the air? New insights into mammalian pheromones. Curr Biol *14*, R81-89.

Broome, B., Jayaraman, V., and Laurent, G. ((submitted)). Encoding and decoding of overlapping odor sequennces.

Brown, S. L., Joseph, J., and Stopfer, M. (2005). Encoding a temporally structured stimulus with a temporally structured neural representation. Nat Neurosci *8*, 1568-1576.

Buck, L. B., Axel, R. (1991). A novel multigene family may encode odorant receptors: a molecular basis for odor recognition. Cell *65*, 175-187.

Burrows, M. (1979). Synaptic potentials effect the release of transmitter from locust nonspiking interneurons. Science *204*, 81-83.

Burrows, M. (1996). Neurobiology of an insect brain (Oxford, Oxford Univ. Press).

Buzsaki, G. (2004). Large-scale recording of neuronal ensembles. Nat Neurosci *7*, 446-451.
Callaway, E. M. (2004). Feedforward, feedback and inhibitory connections in primate visual cortex. Neural Netw *17*, 625-632.

Chapman, R. (1998). The Insects: Structure and Function, 4th edn (Cambridge, Cambridge University Press).

Christensen, T. A., and Hildebrand, J. G. (2002). Pheromonal and host-odor processing in the insect antennal lobe: how different? Curr Opin Neurobiol *12*, 393-399.

Christensen, T. A., Hildebrand, T.J. (1988). Frequency coding by central olfactory neurons in the sphinx moth Manduca sexta. Chem Senses *13*, 123-130.

Coolen, I., Dangles, O., and Casas, J. (2005). Social learning in noncolonial insects? Curr Biol *15*, 1931-1935.

Couto, A., Alenius, M., and Dickson, B. J. (2005). Molecular, anatomical, and functional organization of the Drosophila olfactory system. Curr Biol *15*, 1535-1547.

Dayan, P., and Abbott, L. (2001). Theoretical Neuroscience: Computational and mathematical modeling of neural systems (Cambridge, MIT Press).

Deadwyler, S. A., and Hampson, R. E. (1997). The significance of neural ensemble codes during behavior and cognition. Annu Rev Neurosci *20*, 217-244.

Delorme, A., and Thorpe, S. J. (2001). Face identification using one spike per neuron: resistance to image degradations. Neural Netw *14*, 795-803.

Drake, K. L., Wise, K. D., Farraye, J., Anderson, D. J., and BeMent, S. L. (1988). Performance of planar multisite microprobes in recording extracellular single-unit intracortical activity. IEEE Trans Biomed Eng *35*, 719-732.

Dubnau, J., Grady, L., Kitamoto, T., and Tully, T. (2001). Disruption of neurotransmission in Drosophila mushroom body blocks retrieval but not acquisition of memory. Nature *411*, 476-480.

Duda, R., Hart, P., and Stork, D. (2000). Pattern Classification (New York, Wiley).

Eccles, J. (1976). From electrical to chemical transmission in the central nervous system. Henry Dale Centennial Symposium. Record of the Royal Scoiety *30*, 219-230.

Engel, A. K., Fries, P., and Singer, W. (2001). Dynamic predictions: oscillations and synchrony in top-down processing. Nat Rev Neurosci *2*, 704-716.

Engel, A. K., and Singer, W. (2001). Temporal binding and the neural correlates of sensory awareness. Trends Cogn Sci *5*, 16-25.

Ernst, K., Boeckh, J., and Boeckh, V. (1977). A neuroanatomical study on the organization of the central antennal pathways in insects. Cell Tissue Res *176*, 285-308.

Fell, J., Fernandez, G., Klaver, P., Elger, C. E., and Fries, P. (2003). Is synchronized neuronal gamma activity relevant for selective attention? Brain Res Brain Res Rev *42*, 265-272.

Firestein, S. (2001). How the olfactory system makes sense of scents. Nature *413*, 211-218.

Foldiak, P. (2002). Decoding neural population activity. In Encyclopedia of Cognitive Science, L. Nadel, ed. (London, Macmillan, Nature Publishing Group).

Fonta, C., Sun, X., and masson, C. (1993). Morphology and spatial distribution of bee antennal lobe interneurons responsive to odors. Chem Senses *18*, 101-119.

Freund, M. S., and Lewis, N. S. (1995). A chemically diverse conducting polymer-based "electronic nose". Proc Natl Acad Sci U S A *92*, 2652-2656.

Friedrich, R. W., and Laurent, G. (2001). Dynamic optimization of odor representations by slow temporal patterning of mitral cell activity. Science *291*, 889-894.

Friedrich, R. W., and Laurent, G. (2004). Dynamics of olfactory bulb input and output activity during odor stimulation in zebrafish. J Neurophysiol *91*, 2658-2669.

Funahashi, K. (1998). Multilayer neural networks and Bayes decision theory. Neural Netw *11*, 209-213.

Gilbert, C. D. (1994). Circuitry, architecture and functional dynamics of visual cortex. Ciba Found Symp *184*, 35-56; discussion 56-70.

Giurfa, M. (2003). Cognitive neuroethology: dissecting non-elemental learning in a honeybee brain. Curr Opin Neurobiol *13*, 726-735.

Giurfa, M., Zhang, S., Jenett, A., Menzel, R., and Srinivasan, M. V. (2001). The concepts of 'sameness' and 'difference' in an insect. Nature *410*, 930-933.

Gronenberg, W. (2001). Subdivisions of hymenopteran mushroom body calyces by their afferent supply. J Comp Neurol *435*, 474-489.

Hallem, E. A., Ho, M. G., and Carlson, J. R. (2004). The molecular basis of odor coding in the Drosophila antenna. Cell *117*, 965-979.

Hansson, B. S., and Anton, S. (2000). Function and morphology of the antennal lobe: new developments. Annu Rev Entomol *45*, 203-231.

Hassanali, A., Njagi, P. G., and Bashir, M. O. (2005). Chemical ecology of locusts and related acridids. Annu Rev Entomol *50*, 223-245.

Hodgkin, A., and Huxley, A. (1952). A quantitative description of membrance current and its application to conduction and excitation in nerve. Journal of Physiology *117*, 500-544.

Homberg, U., Christensen, T., and Hildebrand, J. (1989). Mechanisms of olfactory discrimination: converging evidence for common principles across phyla. Annu Rev Entomol, 477-501.

Homberg, U., Montague, R., and Hildebrand, J. (1988). Anatomy of antenno-cerebral pathways in the brain of the sphinx moth Manduca-sexta. Cell Tissue Res *254*, 255-281.

Hughes, J., and Mazurowski, J. (1962). Studies on the supracallosial mesial cortex of unanesthetized, conscious mammals. II. Monkeys. B. Responses from the olfactory bulb. EEG Clin Neurophysiol *14*, 635-645.

Jefferis, G. S., Marin, E. C., Stocker, R. F., and Luo, L. (2001). Target neuron prespecification in the olfactory map of Drosophila. Nature *414*, 204-208.

Jinks, A., and Laing, D. G. (1999). A limit in the processing of components in odour mixtures. Perception *28*, 395-404.

Kandel, E., Schwartz, J., and Jessell, T. (2000). Priciples of Neural Science, 4th edn (New York, McGraw-Hill).

Keil, T. (1989). Fine-structure of the pheromone-sensitive sensilla on the antenna of the hawkmoth, Manduca-sexta. Tissue Cell *21*, 139-151.

Knusel, P., Wyss, R., Konig, P., and Verschure, P. F. (2004). Decoding a temporal population code. Neural Comput *16*, 2079-2100.

Koehl, M. A., Koseff, J. R., Crimaldi, J. P., McCay, M. G., Cooper, T., Wiley, M. B., and Moore, P. A. (2001). Lobster sniffing: antennule design and hydrodynamic filtering of information in an odor plume. Science *294*, 1948-1951.

König, P., Engel, A. K., and Singer, W. (1996). Integrator of coincidence detector? The role of the coritcal neuron revisited. Trends Neurosci *19*, 130-137.

Konishi, M. (2003). Coding of auditory space. Annu Rev Neurosci *26*, 31-55.

Kurahashi, T., and Menini, A. (1997). Mechanism of odorant adaptation in the olfactory receptor cell. Nature *385*, 725-729.

Lagnado, L., and Baylor, D. (1992). Signal flow in visual transduction. Neuron *8*, 955-1002.

Laing, D. G., and Francis, G. W. (1989). The capacity of humans to identify odors in mixtures. Physiol Behav *46*, 809-814.

Laurent, G. (1993). A dendritic gain control mechanism in axonless neurons of the locust, *Schistocerca Americana*. J Physiol Lond *470*, 45-54.

Laurent, G. (1997). Olfactory processing: maps, time and codes. Curr Opin Neurobiol *7*, 547-553.

Laurent, G. (1999). A systems perspective on early olfactory coding. Science *286*, 723-728.

Laurent, G. (2002). Olfactory network dynamics and the coding of multidimensional signals. Nat Rev Neurosci *3*, 884-895.

Laurent, G., and Davidowitz, H. (1994). Encoding of olfactory information with oscillating neural assemblies. Science *265*, 1872-1875.

Laurent, G., and Naraghi, M. (1994). Odorant-induced oscillations in the mushroom bodies of the locust. J Neurosci *14*, 2993-3004.

Laurent, G., Stopfer, M., Friedrich, R. W., Rabinovich, M. I., Volkovskii, A., and Abarbanel, H. D. (2001). Odor encoding as an active, dynamical process: experiments, computation, and theory. Annu Rev Neurosci *24*, 263-297.

Laurent, G., Wehr, M., and Davidowitz, H. (1996). Temporal representations of odors in an olfactory network. J Neurosci *16*, 3837-3847.

Lee, H., Simpson, G. V., Logothetis, N. K., and Rainer, G. (2005). Phase locking of single neuron activity to theta oscillations during working memory in monkey extrastriate visual cortex. Neuron *45*, 147-156.

Lee, J. K., and Strausfeld, N. J. (1990). Structure, distribution and number of surface sensilla and their receptor cells on the olfactory appendage of the male moth Manduca sexta. J Neurocytol *19*, 519-538.

Leitch, B., and Laurent, G. (1996). GABAergic synapses in the antennal lobe and mushroom body of the locust olfactory system. J Comp Neurol *372*, 487-514.

Livingstone, M., and Hubel, D. (1988). Segregation of form, color, movement, and depth: anatomy, physiology, and perception. Science *240*, 740-749.

Loewi, O., and Navratil, E. (1926). On the humoral propogation of cardiac nerve action. Commmunication X. The fate of the vagus substance. In Cellular Neurophysiology: A Source Book, I. Cooke, and M. Lipkin Jr., eds. (New York, Holt, Rinehart and Winston), pp. 478-485.

Maass, W., Natschlager, T., and Markram, H. (2002). Real-time computing without stable states: a new framework for neural computation based on perturbations. Neural Comput *14*, 2531-2560.

MacLeod, K., Backer, A., and Laurent, G. (1998). Who reads temporal information contained across synchronized and oscillatory spike trains? Nature *395*, 693-698.

MacLeod, K., and Laurent, G. (1996). Distinct mechanisms for synchronization and temporal patterning of odor-encoding neural assemblies. Science *274*, 976-979.

Maei, H., and Latham, P. (2004). How can realistic networks process time-varying signals? . Society for Neuroscience Absrtact *30*, 81.89.

Marder, E. (2002). Non-mammalian models for studying neural development and function. Nature *417*, 318-321.

Martin, K. A. (2002). Microcircuits in visual cortex. Curr Opin Neurobiol *12*, 418-425.

Matzger, A. J., Lawrence, C. E., Grubbs, R. H., and Lewis, N. S. (2000). Combinatorial approaches to the synthesis of vapor detector arrays for use in an electronic nose. J Comb Chem *2*, 301-304.

Mazor, O., and Laurent, G. (2005). Transient Dynamics versus Fixed Points in Odor Representations by Locust Antennal Lobe Projection Neurons. Neuron *48*, 661-673.

McGuire, S. E., Le, P. T., and Davis, R. L. (2001). The role of Drosophila mushroom body signaling in olfactory memory. Science *293*, 1330-1333.

Mehta, M. R. (2005). Role of rhythms in facilitating short-term memory. Neuron *45*, 7-9.

Meister, M. (1996). Multineuronal codes in retinal signaling. Proc Natl Acad Sci U S A *93*, 609-614.

Mombaerts, P. (1996). Targeting olfaction. Curr Opin Neurobiol *6*, 481-486.

Mombaerts, P. (1999). Molecular biology of odorant receptors in vertebrates. Annu Rev Neurosci *22*, 487-509.

Mombaerts, P., Wang, F., Dulac, C., Chao, S. K., Nemes, A., Mendelsohn, M., Edmondson, J., and Axel, R. (1996). Visualizing an olfactory sensory map. Cell *87*, 675-686.

Mori, K., Nagao, H., and Yoshihara, Y. (1999). The olfactory bulb: coding and processing of odor molecule information. Science *286*, 711-715.

Murlis, J., Elkinton, J. S., and Cardé, R. T. (1992). Odor plumes and how insects use them. Annu Rev Entomol *37*, 505-532.

Murlis, J., Jones, C.D. (1982). Fine-scale structure of odour plumes in relation to insect orientation to distant pheromone and other attractant sources. Physiol Entomol *6*, 71-86.

Mustaparta, H. (1996). Central mechanisms of pheromone information processing. Chem Senses *21*, 269-275.

Nicolelis, M. A., Dimitrov, D., Carmena, J. M., Crist, R., Lehew, G., Kralik, J. D., and Wise, S. P. (2003). Chronic, multisite, multielectrode recordings in macaque monkeys. Proc Natl Acad Sci U S A *100*, 11041-11046.

Nicolelis, M. A., and Ribeiro, S. (2002). Multielectrode recordings: the next steps. Curr Opin Neurobiol *12*, 602-606.

Nicoll, R. (1971b.). Recurrent excitation of secondary olfactory neurons: a possible mechanism for signal amplication. Science *171*, 824-825.

Ochieng, S. A., Hallberg, E., and Hansson, B. S. (1998). Fine structure and distribution of antennal sensilla of the desert locust, Schistocerca gregaria (Orthoptera: Acrididae). Cell Tissue Res *291*, 525-536.

Oram, M. W., Foldiak, P., Perrett, D. I., and Sengpiel, F. (1998). The 'Ideal Homunculus': decoding neural population signals. Trends Neurosci *21*, 259-265.

Park, K., and Hardie, J. (1998). An improved aphid electroantennogram. J Insect Physiol *44*, 919-928.

Park, K. C., Ochieng, S. A., Zhu, J., and Baker, T. C. (2002). Odor discrimination using insect electroantennogram responses from an insect antennal array. Chem Senses *27*, 343-352.

Parker, A., and Newsome, W. (1998). Sense and the single neuron: probing the physiology of perception. Annu Rev Neurosci *21*, 227-277.

Perez-Orive, J., Bazhenov, M., and Laurent, G. (2004). Intrinsic and circuit properties favor coincidence detection for decoding oscillatory input. J Neurosci *24*, 6037-6047.

Perez-Orive, J., Mazor, O., Turner, G., Cassenaer, S., and Laurent, G. (2002). Oscillations and sparsening of odor representations in the mushroom body. Science *297*, 359-365.

Pouget, A., Dayan, P., and Zemel, R. (2000). Information processing with population codes. Nat Rev Neurosci *1*, 125-132.

Pouzat, C., Mazor, O., and Laurent, G. (2002). Using noise signature to optimize spike-sorting and to assess neuronal classification quality. J Neurosci Methods *122*, 43-57.

Rabinovich, M. I., Huerta, R., Volkovskii, A., Abarbanel, H. D., Stopfer, M., and Laurent, G. (2000). Dynamical coding of sensory information with competitive networks. J Physiol Paris *94*, 465-471.

Reid, R. C., and Alonso, J. M. (1996). The processing and encoding of information in the visual cortex. Curr Opin Neurobiol *6*, 475-480.

Reid, R. C., Victor, J. D., and Shapley, R. M. (1997). The use of m-sequences in the analysis of visual neurons: linear receptive field properties. Vis Neurosci *14*, 1015-1027.

Rieke, F., Warland, D., de Ruyter van Steneninck, R., and Bialek, W. (1997). Spikes (Cambridge, MIT Press).

Roweis, S. T., and Saul, L. K. (2000). Nonlinear dimensionality reduction by locally linear embedding. Science *290*, 2323-2326.

Sanger, T. D. (2003). Neural population codes. Curr Opin Neurobiol *13*, 238-249.

Schnitzer, M. J., and Meister, M. (2003). Multineuronal firing patterns in the signal from eye to brain. Neuron *37*, 499-511.

Schwartz, A. B., and Moran, D. W. (2000). Arm trajectory and representation of movement processing in motor cortical activity. Eur J Neurosci *12*, 1851-1856.

Scott, J. W., and Brierley, T. (1999). A functional map in rat olfactory epithelium. Chem Senses *24*, 679-690.

Scott, J. W., Shannon, D. E., Charpentier, J., Davis, L. M., and Kaplan, C. (1997). Spatially organized response zones in rat olfactory epithelium. J Neurophysiol *77*, 1950-1962.

Shadlen, M. N., and Newsome, W. T. (1994). Noise, neural codes and cortical organization. Curr Opin Neurobiol *4*, 569-579.

Siapas, A. G., Lubenov, E. V., and Wilson, M. A. (2005). Prefrontal phase locking to hippocampal theta oscillations. Neuron *46*, 141-151.

Siapas, A. G., and Wilson, M. A. (1998). Coordinated interactions between hippocampal ripples and cortical spindles during slow-wave sleep. Neuron *21*, 1123-1128.

Sincich, L. C., and Horton, J. C. (2005). The circuitry of V1 and V2: integration of color, form, and motion. Annu Rev Neurosci *28*, 303-326.

Singer, W. (1999). Neuronal synchrony: a versatile code for the definition of relations? Neuron *24*, 49-65, 111-125.

Singer, W., Gray, C. (1995). Visual feature integration and the temporal correlation hypothesis. Annu Rev Neurosci *18*, 555-586.

Smith, D., and Spanel, P. (2005). Selected ion flow tube mass spectrometry (SIFT-MS) for on-line trace gas analysis. Mass Spectrom Rev *24*, 661-700.

Smith, D., Wang, T., and Spanel, P. (2002). On-line, simultaneous quantification of ethanol, some metabolites and water vapour in breath following the ingestion of alcohol. Physiol Meas *23*, 477-489.

Srinivasan, M. V. (2003). Honeybee navigation. Curr Biol *13*, R894.

Steinbrecht, R. (1980). Cryofixation without cryorotectants - freeze substitution and freeze etching of an insect olfactory receptor. Tissue Cell *12*, 73-100.

Stocker, R. F., Lienhard, M. C., Borst, A., and Fischbach, K. F. (1990). Neuronal architecture of the antennal lobe in Drosophila melanogaster. Cell Tissue Res *262*, 9-34.

Stopfer, M., Bhagavan, S., Smith, B. H., and Laurent, G. (1997). Impaired odour discrimination on desynchronization of odour-encoding neural assemblies. Nature *390*, 70-74.

Stopfer, M., Jayaraman, V., and Laurent, G. (2003). Intensity versus identity coding in an olfactory system. Neuron *39*, 991-1004.
Stopfer, M., and Laurent, G. (1999). Short-term memory in olfactory network dynamics. Nature *402*, 664-668.

Stopfer, M., Wehr, M., MacLeod, K., and Laurent, G. (1999). Neural dynamics, oscillatory synchronization, and odour codes. In Insect Olfaction, B. S. Hansson, ed. (Berlin, Springer), pp. 163-180.

Strausfeld, N. J., Hansen, L., Li, Y., Gomez, R. S., and Ito, K. (1998). Evolution, discovery, and interpretations of arthropod mushroom bodies. Learn Mem *5*, 11-37.

Strausfeld, N. J., Sinakevitch, I., and Vilinsky, I. (2003). The mushroom bodies of Drosophila melanogaster: an immunocytological and golgi study of Kenyon cell organization in the calyces and lobes. Microsc Res Tech *62*, 151-169.

Suh, G. S., Wong, A. M., Hergarden, A. C., Wang, J. W., Simon, A. F., Benzer, S., Axel, R., and Anderson, D. J. (2004). A single population of olfactory sensory neurons mediates an innate avoidance behaviour in Drosophila. Nature.

Sutter, E. E. (1987). A practical nonstochastic approach to nonlinear time-domain analysis. In Advanced Methods in Physiological System Modelling, V. Z. Marmarelis, ed. (Los Angeles, University of Southern California), pp. 303-315.

Takeuchi, H., Imanaka, Y., Hirono, J., and Kurahashi, T. (2003). Cross-adaptation between olfactory responses induced by two subgroups of odorant molecules. J Gen Physiol *122*, 255-264.

Theunissen, F., and Miller, J. P. (1995). Temporal encoding in nervous systems: a rigorous definition. J Comput Neurosci *2*, 149-162.

Thorpe, S., Delorme, A., and Van Rullen, R. (2001). Spike-based strategies for rapid processing. Neural Netw *14*, 715-725.

Tiesinga, P. H., Fellous, J. M., Salinas, E., Jose, J. V., and Sejnowski, T. J. (2004). Inhibitory synchrony as a mechanism for attentional gain modulation. J Physiol Paris *98*, 296-314.

Uchida, N., and Mainen, Z. F. (2003). Speed and accuracy of olfactory discrimination in the rat. Nat Neurosci *6*, 1224-1229.

Van Rullen, R., Gautrais, J., Delorme, A., and Thorpe, S. (1998). Face processing using one spike per neurone. Biosystems *48*, 229-239.

van Ruth, S. M. (2001). Methods for gas chromatography-olfactometry: a review. Biomol Eng *17*, 121-128.

van Ruth, S. M. (2004). Evaluation of two gas chromatography-olfactometry methods: the detection frequency and perceived intensity method. J Chromatogr A *1054*, 33-37.

Vickers, N. J., Christensen, T. A., Baker, T. C., and Hildebrand, J. G. (2001). Odour-plume dynamics influence the brain's olfactory code. Nature *410*, 466-470.

Vickers, N. J., Christensen, T. A., and Hildebrand, J. G. (1998). Combinatorial odor discrimination in the brain: attractive and antagonist odor blends are represented in distinct combinations of uniquely identifiable glomeruli. J Comp Neurol *400*, 35-56.

Vosshall, L. B., Amrein, H., Morozov, P. S., Rzhetsky, A., and Axel, R. (1999). A spatial map of olfactory receptor expression in the Drosophila antenna. Cell *96*, 725-736.

Vosshall, L. B., Wong, A. M., and Axel, R. (2000). An olfactory sensory map in the fly brain. Cell *102*, 147-159.

Warland, D. K., Reinagel, P., and Meister, M. (1997). Decoding visual information from a population of retinal ganglion cells. J Neurophysiol *78*, 2336-2350.

Wehr, M., and Laurent, G. (1996). Odor encoding by temporal sequences of firing in oscillating neural assemblies. Nature *384*, 162-166.

Wehr, M., and Laurent, G. (1999). Relationship between afferent and central temporal patterns in the locust olfactory system. J Neurosci *19*, 381-390.

Wilson, M. A., and McNaughton, B. L. (1993). Dynamics of the hippocampal ensemble code for space. Science *261*, 1055-1058.

Wilson, M. A., and McNaughton, B. L. (1994). Reactivation of hippocampal ensemble memories during sleep. Science *265*, 676-679.

Wilson, R. I., Turner, G. C., and Laurent, G. (2004). Transformation of olfactory representations in the Drosophila antennal lobe. Science *303*, 366-370.

Wong, A. M., Wang, J. W., and Axel, R. (2002). Spatial representation of the glomerular map in the Drosophila protocerebrum. Cell *109*, 229-241.

Yang, Z., and Purves, D. (2003). Image/source statistics of surfaces in natural scenes. Network *14*, 371-390.

Young, M. P., and Yamane, S. (1992). Sparse population coding of faces in the inferotemporal cortex. Science *256*, 1327-1331.

Yuille, A., Grzywacs, N. (1989). A winner-take-all mechanism based on presynaptic inhibition. Neural Comput *1*, 334-347.

Zhang, K., Ginzburg, I., McNaughton, B. L., and Sejnowski, T. J. (1998). Interpreting neuronal population activity by reconstruction: unified framework with application to hippocampal place cells. J Neurophysiol *79*, 1017-1044.

Zufall, F., and Leinders-Zufall, T. (1998). Role of cyclic GMP in olfactory transduction and adaptation. Ann N Y Acad Sci *855*, 199-204.

Zufall, F., and Leinders-Zufall, T. (2000). The cellular and molecular basis of odor adaptation. Chem Senses *25*, 473-481.